eCAM Evidence-Based Complementary and Alternative Medicine

Traditional Chinese Medicine and Autonomic Disorders

Guest Editors: Kazuo Toda, Jorge L. Zeredo, Sae Uchida, and Vitaly Napadow

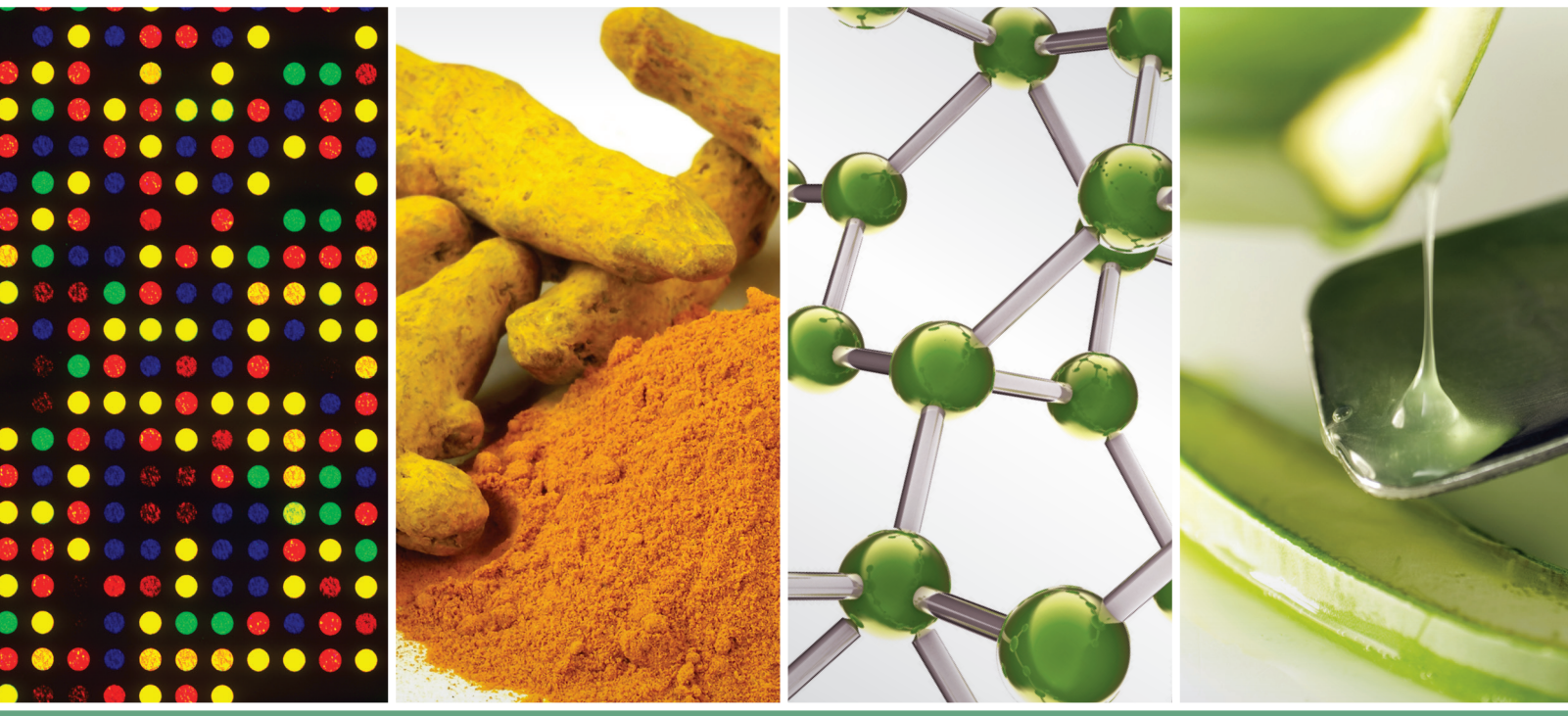

Traditional Chinese Medicine and Autonomic Disorders

Evidence-Based Complementary
and Alternative Medicine

Traditional Chinese Medicine and Autonomic Disorders

Guest Editors: Kazuo Toda, Jorge L. Zeredo, Sae Uchida, and Vitaly Napadow

Editorial Board

Contents

Hindawi Publishing Corporation
Evidence-Based Complementary and Alternative Medicine
Volume 2015, Article ID 429181, 2 pages
http://dx.doi.org/10.1155/2015/429181

Editorial

Traditional Chinese Medicine and Autonomic Disorders

Kazuo Toda,[1] Jorge L. Zeredo,[2] Sae Uchida,[3] and Vitaly Napadow[4]

[1]*Integrative Sensory Physiology, Graduate School of Biomedical Sciences, Nagasaki University, Nagasaki 8528588, Japan*
[2]*Graduate Program in Health Sciences, University of Brasilia, 70910-900 Brasilia, DF, Brazil*
[3]*Department of the Autonomic Nervous System, Tokyo Metropolitan Institute of Gerontology, Itabashi, Tokyo 1730015, Japan*
[4]*Athinoula A. Martinos Center for Biomedical Imaging, Massachusetts General Hospital, Harvard Medical School, Charlestown, MA 02129, USA*

Correspondence should be addressed to Kazuo Toda; k-toda@nagasaki-u.ac.jp

Received 16 June 2015; Accepted 17 June 2015

Traditional Chinese Medicine (TCM) consists of acupuncture, moxibustion, qigong, and herbal medicine. In modern times, TCM has often been used as complementary treatment for diseases that do not respond satisfactorily to conventional medicine. Autonomic disorders, which are caused by chronic imbalance of vegetative organs as well as autonomic-related areas in the central nervous system, fall into this category of difficult-to-treat conditions. Therefore, a significant role for TCM has been increasingly accepted in both Asian and Western countries for the treatment of autonomic disorders. The purpose of this special issue was to gather the most up-to-date evidence concerning the effective use of TCM for the treatment of autonomic disorders. Particular focus in this issue was placed on the effective use of herbal medicine.

Three papers are related to digestive function. Inflammatory bowel disease (IBD) is a chronic intestinal disorder which is characterized by bouts of severe intestinal inflammation and colonic mucosal ulcer. D. Liu et al. showed that Si Shen Wan significantly inhibited apoptosis of IECs (intestinal epithelial cells) through activation of PLC-γ1 and suppression of P13K/Akt signal pathway. Their results indicate that Si Shen Wan (which consist of four components) can effectively treat colitis by inhibiting excessive apoptosis of IECs.

A basic study on the effects of Huqi San (Qi-protecting powder) for cholestasis was conducted by X. Xue et al. They investigated the positive effects of Huqi San in the rat, indicating that it can stimulate Cl ion secretion in the distal colon by means of increasing the mRNA transcript and protein content of the cystic fibrosis transmembrane regulator in the liver, distal colon, and pancreas. They suggest that transporter modulation at a transcriptional level may serve as a potential target for a new therapeutic strategy for cholestasis.

Swertianlarin, isolated from *Swertia mussotii* Franch. and *Enicostemma axillare*, has hepatoprotective effects against cholestasis. In China, it is often used for treatment of jaundice. A pilot study was conducted by L. Zhang et al. using a rat bile duct-ligation (BDL) model. Serum bile acid levels were reduced in BDL rats treated for 14 days with Swertianlarin. This observation suggests that *Swertia mussotii* Franch. attenuates liver injury, inflammation, and cholestasis. Further studies are critically needed on whether Swertianlarin exerts the protective role in other cholestatic models and what the molecular mechanism underlying Swertianlarin-induced protective effects on liver injury, inflammation, and cholestasis is.

Hyperglycemia and diabetes-related depression can be improved by Chinese herbal medicine, Zuogui jiangtang jieyu (ZGJTJY) in rats. Y. Wang et al. conducted an interesting study using a 28-day mild stress model together with consistent high-fat diet and injection of streptozotocin. They investigated whether ZGJTJY prescription has hypoglycemic and antidepressant effects and found that ZGJTJY inhibits the expression of 11β-hydroxysteroid dehydrogenase type 1 (11β-HSD1) and increases glucocorticoid (GR) levels in the hippocampus and subsequently modulates blood glucose

levels. They concluded that this potential property of ZGJTJY could be of benefit for the treatment of behavior and cognitive function in diabetes-related depression.

Shenfu Decoction (SFD) is one of the most popular herbal medicine formulas with a long history of use in China. This herbal medicine consists of a mixture of *Panax ginseng* and Radix Aconiti Lateralis Preparata. Decoction is a typical traditional method of extraction by boiling of dissolved chemicals from herbal material and widely conducted in China, Japan, Korea, and other Asian countries. A study by J. He et al. had the main purpose of developing a rapid and sensitive Ultra Performance Liquid Chromatography/Quadrupole Time-of-flight Mass Spectrometry method. This technique is thought to be important to analyze pharmacokinetics of multiple components in various herbal medicines.

We believe that this special issue will provide many readers with relevant up-to-date information in the fields of autonomic nervous system and traditional medicines.

Kazuo Toda
Jorge L. Zeredo
Sae Uchida
Vitaly Napadow

Hindawi Publishing Corporation
Evidence-Based Complementary and Alternative Medicine
Volume 2015, Article ID 301640, 12 pages
http://dx.doi.org/10.1155/2015/301640

Research Article

Huqi San-Evoked Rat Colonic Anion Secretion through Increasing CFTR Expression

Xiaowei Xue,[1,2] Zhengming Shi,[3] Wen Wang,[4] Xiaotong Yu,[1] Ping Feng,[1] Min Zhang,[5,6] Xuejiang Wang,[1] and Jingdong Xu[1]

[1] *Department of Physiology and Pathophysiology, School of Basic Medical Science, Capital Medical University, Beijing 100069, China*
[2] *Department of Pathology, Peking Union Medical College Hospital, Chinese Academy of Medical Sciences & Peking Union Medical College, Beijing 100730, China*
[3] *Department of General Surgery, Beijing Jishuitan Hospital, Beijing 100035, China*
[4] *Department of Pharmacology, Xuanwu Hospital of Capital Medical University, Beijing 100053, China*
[5] *Alzheimer's Disease Center, Beijing Institute for Brain Disorders, Capital Medical University, Beijing 100069, China*
[6] *Department of Statistics, Purdue University, West Lafayette, IN, USA*

Correspondence should be addressed to Jingdong Xu; xujingdong@163.com

Received 13 August 2014; Revised 6 October 2014; Accepted 12 October 2014

Academic Editor: Sae Uchida

Huqi San (HQS) is a Chinese herbal preparation of eight medicinal herbs that promote diuresis, detoxification, blood circulation, and cholestasis. Defects in transporter expression and function can cause cholestasis and jaundice. However, the mechanism of the cholestasis underlying HQS effects, especially on the gastrointestinal tract ion secretion, has not been elucidated. Real-time RT-PCR and Western blotting were used to study the expression and localization of cystic fibrosis transmembrane conductance regulator (CFTR) and α-ENaC in rat alimentary tract, and then the effect of HQS on the ion transport in rat distal colon mucosa was investigated using the short-circuit current (I_{SC}) technique. The results showed that pretreatment with HQS significantly enhanced mRNA transcripts and protein content of CFTR in liver and distal colon but not α-ENaC in alimentary organs. HQS increases I_{SC} and decreases the transepithelial resistance. Pretreatment with epithelial Na^+ channel blocker did not affect the I_{SC} responses elicited by HQS, but removal of extracellular Cl^- or pretreatment with Cl^- channel or Na^+-K^+-$2Cl^-$ cotransporter blocker inhibited HQS-elicited I_{SC} responses. These findings demonstrated that HQS, RA, and RP can stimulate Cl^- secretion in the distal colon by increasing the mRNA transcripts and protein content of CFTR in liver and distal colon.

1. Background

Huqi San (HQS) is a Chinese herbal preparation of eight medicinal herbs, including Ramulus Visci, Radix Astragali seu Hedysari, Radix Curcumae, Radix Salviae Miltiorrhizae, Spica Prunellae, Semen Persicae, Semen Cuscutae, and Radix Sophorae Flavescentis, purchased from Tongrentang (Beijing, China) and authenticated by Professor Wen Wang, a botanist at Xuanwu Hospital, Beijing, China. HQS supplements qi and tonifies the kidney. HQS, especially its principal drug Ramulus Visci alkali (RA), the major active constituent of mistletoe extracts, is widely used for the treatment of tumour [1], hypertensive rats, and renal hypertensive dogs [2]. Previous studies showed that RA can inhibit Ca^{2+} mobilization from intracellular stores [3], block and reverse hepatocarcinogenesis [1], gynecological and breast cancer treatment [4], and even enhance immunosurveillance to prevent intestinal infections or other intestinal pathologies by the induction of cytokines in intestinal epithelial cells [5]. As an adjuvant, polysaccharides of Ramulus Visci (RP) can inhibit cancer cell proliferation and promote cancer cell apoptosis *in vivo* [6]. Our previous experiment has confirmed the effect of HQS on hepatocarcinogenesis [7]. Laboratory tests revealed hepatic cell damage with cholestasis, lipid abnormalities, and hypocholesterolemia with cystic fibrosis associated with liver disease as the only manifestation of cystic fibrosis [8].

Cholangiocytes alkalinize and dilute canalicular bile through the secretion of a bicarbonate rich fluid. Cystic fibrosis transmembrane conductance regulator (CFTR), a cAMP-regulated chloride channel expressed in biliary tract, is the major driving force for this ductular secretion [9, 10]. Both human and animal studies have provided evidence that any impairment in the expression and/or function of these different hepatobiliary transporters may lead to cholestatic disorders [11]. The disruption and dysregulation of this excretory pathway may result in cholestasis [12] and lead to intrahepatic accumulation of bile acids and other toxic compounds with progression of hepatic pathological changes [13]. Although the transcriptional regulation of hepatic organic anion transporters by liver-enriched hepatocyte nuclear factors and ligand activated nuclear receptors is the key to understand the molecular mechanisms of cholestasis [14], the transporter changes at a transcriptional level may represent potential targets for therapy [14]. In this study we investigate the effects of HQS, RA, and RP on hepatic organic anion transporter regulation in the liver, distal colon, and pancreas of rat.

2. Materials and Methods

2.1. Preparation of HQS. *HQS* was prepared from eight medicinal herbs by soaking the herbs, which include Hujisheng 1800 g (*Viscum coloratum* (Komar.) Nakai, Shanxi), Huangqi 1600 g (*Astragalus membranaceus* (Fisch.) Bge. var. mongholicus (Bge.) *Hsiao*, Gansu), Yujin 1200 g (*Curcuma wenyujin* Y. H. Chen and C. Ling., Sichuan), Danshen 800 g (*Salvia miltiorrhiza* Bge., Gansu), Xiakucao 800 g (*Prunella vulgaris* L., Henan), Taoren 600 g (*Prunus persica* (L.) Batsch, Beijing), Buguzhi 1200 g (*Psoralea corylifolia* L., Yunnan), and Kushen 800 g (*Sophora flavescens* Ait., Jiangsu) which were extracted with 95% ethanol in the proportion of 1 : 8 (w/v) for 2 h and repeated twice, and then the ethanol extracts were concentrated with a rotary evaporator (RE-52AA, Shanghai, China) and lyophilized (Thermo Savant, USA). The extracts were dissolved in water and extracted with petroleum ether. Subsequently, the defatted fraction was extracted with ethyl acetate and then concentrated to ointment under reduced pressure. The ointment was subjected to vacuum drying to form extractum which was then crushed into pieces, granulated, and stored in 4°C refrigerator until use. The HQS granules were diluted with water in the concentration 0.38 g dry grains/mL [15].

2.2. Preparation of Alkalies and Polysaccharides. The regular experiment method was performed for qualitative analyses of the alkalies or polysaccharides in Ramulus Visci. Ramulus Visci was ground to powder. Before soaking in acidity aqueous for 48 h, alkalies in Ramulus Visci (RA) were proceeded to precipitate with the alkali and then the insoluble were filtered. The partial precipitates were achieved using different alkalinity ratios to get the total alkali, and the polysaccharides of Ramulus Visci (RP) were prepared according to the previous report [16].

2.3. Solutions and Reagents. Hank's balanced salt solution (HBSS), glibenclamide, amiloride hydrochloride, bumetanide, and forskolin are from Sigma (St. Louis, MO, USA). The stock solutions of glibenclamide, forskolin, and bumetanide were prepared in dimethyl sulfoxide (DMSO). Final concentrations of DMSO never exceeded 0.1% (v/v). Preliminary experiments indicated that the vehicle did not change any baseline electrophysiological parameters.

Krebs-Henseit solution (K-HS) includes the following ingredients (mM): NaCl, 117; KCl, 4.5; $CaCl_2$, 2.5; $MgCl_2$, 1.2; $NaHCO_3$, 24.8; KH_2PO_4, 1.2; glucose, 11.1. In Cl^--free solution, NaCl, KCl, and $CaCl_2$ were replaced by sodium gluconate, potassium gluconate, and calcium gluconate, respectively. The solution was gassed with 95% O_2-5% CO_2 (V/V), pH 7.4, at temperature 37°C.

2.4. Tissue Preparation. Animal protocols followed guidelines established by the NIH and were approved by Animal Care and Use Committee, Capital Medical University. Male Sprague-Dawley rats (Laboratory Animal Services Center, Capital Medical University) ranging from 135 to 150 g (6 weeks old) had free access to standard rodent laboratory food and water until the day of the experiments. Eighty rats were equally divided (20 rats/group) into HQS therapeutic group (8 g/kg body weight), RA therapeutic group (10 mg/kg body weight), RP therapeutic group (10 mg/kg body weight), and control group with the physiological saline. All the drugs were given through intragastric administration for seven days *in vivo* experiment. The animals were killed by cervical dislocation. The distal colon was removed and defined as the *ca.* 7 cm long segment proximal to the lymph node (typically situated 3 cm apart from the anus). Then the distal colon was divided into 4 segments, which were cut along the mesenteric border into a flat sheet and flushed with ice-cold Kreb's-Henseit solution (K-HS). The tissue was pinned flat with the mucosal side down in a Sylgard-lined petri dish containing ice-cold oxygenated solution. The colon was longitudinally cut close to the mesentery, and the serosal muscle layers were carefully stripped away by blunt dissection to obtain a mucosa preparation. All the herbs and the routine drugs were supplied by means of directly apical or basolateral side in Ussing chamber system.

2.5. Short-Circuit Current Measurement. The short-circuit current was measured *in vitro* in Ussing chambers. Flat sheet of colonic mucosa preparations was mounted between two halves of modified Ussing chambers, in which the total cross-sectional area was 0.5 cm^2. The mucosal and serosal surfaces of tissue were bathed with 5 mL K-HS by recirculation from a reservoir maintained at 37°C during the experiments. The K-HS was bubbled with 95% O_2-5% CO_2 to maintain the pH of the solution at 7.4. Drugs could be added directly to the apical or basolateral side of mucosa. Responses were continuously recorded by computer. Transepithelial potential difference for every colonic mucosa was measured by the Ag/AgCl reference electrodes (Physiologic Instruments, P2020S) connected

to a preamplifier that was in turn connected to a voltage-clamp amplifier VCC MC6 (Physiologic Instruments). The change in I_{SC} was calculated using the value before and after simulation and was normalized as current per unit area of epithelial tissue ($\mu A \cdot cm^{-2}$), which allowed the curve area for 15 minutes to be calculated ($\mu A \cdot min$). The change in current in response to the applied potential was used to calculate the transepithelial resistance of the monolayer by Ohm's law. Experiments were repeated in different batches of colon mucosa to ensure that the data were reproducible. Positive I_{SC} corresponded to the movement of anions from the serosal to mucosal compartments or movement of cations from the mucosal to serosal compartments or a combination of both.

2.6. Preparation of RNA and cDNA. The distal colonic, liver, and pancreas tissues were collected in phosphate buffered saline (PBS; 0.9% NaCl in 0.01 M sodium phosphate buffer, pH 7.4), which had been treated with 0.1% diethylpyrocarbonate (DEPC-PBS). After the wall of each piece of tissue had been opened, the tissue was cleaned with DEPC-PBS and transferred to Trizol (Invitrogen) for extraction of total RNA, which was isolated according to the manufacturer's instructions and stored at −80°C for later use. Samples of cDNA were generated by reverse transcription with 5 μg total RNA, 50 ng random hexamer primers, and 10 nM dNTPs, incubated at 65°C for 5 min, and placed on ice for at least 1 min, with the addition of 40 URNase OUT, 200U SuperScript III RT, 10 mM dithiothreitol, and 5 mM $MgCl_2$ (Invitrogen), in a 20 μL reaction volume. Following brief centrifugation, the reactions were incubated at 50°C for 50 min and then at 70°C for 15 min. The completed reverse transcription reactions were stored at −20°C and used for the polymerase chain reaction (PCR) without further treatment.

2.7. Real-Time RT-PCR and Sequencing. Total RNA of the liver, colon, and pancreas was extracted using the Trizol reagent (Invitrogen, Carlsbad, CA, USA) according to the protocol of the manufacturer. Primers for CFTR were designed according to the rat mRNA sequence of CFTR (Sangon, Shanghai, China): 5′-cgc agg ttc tca gtg gac gat gcc-3′ (forward) and 5′-cct caa cca gaa aaa cca gca cgc-3′ (reverse) (estimated amplicon size: product length 269 bp). mRNA sequence of α-ENaC (Sangon, Shanghai, China): 5′-cag-ggt-gat-ggt-gca-tgg-3′ (forward) and 5′-cca cgc cag gtc aag-3′ (reverse) (estimated amplicon size: product length 239 bp), GAPDH forward primer: 5′-tgg agt cta ctg gcg tct-3′, reverse primer: 5′-agt gag ctt ccc gtt cag-3′ was used as an internal control (Table 1). All RT-qPCRs were performed with a Bio-Rad CFX 96 Real-time Detection Systems (Bio-Rad, Hercules, CA, USA). Protocols for all cycle RT-qPCRs were adjusted to the same thermal profile. Data were collected during the annealing phase.

2.8. Western Blotting. Tissue was harvested from the rat liver, distal colon, and pancreas, washed with PBS, and homogenized in 300 μL cold lysis buffer, pH 7.5, containing Nonidet P-40 (1%), TRIS-HCl (10 mM, pH 8.0), EDTA (1.0 mM), NaCl (150 mM), EGTA (2.0 mM), 10% SDS (0.1%), sodium orthovanadate (1 mM), deoxycholic acid (0.5%), phenylmethanesulfonyl fluoride (1.0 mM), aprotinin (5 μg/mL), and leupeptin (5 μg/mL), all purchased from Sigma. Total tissue homogenates were sonicated to dissolve completely and then centrifuged at 12,000 rpm for 30 min at 4°C to separate the membrane-containing fraction (pellet) from the cytosol. Proteins (100 μg) were separated by 10% SDS-polyacrylamide gel electrophoresis. The separated proteins were electroblotted onto nitrocellulose membrane (NC membrane, Millipore), and then the membrane was washed for 10 min with TBST (20 mM TRIS-HCl, pH 7.5, containing 0.15 M NaCl and 0.05% Tween 20) and immersed in blocking buffer containing 5% nonfat dry milk in TBST for 1 h at room temperature. The blot was washed with TBST and finally incubated overnight at 4°C with polyclonal primary antibodies to CFTR and α-ENaC (Affinity Bio Reagents, USA; diluted 1 : 500 in 5% nonfat dry milk). After being washed in TBST, the blot was incubated with secondary antibody to rabbit lgG (Zhongshan Goldenbridge, China) for 1 h at room temperature. The blot was finally washed with TBST, scanned by infrared rays with the Odyssey Infrared Imager (LI-COR, Nebraska, USA), and analyzed by Odyssey software (version 1.2).

Table 1: Sequences of primers.

Primer	Primer sequence	Product length (bp)
CFTR	F: 5′-cgc agg ttc tca gtg gac gat gcc-3′ R: 5′-cct caa cca gaa aaa cca gca cgc-3′	269 bp
α-ENaC	F: 5′-cag ggt gat ggt gca tgg-3′ R: 5′-cca cgc cag gtc aag-3′	239 bp
GAPDH	F: 5′-tgg agt cta ctg gcg tct-3′ R: 5′-agt gag ctt ccc gtt cag-3′	401 bp

2.9. Statistical Analysis. All values were expressed as means and standard error of mean (S.E.M.), and n was the number of animals in each experiment. All data were analyzed using the GraphPad Prism software 5.0 package (GraphPad Software Inc., San Diego, CA, USA). The increase in I_{SC} was quantified by subtracting the peak of an I_{SC} response from its respective baseline value before drug administration. The differences between control and treatment means were analyzed using Student's paired or unpaired t-test when appropriate. The differences among groups were analyzed using a one-way analysis of variance followed by Dunnett's multiple comparison. A P value of less than 0.05 was considered statistically significant.

3. Results

3.1. Effects of HQS, RP, and RA on the mRNA Expressions of CFTR and α-ENaC. In order to investigate whether the effects of HQS, RP, or RA on the depressed liver energy and cholestasis were related to the expressions of CFTR and α-ENaC, we used real-time RT-PCR analysis to examine the expression levels of CFTR and α-ENaC in liver, pancreas, and

Table 2: Effect of HQS on CFTR and α-ENaC protein level in different tissue (mean ± SEM, mm^2).

Tissue	CFTR			α-ENaC		
	Liver	Pancreas	Distal colon	Liver	Pancreas	Distal colon
Control	0.18 ± 0.02 ($n = 6$)	0.14 ± 0.02 ($n = 6$)	0.66 ± 0.11 ($n = 6$)	0.14 ± 0.02 ($n = 6$)	0.05 ± 0.02 ($n = 6$)	0.21 ± 0.04 ($n = 6$)
RP	0.31 ± 0.03 ($n = 6$)	0.15 ± 0.02 ($n = 6$)	0.68 ± 0.08 ($n = 6$)	0.14 ± 0.00 ($n = 6$)	0.06 ± 0.03 ($n = 6$)	0.25 ± 0.02 ($n = 6$)
RA	0.34 ± 0.05 ($n = 6$)	0.16 ± 0.03 ($n = 6$)	1.08 ± 0.35* ($n = 6$)	0.15 ± 0.02 ($n = 6$)	0.07 ± 0.03 ($n = 6$)	0.24 ± 0.03 ($n = 6$)
HQS	0.64 ± 0.22** ($n = 6$)	0.22 ± 0.08* ($n = 6$)	1.05 ± 0.26* ($n = 6$)	0.16 ± 0.04 ($n = 6$)	0.07 ± 0.04 ($n = 6$)	0.24 ± 0.06 ($n = 6$)

*$P < 0.05$, **$P < 0.01$ versus control group.

colon (Figures 1(c)–1(e)). The quantitative analyses showed that the expression levels of CFTR but not α-ENaC were significantly elevated after HQS, RP, or RA pretreatment, respectively. The CFTR mRNA level (%) in liver increased to 2.83 ± 0.62 in RA ($n = 6$, $P < 0.05$) and to 5.15 ± 0.42 in HQS ($n = 6$, $P < 0.001$) but not in RP (Figure 1(c)). The CFTR mRNA level (%) in colon was increased to 2.72 ± 0.45 in HQS ($n = 6$, $P < 0.001$) (Figure 1(d)) but no obvious changes in RA or RP. However, the CFTR in pancreas has no obvious changes after treatment with HQS, RA, or RP (Figure 1(e)). As shown in Figures 1(f)–1(h), α-ENaC has no significant change in liver, pancreas, or colon after treatment with HQS, RA, or RP.

3.2. Effects of HQS on the Protein Expression of CFTR and α-ENaC. Western blotting was performed to investigate CFTR and α-ENaC protein content in gastrointestinal tract. We probed lysates from liver, distal colon, and pancreas with anti-CFTR and α-ENaC antibody (Figures 2(a)–2(c)). The immunoblots were located at the same level as their corresponding positive controls. The immunoblot detected with CFTR and α-ENaC antibody was 165 KD and 95 KD which was in the range reported for CFTR and α-ENaC protein previously. As expected, the content levels of CFTR protein significantly increased in the liver from 0.18 ± 0.02 to 0.64 ± 0.22 ($n = 6$, $P < 0.05$, about 255.5%), distal colon from 0.66 ± 0.11 to 1.05 ± 0.26 ($n = 6$, $P < 0.05$, about 59.1%), and pancreas from 0.14 ± 0.02 to 0.22 ± 0.08 ($n = 6$, $P < 0.05$, about 57.1%) in the HQS group more than that in the control. However, there was no significant difference in the other groups, except RA in colon group. Meanwhile, α-ENaC protein contents have no significant changes in all tissues (shown in Table 2 and Figures 2(a)–2(c)).

In order to reconfirm the ion species involved in the HQS-induced I_{SC}, Cl^- was removed from the bathing solution. The HQS response significantly decreased in Cl^--free solution (Figures 2(d) and 2(e)), from 27.81 ± 1.98 $\mu A/cm^2$ ($n = 12$) to 11.73 ± 0.88 $\mu A/cm^2$ ($n = 12$, $P < 0.001$, 57.82%), indicating Cl^--dependence of the HQS-induced current, and the transmembrane resistance has no obvious changes, while pretreatment with 10 mM amiloride (Ami), an epithelial Na^+ channel blocker, had no effect on the HQS-induced ΔI_{SC} ($n = 13$, $P > 0.05$; Figures 2(g)–2(i)), which excluded the involvement of Na^+ absorption. The effect of the Cl^- channel blocker, glibenclamide, on the HQS-induced I_{SC} was also examined. As shown in Figures 2(j) and 2(k), apically applied glibenclamide (1 mM) reduced the HQS-induced ΔI_{SC} response by 29.9% from 62.67 ± 4.09 $\mu A/cm^2$ to 48.25 ± 1.38 $\mu A/cm^2$ ($n = 6$, $P < 0.01$). Basolateral addition of 100 mM bumetanide, which is a strong inhibitor of the Na^+-K^+-$2Cl^-$ cotransporter, reduced the HQS-induced I_{SC} more than 37.6% ($n = 6$, $P < 0.01$) as shown in Figures 2(j) and 2(k).

3.3. HQS-Induced I_{SC} Responses. Given that HQS can enhance the expression of CFTR protein in the liver, pancreas, and colon, a mucosal preparation of the rat distal colon was chosen as a model to study the colonic secretion and analyze the potential mechanism by improving the bile from the gallbladder [17]. After the freshly isolated rat colonic mucosa had been equilibrated for 30 min, the basolateral addition of HQS produced a transient increase in I_{SC} that lasted approximately 10 min. The effect of HQS was concentration independent. As shown in Figure 3(a), the I_{SC} increase evoked by HQS at a dosage of 0.1, 1.0, and 5.0 mg/mL was from 35.49 ± 1.95 $\mu A/cm^2$ to 35.03 ± 4.90 $\mu A/cm^2$ ($n = 9$, $P > 0.05$), 56.03 ± 4.95 $\mu A/cm^2$ ($n = 27$, $P < 0.01$), and 32.14 ± 1.10 $\mu A/cm^2$ ($n = 8$, $P > 0.05$) about 8.48%, 57.88%, or 1.69%, respectively. The HQS-induced I_{SC} response was accompanied by a significant dose-independent decrease in transepithelial resistance from 63.33 ± 5.06 $\Omega \cdot cm^2$ to 54.17 ± 1.20 $\Omega \cdot cm^2$ ($n = 12$, $P > 0.05$), 39.79 ± 3.38 $\Omega \cdot cm^2$ ($n = 9$, $P < 0.01$), and 60.72 ± 3.88 $\Omega \cdot cm^{-2}$ ($n = 6$, $P > 0.05$) at the dosage of 0.1, 1, and 5 mg/mL by 15.90%, 37.20%, and 4.12%, respectively, which indicated that mucosa conductance might be activated at the dosage of 1 mg/mL. However, at a dosage of 5 mg/mL, HQS did not affect significantly the I_{SC} and transepithelial resistance as compared with the baseline (Figures 3(a)–3(c)).

3.4. RA and RP-Induced I_{SC} Responses. As shown in Figure 2(b), RA could enhance the expression of CFTR protein in colon from 0.66 ± 0.11 to 1.05 ± 0.26 ($n = 6$, $P < 0.05$, about 59.1%) but not in liver and pancreas. So RA-induced I_{SC} response was observed. The result showed that RA in 0.75 mg/mL or 1.50 mg/mL increased I_{SC} response about 13.10% or 59.89% from 53.85 ± 3.82 $\mu A/cm^2$ to 60.90 ± 7.39 $\mu A/cm^2$ ($n = 11$, $P > 0.05$) and 86.10 ± 8.91 $\mu A/cm^2$

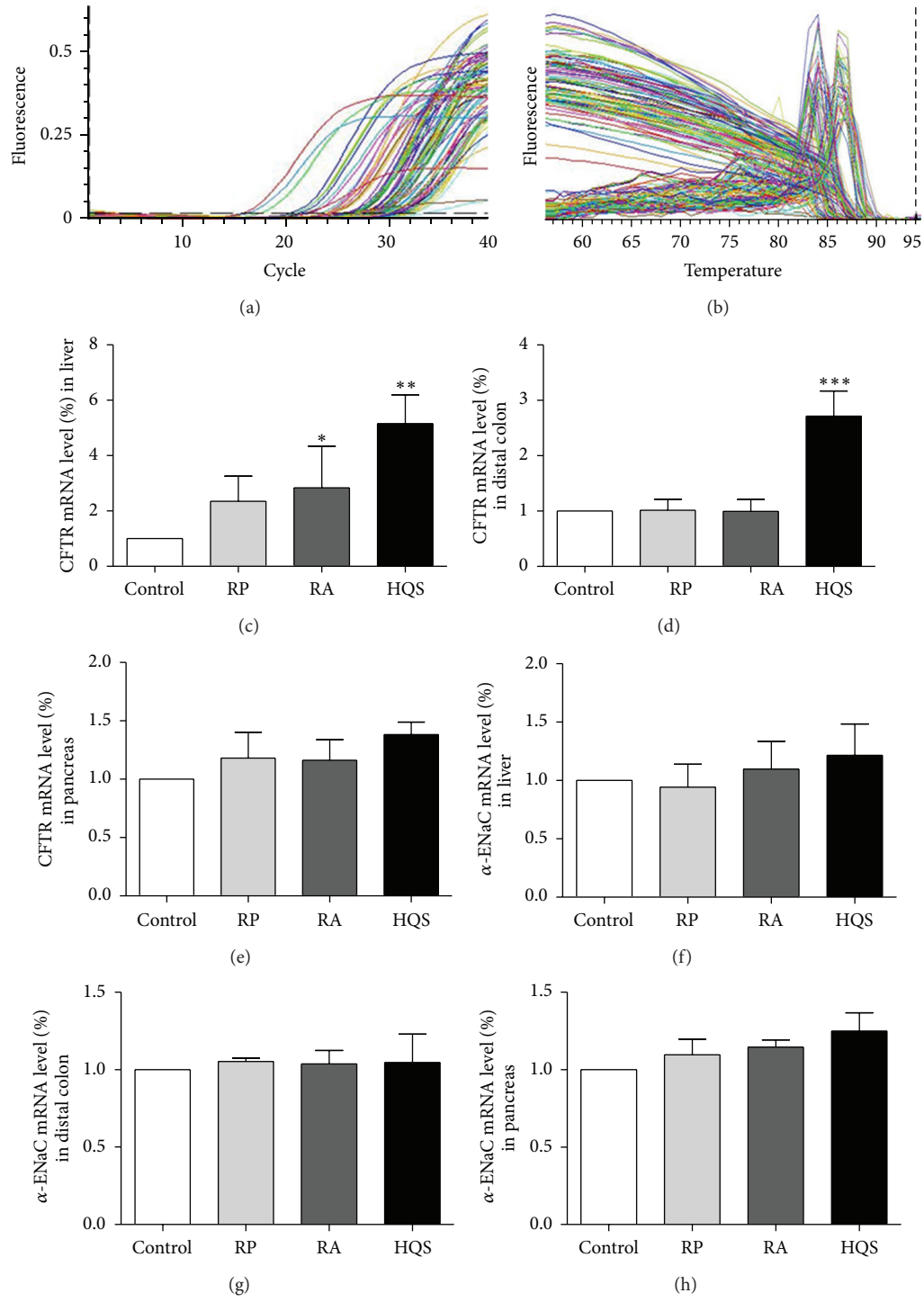

Figure 1: Real-time RT-PCR analysis of mRNA expression of CFTR and α-ENaC in rat liver, distal colon, and pancreas. (a) Continuous monitoring of fluorescence emission during cycle PCR of template DNA from strains tested. The number of samples for liver, pancreas, and distal colon is 35 and 40, respectively. The error bars represent standard error. (b) Representative different tissues experiment by melting analysis based on real-time PCR using SYBR Green I. The melting point peaks were clearly separated among liver, pancreas, and distal colon using SYBR Green I at 2.5 mM $MgCl_2$. Real time RT-PCR results with products of CFTR found in rat liver, pancreas, and distal colon quantitative analysis of CFTR expression pretreatment with RP, RA, and HQS, respectively, and GAPDH (internal marker) ratio shown. RA and HQS could enhance the CFTR expression in rat liver and distal colon but not in pancreas ((c)–(e)). Quantitative analysis of α-ENaC expression pretreatment with RP, RA, and HQS, respectively, and GAPDH (internal marker) ratio were shown. There is no statistically significant change in liver, pancreas, or distal colon ((f)–(h)). Data analysis was used with one-way analysis of variance followed by Dunnett's multiple comparison. Values are represented as means ± SEM; $^{*}P < 0.05$, $^{**}P < 0.01$.

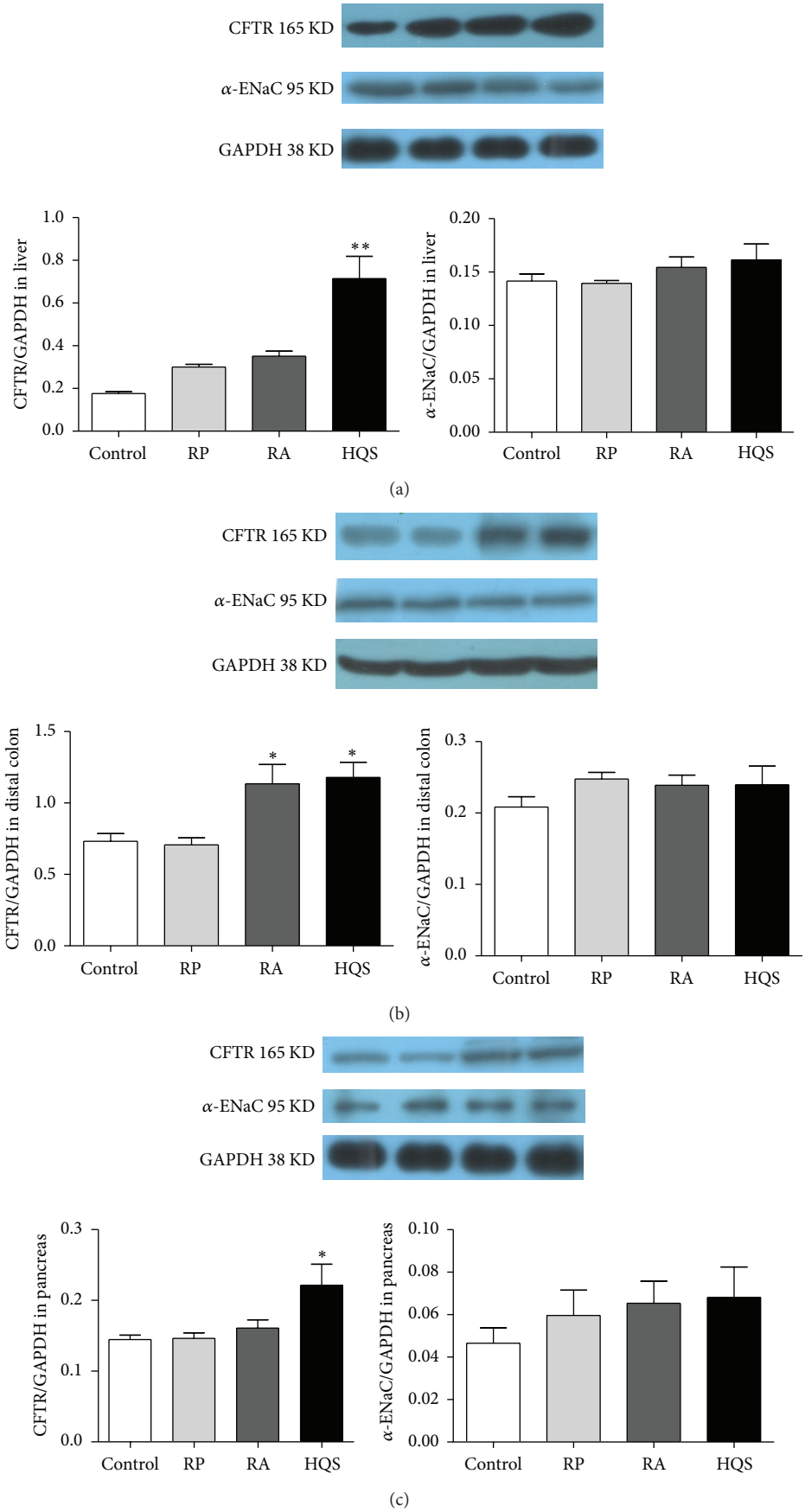

Figure 2: Continued.

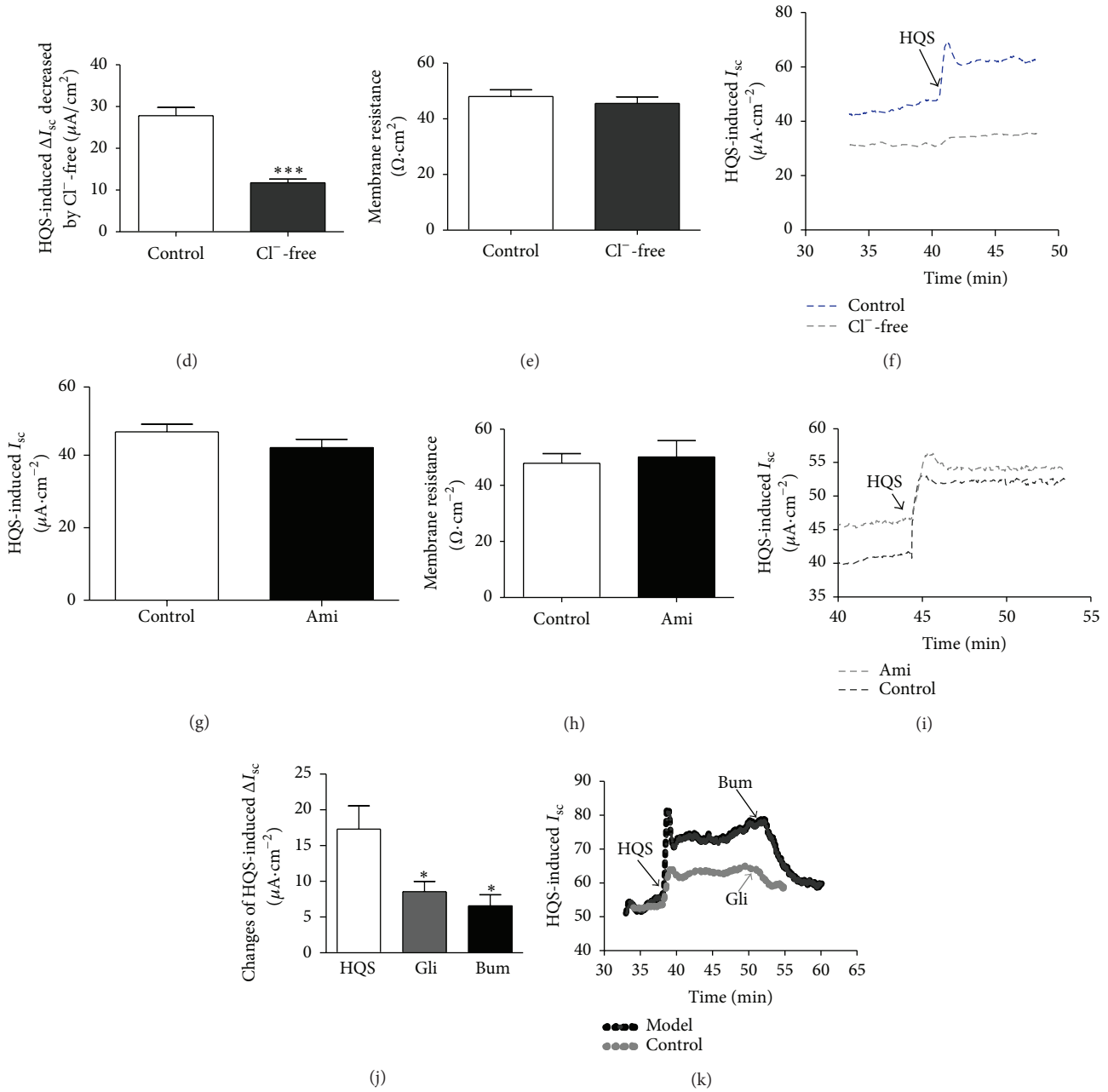

Figure 2: Western blot confirmed the expression of CFTR and α-ENaC in rat liver, distal colon, and pancreas. Densitometric analysis of CFTR and α-ENaC protein levels (normalized to GAPDH) in rat liver. HQS (1.0 mg/mL) can significantly increase the expression of CFTR in liver (a). Densitometric analysis of CFTR and α-ENaC protein levels (normalized to GAPDH) in rat distal colon. HQS (1.0 mg/mL) and RA can significantly increase the expression of CFTR in colon (b). Densitometric analysis of CFTR and α-ENaC protein levels (normalized to GAPDH) in rat pancreas. HQS (1.0 mg/mL) can significantly increase the expression of CFTR in pancreas (c). α-ENaC has no conspicuous changes across different groups ((a)–(c)). (d) Effects of Cl^- replacement and transporter inhibitors on the HQS I_{SC}. The bar graph illustrates the effects of removing extracellular Cl^- on the HQS I_{SC} and transepithelial resistance (e). Representative traces of HQS-evoked Cl^- flux in the absence and presence of Cl^-. Arrows indicate the time of the response to HQS (1.0 mg/mL) added basal in normal and Cl^--free K-H solutions (f). The bar graph illustrates the effects of apical addition of amiloride (10 μmol/L) on the I_{SC}. HQS (1.0 mg/mL) added basal in normal and Na^+ channel blocker, amiloride (10 μmol/L) (g). The bar graph illustrates of the amiloride on the transepithelial resistance of HQS (1.0 mg/mL) (h). Representative traces of HQS-evoked I_{SC} in the absence and presence of amiloride (100 μM). Arrowheads indicate the time of HQS addition (i). The bar graph illustrates the application of glibenclamide (1 mmol/L, apical), an inhibitor of the CFTR transporter or bumetanide (100 μmol/L, basal), and the Na^+-K^+-$2Cl^-$ cotransporter on HQS-induced I_{SC} comparison of HQS- (1.0 mg/mL) induced I_{SC} (j). Representative traces of I_{SC} recording with arrows indicating the time for the apical application of glibenclamide (1 mm/L) or basolateral application of bumetanide (100 μmol/L), respectively, and addition of HQS (1.0 mg/mL) (k). Data analysis was used with one-way analysis of variance followed by Dunnett's multiple comparison. Values are represented as mean ± SEM; $^*P < 0.05$, $^{**}P < 0.01$.

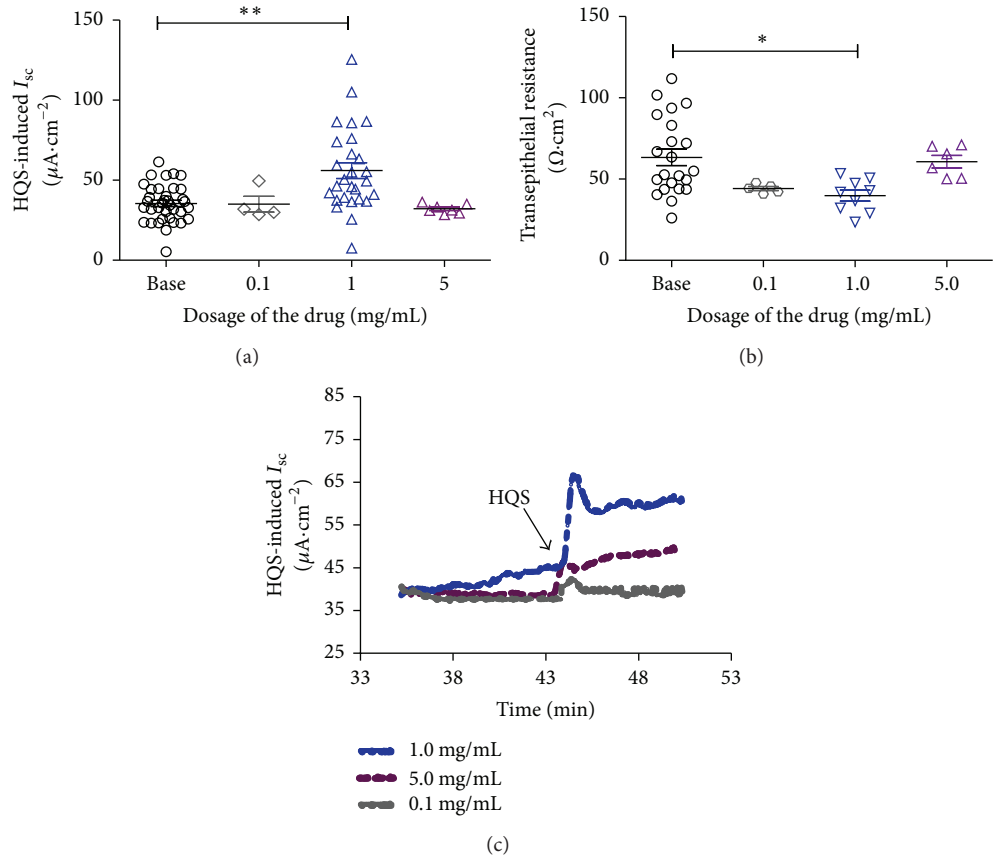

Figure 3: Concentration-response curve for HQS-induced response in the mucosa/submucosa preparations of the rat distal colon. Application of different dosage of HQS (0.1, 1.0, and 5.0 mg/mL) on the I_{SC} responses (a). The scattergram illustrates the effect of basolateral application of different concentrations of HQS on the transepithelial resistance. At the dosage of HQS (1.0 mg/mL), the colonic transepithelial resistance was significantly reduced by 58.33% ($P < 0.05$, $n = 6$) (b). Representative traces of basolateral addition of HQS-evoke I_{SC} responses at the concentration of 0.1, 1.0, and 5.0 mg/mL. Arrowheads indicate the time of HQS addition (c). Unpaired t-test was used. Values are represented as means ± SEM; $^{*}P < 0.05$, $^{**}P < 0.01$.

($n = 13$, $P < 0.01$) and with the decrease in transepithelial resistance about 24.6% from 48.01 ± 2.48 Ω·cm^2 to 36.2 ± 1.84 Ω·cm^2 ($n = 14$, $P < 0.01$) in the dosage of 1.50 mg/mL but not in other dosage groups (Figure 4(c)).

As shown in Figure 4(d), RP could not induce I_{SC} increasing in the dosage of 1.0, 10, and 100 mg/mL about 17.36%, 16.00%, and 17.90%, respectively, from 14.69 ± 0.92 μA/cm^2 ($n = 15$) to 17.04 ± 0.92 μA/cm^2 ($n = 15$, $P > 0.05$) and 17.32 ± 1.05 μA/cm^2 ($n = 16$, $P > 0.05$). It also showed that RP might have no effect on transepithelial resistance from 40.39 ± 1.26 Ω·cm^2 to 38.00 ± 1.44 Ω·cm^2 ($n = 18$, $P > 0.05$), 36.91 ± 1.67 Ω·cm^2 ($n = 15$, $P > 0.05$), and 38.42 ± 1.75 Ω·cm^2 ($n = 17$, $P > 0.05$), respectively. All these results indicated that ion channels might be partly activated and the mucosal barrier had not obviously changed treatment with RP but with RA (Figures 4(a)–4(f)).

3.5. HQS-Induced I_{SC} Responses in Rat Model. In order to further investigate whether HQS has the choleretic action. The model rats had been administered the HQS with 8 g/kg body weight for 6 weeks. As shown in Figures 5(a) and 5(d), the baseline of I_{SC} in the model rat is 59.27 ± 6.22 μA/cm^2 higher than that in the control group 47.46±6.91 μA/cm^2 ($n = 8$, $P > 0.05$, 19.9%), while in Figure 5(b), the transmembrane resistance in the model is 40.14 ± 2.32 Ω·cm^2 lower than that in the control group 49.79 ± 2.36 Ω·cm^2 about 19.90% ($n = 8$, $P > 0.05$). As indicated in Figures 5(c) and 5(d), basolateral addition of forskolin (100 μM) induced a rapid I_{SC} rise from 59.27 ± 6.22 μA/cm^2 to 221.50 ± 24.29 μA/cm^2 ($n = 8$, $P < 0.01$) in model group, which was higher than in the control group from 45.67 ± 2.86 μA/cm^2 to 107.50 ± 11.72 μA/cm^2 ($n = 8$, $P < 0.01$) in model group, respectively. The results indicate that the ΔI_{SC} obviously increased after forskolin application was cAMP-dependent on the CFTR expression of the apical side, while basolaterally applied bumetanide, Na^+-K^+-$2Cl^-$cotransporter inhibitor (100 μM), or apically applied glibenclamide (1 mM), CFTR channel inhibitor, decreased the forskolin-induced I_{SC} response to 53.65 ± 0.09 μA/cm^2 (Figure 5(d)), which was close to the baseline.

4. Discussion

Both human and animal studies have shown that any impairment in the expression and/or function of different

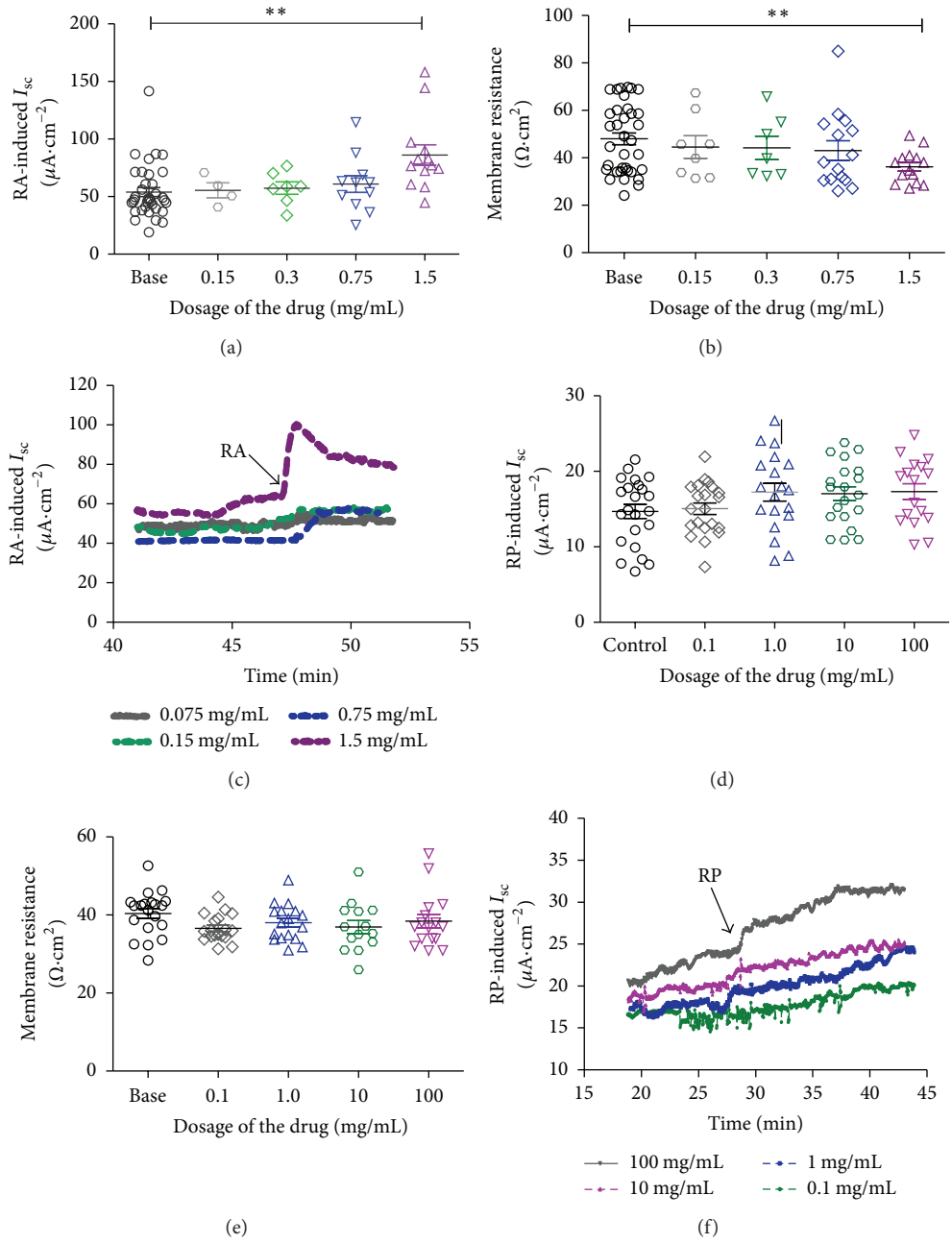

FIGURE 4: Effects of the RA and RP on the I_{SC} in the mucosa/submucosa preparations of the rat distal colon. The scattergram illustrates the application of different concentrations of RA (0.15, 0.3, 0.75, and 1.5 mg/mL) on the I_{SC} responses (a). Summary of the effects of different concentration of RA on the transepithelial resistance in the dosage of RA (1.5 mg/mL) significantly reduced colonic transepithelial resistance (b). The effect of different concentrations of RA (0.15, 0.3, 0.75, and 1.5 mg/mL) on the distal colon mucosa I_{SC}. Arrowheads indicate the time of RA addition (c). The scattergram illustrates the application of different concentrations of RP (0.1, 1.0, 10.0, and 100 mg/mL) on the I_{SC} responses (d). Summary of the effects of different concentration of RP on the transepithelial resistance higher dosage of RP (1.0, 10.0, and 100.0 mg/mL) had no significant changes on colonic transepithelial resistance (e). The effect of different concentrations of RP (0.1, 1.0, 10.0, and 100.0 mg/mL) on the distal colon mucosa I_{SC}. Arrowheads indicate the time of RP addition (f). Unpaired t-test was used. Data represents mean ± S.E.M., $^{*}P < 0.05$, $^{**}P < 0.01$ when compared with control group alone.

hepatobiliary transporters may lead to cholestatic disorders [9]. The impaired secretory function of the biliary epithelium is considered responsible for reduced biliary fluidity and alkalinity for subsequent bile duct damage by cytotoxic compounds or infectious agents [18]. Some experiment results indicate that treatment with ursodeoxycholic acid [19], aimed at improving biliary secretion in terms of bile viscosity and bile acid composition, is currently the most useful therapeutic approach in cystic fibrosis-associated liver disease. Similarly, it was previously shown that tight junctional integrity and

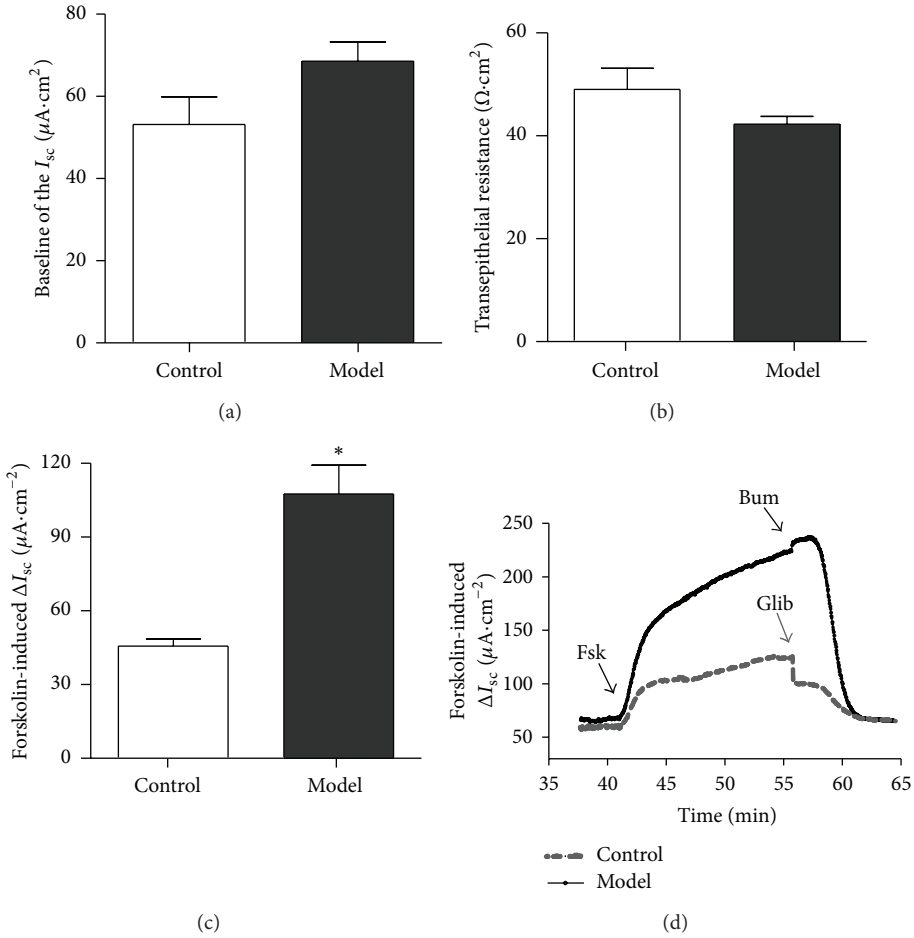

FIGURE 5: Effects of forskolin-induced I_{SC} responses in model rat. The baseline indicates the anion secretion of distal colon in control group and model group (a). The colonic transepithelial resistance has no significant attenuation in the model group (b). Summary of the effects of forskolin- (10 μmol/L, apical) induced ΔI_{SC} in model rats distal colon comparison of normal rats (c). Representative I_{SC} recording with arrows indicating the time for the apical application of glibenclamide (1 mm/L) or basolateral application of bumetanide (100 μmol/L), respectively, and pretreatment with forskolin (10 μmol/L, apical) (d). Unpaired t-test was used. Values are represented as mean ± SEM; $^*P < 0.05$.

transepithelial resistance are relatively resistant to ischemia in bile ducts [20]. The principal effect of HQS is to regulate the functional activities of qi, eliminate stagnation of qi, and enable qi to flow smoothly [15], while Cl^- channels have been shown to be important in the regulation of the hepatocyte volume in the presence of altered osmotic conditions; however, the role of this channel in bile flow has not been demonstrated [21].

Electrical parameters, which are monitored in the Ussing chambers, are widely accepted for monitoring the viability and integrity of tissue in the Ussing Chambers. I_{SC} reflects the ionic fluxes across the epithelium. In the present study, basal electrical parameters varied over a wide range. This variability has also been observed in previous studies on human tissue samples from jejunum and colon. Formation of bile requires the coordinated function of two epithelial cell types: hepatocytes that are responsible for secretion of the major osmolytes and biliary constituents and cholangiocytes that regulate the fluidity and alkalinity of bile through secretion of osmolytes such as Cl^- and HCO_3^- [22]. Studies in isolated cholangiocyte preparations have elucidated the basic transport mechanisms involved in constitutive and stimulated secretory activities in the biliary epithelium. Primary damage to the biliary epithelium is the cause of several chronic cholestatic disorders [23]. From a pathophysiological point of view, common to all cholangiopathies is the coexistence of cholangiocyte death and proliferation and various degrees of portal inflammation and fibrosis. Cholestasis dominates the clinical picture and may initiate or worsen the process. Alterations in biliary electrolyte transport can contribute to the pathogenesis of cholestasis in primary bile duct diseases. Cystic fibrosis-related liver disease represents an example of biliary cirrhosis secondary to a derangement of cholangiocyte ion transport [23].

Epithelial Cl^- channels play an important role in regulating and maintaining the normal physiological functions of the GI tract [24]. In this epithelium, Cl^- secretion is mediated by two steps, that is, the accumulation of cytosolic Cl^- by Na^+-K^+-$2Cl^-$ cotransporters in the basolateral membrane and then the exit of Cl^- through Cl^- channels in the apical

membrane [25, 26], namely, cystic fibrosis transmembrane regulator (CFTR). Since Cl^- secretion requires both the basolateral accumulation of Cl^- by Na^+-K^+-$2Cl^-$ cotransporter and an apical exit through Cl^- channels, it is not clear at this point which site is the primary target of HQS. Our results have demonstrated that HQS ethanol extract exerted a stimulatory effect on colon mucosa Cl^- secretion by predominantly activating apical cAMP-dependent Cl^- channels, namely, CFTR and possibly the Na^+-K^+-$2Cl^-$ cotransporter [23]. The ability of HQS to stimulate Cl^- secretion in the GI tract may contribute to its beneficial effects [27], such as smoothing bowl movement [28] and enhancing fluid clearance during host defense response [29]. It remains uncertain whether the stimulatory effect of HQS on Cl^- secretion is due to the collective effect of all the constituent herbal components or some active ingredients contained in the ethanol extract. The general objective of the experiments was to investigate the relation between electrical activity of the intestinal epithelium and capacity to transfer fluid and various solutes. This involved the measurement of the transfer of fluid and solutes by means of short-circuit current. Nevertheless, the current study has established a model for the quantitative measurement of HQS effect on the GI tract to further investigate its possible active ingredients. This effect can potentially improve GI disorders, such as constipation, a condition commonly associated with aged people [30]. The present study demonstrated the stimulation of HQS on the colonic epithelial Cl^- secretion. The supporting evidence for the stimulatory effect of HQS on Cl^- secretion includes the following: (1) HQS-induced I_{SC} increase was insensitive to the Na^+ channel blocker amiloride but sensitive to Cl^- channel blocker glibenclamide and removal of extracellular Cl^-; (2) the response was inhibited by the inhibitor of Na^+-K^+-$2Cl^-$ cotransporters, bumetanide. These confirmed the stimulation of Cl^- secretion by HQS. Furthermore, Cl^- secretion requires both the basolateral accumulation of Cl^- by Na^+-K^+-$2Cl^-$ cotransporter and apical exit through Cl^- channels [31]; (3) CFTR, but not α-ENaC, in liver, pancreas, and colon, was much higher in the HQS group than those in other groups. As shown in Figures 1, 2, and 4, RA could stimulate the Cl^- secretion with the enhancement of I_{SC}. Our hypothesis is supported by the observation of increased mRNA and protein of CFTR in colon and liver of the treatment group compared with controls. Using multiple methods, these data demonstrate that HQS is inherently altered in alimentary tract CFTR both in *in vitro* colon mucosa and *in vivo* models. These results suggest dominant pathway for regulation of biliary secretion to improve hepatic function [32].

In summary, the results of this study support that HQS and RA can upregulate the expression of CFTR in alimentary tract and evoke colonic ion secretion via CFTR activation, but not α-EnaC. Future studies are needed to better delineate this question.

Abbreviations

HQS: Huqi San
RA: Ramulus Visci alkali
RP: Polysaccharides of Ramulus Visci
CFTR: Cystic fibrosis transmembrane conductance regulator
α-ENaC: Epithelial Na^+ channel
I_{SC}: Short-circuit current
HBSS: Hank's balanced salt solution
Gli: Glibenclamide
Bum: Bumetanide
Ami: Amiloride.

Conflict of Interests

The authors declare that they have no conflict of interests.

Authors' Contribution

Xiao-Wei Xue and Jing-Dong Xu conducted the experiment. Zheng-Ming Shi and Wen Wang provided the reagents and materials. Xiao-Tong Yu performed Western blot. Min Zhang, Xue-Jiang Wang, and Jing-Dong Xu designed the experiment and modified the paper.

Acknowledgments

This research was supported by grants from the Program Foundation: National Science and Technology Major Project "Created a Major New Drug" "12-5" Program Foundation (no. 2009ZX09103-366); National Natural Science Foundation of China (nos. 81274173 and 81272757); Beijing Natural Science Foundation, China (nos. 7122017 and 7112010); Beijing Municipal Commission of Education (nos. KM201010025004 and KM201410025013); Beijing Institute for Brain Disorders (no. BIBDPXM2014_014226_000016); and Foundation Clinic Research Program of Capital Medical University (nos. 2013JL70 and 2013JL08).

References

[1] J. Eck, M. Langer, B. Möckel et al., "Cloning of the mistletoe lectin gene and characterization of the recombinant A-chain," *European Journal of Biochemistry*, vol. 264, no. 3, pp. 775–784, 1999.

[2] F. Ye, G. Z. Du, A. Q. Cui, and X. T. Lu, "Study on the mechanism of compound mistletoe fluidextract in relieving hypertension," *Journal of Traditional Chinese Medicine*, vol. 29, no. 4, pp. 291–295, 2009.

[3] F. B. Mojiminiyi, M. E. Owolabi, U. V. Igbokwe, and O. P. Ajagbonna, "The vasorelaxant effect of Viscum album leaf extract is mediated by calcium-dependent mechanism," *Nigerian Journal of Physiological Sciences*, vol. 23, no. 1-2, pp. 115–120, 2008.

[4] G. S. Kienle, A. Glockmann, M. Schink, and H. Kiene, "*Viscum album* L. extracts in breast and gynaecological cancers: a systematic review of clinical and preclinical research," *Journal of Experimental & Clinical Cancer Research*, vol. 28, no. 1, article 79, 2009.

[5] S.-Y. Lyu and W.-B. Park, "Mistletoe lectin modulates intestinal epithelial cell-derived cytokines and B cell IgA secretion," *Archives of Pharmacal Research*, vol. 32, no. 3, pp. 443–451, 2009.

[6] Y. Xiao, Y. Fan, B. Chen, Q. Zhang, and H. Zeng, "Polysaccharides from *Scurrula parasitica* L. inhibit sarcoma S180 growth in

mice," *Zhongguo Zhong Yao Za Zhi*, vol. 35, no. 3, pp. 381–384, 2010.

[7] X. Li, Z.-M. Shi, P. Feng, Z.-Y. Wen, and X.-J. Wang, "Effect of Qi-protecting powder (Huqi San) on expression of c-jun, c-fos and c-myc in diethylnitrosamine-mediated hepatocarcinogenesis," *World Journal of Gastroenterology*, vol. 13, no. 31, pp. 4192–4198, 2007.

[8] T. Pytrus, B. IwaNczak, R. Smigiel, J. Ryzko, P. Socha, and E. Iwanczak, "Ascites and extreme lipid abnormalities as initial symptoms of cystic fibrosis in a 5-years-old girl—case report," *Polski Merkuriusz Lekarski*, vol. 27, no. 161, pp. 388–392, 2009.

[9] N. Kanno, G. LeSage, S. Glaser, and G. Alpini, "Regulation of cholangiocyte bicarbonate secretion," *The American Journal of Physiology—Gastrointestinal and Liver Physiology*, vol. 281, no. 3, pp. G612–G625, 2001.

[10] M. J. C. Bijvelds, H. Jorna, H. J. Verkade et al., "Activation of CFTR by ASBT-mediated bile salt absorption," *American Journal of Physiology: Gastrointestinal and Liver Physiology*, vol. 289, no. 5, pp. G870–G879, 2005.

[11] H. Higuchi, S. F. Bronk, M. Taniai, A. Canbay, and G. J. Gores, "Cholestasis increases tumor necrosis factor-related apoptotis-inducing ligand (TRAIL)-R2/DR5 expression and sensitizes the liver to trail-mediated cytotoxicity," *Journal of Pharmacology and Experimental Therapeutics*, vol. 303, no. 2, pp. 461–467, 2002.

[12] L. D. Beilke, D. G. Besselsen, Q. Cheng, S. Kulkarni, A. I. Slitt, and N. J. Cherrington, "Minimal role of hepatic transporters in the hepatoprotection against LCA-induced intrahepatic cholestasis," *Toxicological Sciences*, vol. 102, no. 1, pp. 196–204, 2008.

[13] R. J. Sokol, M. Devereaux, R. Dahl, and E. Gumpricht, ""Let there be bile"—understanding hepatic injury in cholestasis," *Journal of Pediatric Gastroenterology & Nutrition*, vol. 43, no. 1, pp. S4–S9, 2006.

[14] A. Geier, M. Wagner, C. G. Dietrich, and M. Trauner, "Principles of hepatic organic anion transporter regulation during cholestasis, inflammation and liver regeneration," *Biochimica et Biophysica Acta*, vol. 1773, no. 3, pp. 283–308, 2007.

[15] Z. Wen, Z. Shi, P. Feng, X. Xue, K. Dong, and X. Wang, "Modulation of energy metabolic enzyme expression in N-nitrosodiethylamine- mediated hepatocarcinogenesis by Chinese herbs, Huqi San," *BioFactors*, vol. 34, no. 4, pp. 303–312, 2008.

[16] J. Wang and Y.-F. Zhu, "Extraction and content determination of polysaccharides in Viscum coloration," *Zhongguo Zhongyao Zazhi*, vol. 32, no. 22, pp. 2387–2390, 2007.

[17] A. Renzi, S. Demorrow, P. Onori et al., "Modulation of the biliary expression of arylalkylamine N-acetyltransferase alters the autocrine proliferative responses of cholangiocytes in rats," *Hepatology*, vol. 57, no. 3, pp. 1130–1141, 2013.

[18] M. S. Tanner and C. J. Taylor, "Liver disease in cystic fibrosis," *Journal of Pediatric Gastroenterology and Nutrition*, vol. 43, no. 4, supplement 1, pp. S49–S55, 2006.

[19] R. Fiorotto, C. Spirlì, L. Fabris, M. Cadamuro, L. Okolicsanyi, and M. Strazzabosco, "Ursodeoxycholic acid stimulates cholangiocyte fluid secretion in mice via CFTR-dependent ATP secretion," *Gastroenterology*, vol. 133, no. 5, pp. 1603–1613, 2007.

[20] R. B. Doctor, "Reorganization of cholangiocyte membrane domains represents an early event in rat liver ischemia," *Hepatology*, vol. 29, no. 5, pp. 1364–1374, 1999.

[21] M. Vore, Y. Liu, and L. Huang, "Cholestatic properties and hepatic transport of steroid glucuronides," *Drug Metabolism Reviews*, vol. 29, no. 1-2, pp. 183–203, 1997.

[22] P. S. Tietz, R. A. Marinelli, X.-M. Chen et al., "Agonist-induced coordinated trafficking of functionally related transport proteins for water and ions in cholangiocytes," *Journal of Biological Chemistry*, vol. 278, no. 22, pp. 20413–20419, 2003.

[23] M. Strazzabosco, "Transport systems in cholangiocytes: their role in bile formation and cholestasis," *Yale Journal of Biology and Medicine*, vol. 70, no. 4, pp. 427–434, 1997.

[24] L. L. Clarke and M. C. Harline, "Dual role of CFTR in cAMP-stimulated HCO_3^- secretion across murine duodenum," *The American Journal of Physiology—Gastrointestinal and Liver Physiology*, vol. 274, no. 4, pp. G718–G726, 1998.

[25] J. Loffing, B. D. Moyer, D. Reynolds, B. E. Shmukler, S. L. Alper, and B. A. Stanton, "Functional and molecular characterization of an anion exchanger in airway serous epithelial cells," *American Journal of Physiology: Cell Physiology*, vol. 279, no. 4, pp. C1016–C1023, 2000.

[26] I. M. Brzuszczak, J. Zhao, C. Bell et al., "Cyclic AMP-dependent anion secretion in human small and large intestine," *Journal of Gastroenterology and Hepatology*, vol. 11, no. 9, pp. 804–810, 1996.

[27] L. P. Sullivan, D. P. Wallace, and J. J. Grantham, "Epithelial transport in polycystic kidney disease," *Physiological Reviews*, vol. 78, no. 4, pp. 1165–1191, 1998.

[28] G. Wegrzyn, J. Kurlenda, A. Liberek et al., "Atypical microbial infections of digestive tract may contribute to diarrhea in mucopolysaccharidosis patients: a MPS I case study," *BMC Pediatrics*, vol. 5, article 9, 2005.

[29] Y. Yang, Y. Cheng, Q.-Q. Lian et al., "Contribution of CFTR to alveolar fluid clearance by lipoxin A4 via PI3K/Akt Pathway in LPS-induced acute lung injury," *Mediators of Inflammation*, vol. 2013, Article ID 862628, 10 pages, 2013.

[30] P. Gallagher and D. O'Mahony, "Constipation in old age," *Best Practice & Research: Clinical Gastroenterology*, vol. 23, no. 6, pp. 875–887, 2009.

[31] S. V. Koltsova, O. G. Luneva, J. L. Lavoie et al., "HCO_3^- dependent impact of Na^+,K^+,$2Cl^-$ cotransport in vascular smooth muscle excitation-contraction coupling," *Cellular Physiology and Biochemistry*, vol. 23, no. 4–6, pp. 407–414, 2009.

[32] M. Gray, C. O'Reilly, J. Winpenny, and B. Argent, "Anion interactions with CFTR and consequences for HCO_3^- transport in secretory epithelia," *Journal of Korean Medical Science*, vol. 15, pp. S12–S15, 2000.

Hindawi Publishing Corporation
Evidence-Based Complementary and Alternative Medicine
Volume 2015, Article ID 158361, 10 pages
http://dx.doi.org/10.1155/2015/158361

Research Article

Zuogui Jiangtang Jieyu Formulation Prevents Hyperglycaemia and Depressive-Like Behaviour in Rats by Reducing the Glucocorticoid Level in Plasma and Hippocampus

YuHong Wang,[1] Hui Yang,[2] Wei Li,[2] Pan Meng,[1] YuanShan Han,[1] Xiuli Zhang,[1] DeLiang Cao,[1] and Yuansheng Tan[1,2]

[1]*Hunan University of Chinese Medicine, No. 300, Bachelor Road, Changsha, Hunan 410208, China*
[2]*First Hospital of Hunan University of Chinese Medicine, Hunan, China*

Correspondence should be addressed to YuHong Wang; wyh_107@163.com and Yuansheng Tan; tys702@126.com

Received 30 September 2014; Revised 8 January 2015; Accepted 9 January 2015

Academic Editor: Kazuo Toda

Aim. To determine whether Zuogui Jiangtang Jieyu prescription (ZGJTJY) has hypoglycemic and antidepressant effects which are mediated by corticosterone through adjustment of 11β-hydroxysteroid dehydrogenase type 1 (11β-HSD1) and glucocorticoid (GR) levels. *Materials and Methods*. The diabetes-related depression rats were randomly divided into four groups: the model group, metformin (1.8 mg/kg) combined with fluoxetine (10.8 mg/kg) group, and ZGJTJY high and low dose groups. Four weeks after modeling, blood glucose, behavior, and cognitive function of depression were detected. The expressions of 11β-HSD1 and GR in hippocampus were measured by western blotting and immunohistochemical experiments. *Results*. We found that (1) the treatment with ZGJTJY (10.26 g/kg) increases the motor activities and improves cognition ability. (2) ZGJTJY (10.26 g/kg) significantly relieves the disorder in blood and the relative indexes. (3) ZGJTJY (10.26 g/kg) can reduce hippocampal corticosterone expression levels and further improve hippocampus pathological changes. (4) ZGJTJY increased the expression of GR accompanied with decreasing 11β-HSD1 in hippocampus. *Conclusions*. ZGJTJY inhibits the expression of 11β-HSD1 and increases GR in hippocampus and subsequently modulates blood glucose levels, and therefore it is potential property that ZGJTJY could be of benefit for the treatment of behavior and cognitive function of diabetes-related depression.

1. Introduction

Diabetes, a global chronic disease, affects almost 382 million people [1]. Although a stable blood glucose can reduce the risk of complications occurring and reduce the impact on patients' normal life [2], it is unfortunately that a well-controlled blood glucose is not the key point that helps to stop the central erosion which is caused by diabetes mellitus. This erosion not only worsens the physical condition and quality of life [3], but also is regarded as the major mortality predictor in patients [4, 5].

It is regretful to mention that the research of type 2 diabetes-related depression is usually assessed in terms of clinical aspect. In the past decade, the experimental research is barely related to the treatment of diabetes with depression, except a study presented in 2014 that evaluated the therapeutic effects of Zuogui Jiangtang Jieyu prescription on the aspects of glucose and behavioral activity [6]. Although this paper is important from an experimental standpoint, a further investigation seems to be necessary at present. Hippocampus is recognized as not only the first tissue that is affected by diabetes mellitus, but also the major part that related to depression [7, 8]. We hypothesized that the protective effect of Zuogui Jiangtang Jieyu prescription in hippocampus is an important contributor to its hypoglycemic and antidepression function.

It is common to improve the classical Chinese prescription through the combination with characters of modern disease to adapt the illness in China. Zuogui Jiangtang Jieyu Fang, a prescription based on the characteristics of diabetes-related depression, is a Chinese herbal prescription on the strength of Zuogui Wan which has a long history in reducing

blood glucose and it was listed in the Chinese authority "Pharmacopoeia" and developed by Jingyue Zhang during Ming dynasty. Zuogui Jiangtang Jieyu prescription including *Astragalus*, *Hypericum perforatum*, cooked *Rehmannia*, cornel, medlar, dodder, *Eucommia ulmoides*, *Salvia miltiorrhiza*, cortex moutan, and radix achyranthis bidentatae and added to turmeric and hyperforin perforatum which have hypoglycemic and antidepressant effects significantly. Various researches indicated that some Chinese medicine herbs including *Astragalus* polysaccharide, corni fructus, and *Achyranthes aspera* are efficiently improving the glucose homeostasis through a variety of pathways [9–11]. Zhang et al. [12] demonstrated that curcumin, a natural polyphenolic compound of *Curcuma longa*, had an antidepression effect by increasing brain-derived neurotrophic factor (BDNF) which is one of the underlying mechanisms in treatment. Tian et al. [13] have studied adhyperforin, a novel constituent of *Hypericum perforatum* L. The effects of inhibited uptake of serotonin, norepinephrine, dopamine, and displayed robust binding affinities for the serotonin and norepinephrine transporters provide the first evidence for *Hypericum perforatum* L.'s antidepressant-like activity.

Recent researches suggest that the biological bases of diabetes and depression are related to HPA axis disorder and then the disorder causes an abnormal increase of cortisol (in human) and corticosterone (CORT in rodents) [14–17], which are easily penetrated into the blood-brain barrier and damage the nerves. Previous studies found that there are two essential proteins, 11β-HSD1 and GR, expressed in hippocampus and closely related to CORT. The functions of these two proteins include CORT activation and stimulation of HPA axis negative feedback activity, and they are activated by binding to CORT, respectively [14, 18, 19]. Thus, a partial increase of CORT and damaged hippocampal neuron usually attribute to the disordered expression of 11β-HSD1 and GR [19, 20]. In addition, hippocampus is a key target organ that regulates emotion and cognitive function, which is essential for occurrence of depression [8]. Therefore, we believe that hyperactivity of HPA axis in diabetes contributes to an abnormal high level of CORT and it has been overtransferred to hippocampus. Moreover, a deregulated 11β-HSD1 leads to the CORT hyperactivity. Meanwhile, decreased expression of GR leads to a situation that CORT fails to cause negative feedback and regulate the HPA axis disorders. And it causes CORT accumulation in hippocampus, which injures neurons and induces diabetes-related depression.

In order to test the above hypothesis, we intend to verify ZGJTJY on the treatment of diabetes-related depression from the aspects of ethology and hematology. And then the expression of 11β-HSD1 and GR in the hippocampus was detected through immunohistochemistry and western blotting, while determining the content of CORT in the hippocampus by ELISA. Finally, hippocampal morphology was observed through HE stain. In addition, the purpose of this study is to determine the reasons of the abnormal increase of CORT in hippocampus in rats with diabetes-related depression, as well as neuronal damage, and verify the therapeutic effect of ZGJTJY.

2. Materials and Methods

2.1. Drugs and Reagent. The raw material of ZGJTJY was purchased and concentrated to oral liquid (1.14 g/mL) in the First Hospital of Hunan University of Chinese Medicine. The prescription consists of 18 g *Astragalus*, 3 g *Hypericum perforatum*, 9 g turmeric, 15 g cooked *Rehmannia*, 12 g cornel, 12 g medlar, 9 g dodder, 9 g *Eucommia ulmoides*, 12 g *Salvia miltiorrhiza*, 6 g cortex moutan, and 9 g radix achyranthis bidentatae. Metformin hydrochloride tablets (0.25 g) and fluoxetine hydrochloride capsules (20 mg) were purchased from Hunan Xiangya Pharmaceutical and Patheon, France, respectively. High fat diet consists of 10% cholesterol, 0.2% propylthiouracil, 20% lard oil, 20% Tween 80, and 20% propylene glycol and then is added to still water to 100 mL.

2.2. Animal Materials. 75 male SD rats weighing 180–200 g were obtained from Hunan Province Slack Scene of Laboratory Animal Company and kept in SPF Laboratory Animal Center in Hunan Chinese Medicine University. The experiment has been ethically acceptable and where relevant conforms to the national guidelines for animal usage in the research.

2.3. Rats Molding. 10 mL/kg high fat diet was given by intragastric injection for 14 days except control group. After that, abrosia with water supply was performed for 24 h before 38 mg/kg streptozotocin (Sigma-Aldrich Co., USA) injection on the tail. Control group was infused with 2 mL/kg 0.1 mol/L citrate buffer instead. After 72 h, fast blood glucose was detected to screen the diabetes rats. And then, the screened rats were exposed to 28 days of unpredictable chronic mild stress (UCMS) including (I) 4°C ice water bath (5 min), (II) 45°C hot stimulus (5 min), (III) pour cage 45°C (24 h), (IV) noise (8 h), (V) day and night upside down (24 h), (VI) damp bedding (200 mL/cage, 24 h), and (VII) clip tail (1 min). The stress was performed once per day randomly.

After molding, diabetes-related depression rats were divided into five groups consisting of vehicle, DMGB/F (treated with 1.8 mg/kg DMGB and 10.8 mg/kg fluoxetine), ZGJTJY/H, and ZGJTJY/L (treated with gradient concentration of Zuogui Jiangtang Jieyu by 2.28 g/m and 0.57 g/mL, resp.). In addition, control group was given equal volume of normal saline instead.

2.4. Open Field Test. Open field test was carried out in an 80 cm × 80 cm × 40 cm open field chamber. The floor of the chamber was divided into 25 equilateral squares. The horizontal movement (four feet within a square counted as one score) and vertical movement (two front paws to vacate counted as one score) were counted within 3 min after 1 min adaptation. The test was taken once every week.

2.5. Morris Water Maze Test. Spatial learning and memory were tested by Morris water maze. The Morris water maze was filled with water and divided into four quadrants. There was an underwater platform placed in one of the quadrants. After that, in the place navigation test, the time for rats to locate

the underwater platform was regarded as evasive latency (EL) and it lasted for four days. And space exploration was carried out on the 5th day, the platform was removed, and time for rats to locate the platform quadrant was recorded as space exploration time (SET).

2.6. Surgery. Rats were anesthetized with 4 mL/kg 10% chloral hydrate and mounted on the operating desk after abrosia for 24 h. The heart was exposed and then 150–200 mL 0.01 M PBS was implanted quickly from aorta on the apex cordis, while scissoring the auricula dextra and implanting 150–200 mL 4% paraformaldehyde through aorta slowly until clear fluid came out from auricula dextra. After that, they were beheaded in brain and the hippocampuswas isolated on the cryostage, and then it was fixed in 4% paraformaldehyde for 6–8 h and kept in ice saline (2.5 mL/g) after infusion and limbs stiffness.

2.7. Blood Test. The blood in serum tubes was centrifuged and the levels of fasting plasma glucose (FPG), fasting insulin (FINS), glycated hemoglobin (HbAlc), total cholesterol (TC), triglyceride (TG), high-density lipoprotein-cholesterol (HDL-C), and low-density lipoprotein-cholesterol (LDL-C) were tested, respectively, as previous study described [10]. The homeostasis model assessment of insulin resistance was calculated as follows:

$$\begin{aligned} (\text{HOMA-IR}) &= \frac{\text{FPG} \times \text{FINS}}{22.5} \\ (\text{ISI}) &= \ln\left[\frac{1}{\text{FPG} \times \text{FINS}}\right] \\ (\text{HOMA-B}) &= 20 \times \frac{\text{FINS}}{\text{FPG} - 3.5}. \end{aligned} \tag{1}$$

2.8. ELISA Experiments. One side of hippocampus was sampled for enzyme-linked immunosorbent assay. The tissue was ground in ice saline by refiner before it was centrifuged for 10000 r/min 10 min. Supernatant was collected in −80°C until the content of CORT was measured by ELISA kit (R&D Systems, USA) following the manufacturer's protocol. Samples were added to Microelisa Stripplate and incubated in 37°C for 30 min before 50 μL HRP-conjugate reagent was added, which followed by 30 min incubation at 37°C. And then, chromogen solution and stop solution were added before the optical density value was measured at 450 nm. In the meantime, the standard curve was made. Moreover, the level of CORT in blood plasma was measured by CORT ELISA kit (R&D Systems, USA).

2.9. Histopathology Experiment. The brain was removed surgically and fixed in 4% formalin before the tissue was dehydrated, paraffin-embedded, and sliced into section. After that, HE stain was performed and then observed under light microscope.

2.10. Western Blotting Experiments. The other side of hippocampus was applied for western blotting (Western Blotting Kit, Beyotime Institute of Biotechnology, China). The tissue was homogenized in cell lysis buffer (NP-40 lysis buffer) with protease inhibitor and it was ground by refiner before supernatant was kept in −20°C after centrifuge. The protein was electrophoretically resolved on 10% SDS-polyacrylamide gels and then transferred to nitrocellulose membranes at 100 mA for 2.5 h. After that, the membranes were blocked in skimmed milk for 1 h at room temperature and overnight at 4°C in anti-11β-HSD1 (1 : 1000; Cell Signaling Technology, USA), anti-GR (1 : 1000; Cell Signaling Technology, USA), and anti-β-actin (1 : 800; Cell Signaling Technology, USA), receptively. Then the membrane was incubated with HRP antibody (Boster Co., Wuhan, China) at dilution of 1 : 1000. Finally, the membranes were observed by the use of enhanced chemiluminescence kit (ECL, Amersham).

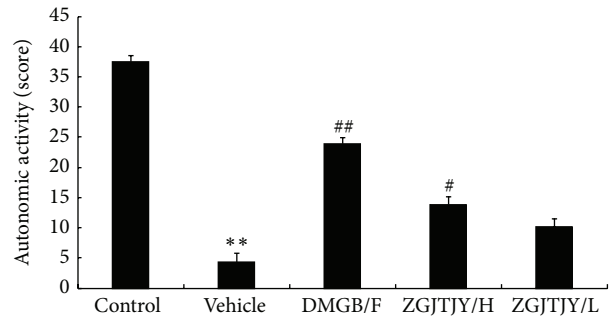

Figure 1: ZGJTJY increases the activity of rats with diabetes-related depression. The autonomic activity was recorded by counting horizontal movement and vertical movement in open field test. $^{*}P < 0.05$ compared with control, $^{**}P < 0.01$ compared with control; $^{\#}P < 0.05$ compared with vehicle; $^{\#\#}P < 0.01$ compared with vehicle.

2.11. Immunohistochemical Experiments. The brain was performed for immunohistochemical experiment. After the tissues were dehydrated, embedded in paraffin, and sliced into sections, the slides were incubated in 3% hydrogen peroxide for 10 min and heated in 0.01 M citrate buffer. After that, they were incubated with the goat serum sealing fluid for 20 min and covered with 50 μL anti-rabbit, which followed by 4°C overnight. Then, the sections were rewarmed at 37°C for 45 min and incubated with SABC for 30 min, which followed by DAB coloration under the microscope and the sections were redyed with hematoxylin (2 min). Finally, dehydration, hyalinization, and mounting were performed and the sections were observed under high magnification (×400) with picture taken.

2.12. Statistics. All the data were based on SPSS16.0 and analyzed by one-way analysis of variance (ANOVA), t-test with two-side test. A level of $P < 0.05$ was set as statistically significant.

3. Results

3.1. ZGJTJY Helps to Increase the State of Behavioral Activity. The mobility of different groups is presented in Figure 1.

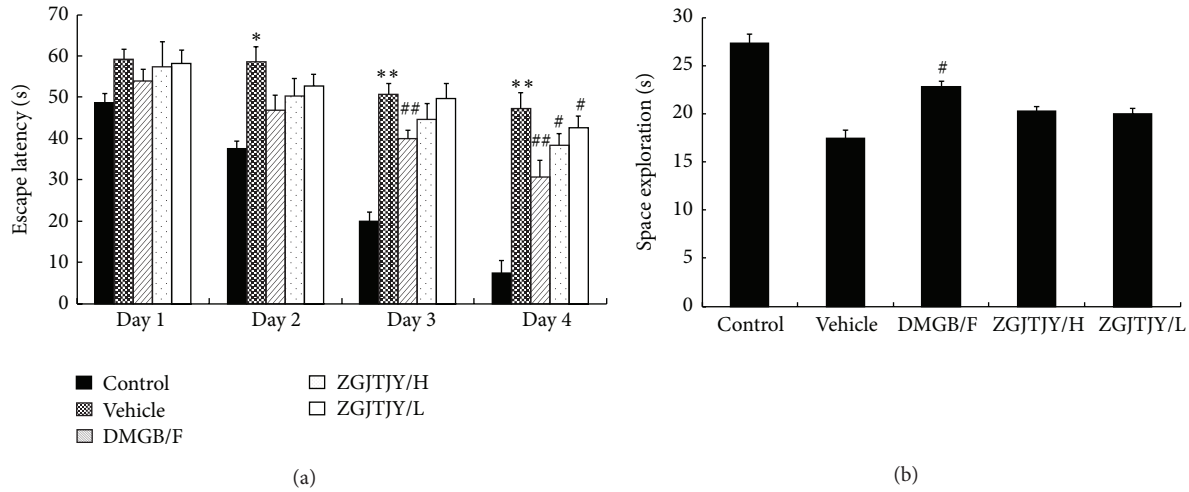

Figure 2: Capability of learning and memory was enhanced after treatment with ZGJTJY. The capabilities of learning were measured by (a) place navigation and the ability of memory was tested by (b) space exploration. $^{*}P < 0.05$ compared with control, $^{**}P < 0.01$ compared with control; $^{\#}P < 0.05$ compared with vehicle; $^{\#\#}P < 0.01$ compared with vehicle.

The activity in vehicle group was obviously lower than that in control group. However, there was a significant increase of mobility in DMGB/F group from 4.38 ± 1.36 to 23.94 ± 1.02. Moreover, the treatment of ZGJTJY witnessed a positive relationship between its dosages where the activities in ZGJTJY/H group rise from 23.94 ± 1.02 to 13.77 ± 1.29, while from 4.38 ± 1.36 to 10.21 ± 0.98 in ZGJTJY/L group.

3.2. Capability of Learning and Memory Was Increased by Treatment of ZGJTJY. The capability of learning and memory was presented in Figure 2.

During the 4 days of place navigation, the escape latency (EL) was higher in vehicle when compared with control group, while it has witnessed a fluctuated decrease in DMGB/F and ZGJTJY groups when compared with vehicle group, especially the 4th day on which the treatment effects were significant where EL was declining from 47.22 S ± 3.86 to 38.32 S ± 2.81 in ZGJTJY/H group. Moreover, there was a positive correlation in the dosage of ZGJTJY.

The space exploration demonstrated that the time spent in target quadrant was shorter in vehicle when compared with control group, while it was increased in DMGB/F and ZGJTJY groups. Noticeably, the treatment effect in high dose of ZGJTJY was more efficient than that in the low dose.

3.3. The Disorder in Blood Glucose and the Relative Indexes Was Relieved by ZGJTJY. The relative indexes in glucose, blood lipid, and insulin are presented in Figure 3.

The levels of blood glucose (Figure 3(a)) and HbAlc (Figure 3(b)) were significantly higher in vehicle group accompanied with severe dysfunction of HOMA-IR (Figure 3(c)) and HOMA-B (Figure 3(d)), and abnormal blood lipid indexes (lipid triad, Figure 3(e)) were performed when compared with control group as well. However, there was a significant treatment influence in DMGB/F and ZGJTJY groups where the levels of blood glucose (Figure 3(a)) and HbAlc (Figure 3(b)) were decreased, the serious HOMA-IR (Figure 3(c)) was relieved, and HOMA-B (Figure 3(d)) was slightly improved. Moreover, the lipid triad has witnessed a back to normal tendency when TC, TG, and LDL-C (Figure 3(e)) were increased and HDL-C has gone down. And the disorder in insulin sensitivity index (Figure 3(f)) was relieved by DMGB/F and ZGJTJY. Moreover, the level of CORT (Figure 3(g)) in blood plasma was obviously high in vehicle, while it was decreased after treatment with DMGB/F and ZGJTJY. Noticeably, there was a positive relationship occurring in ZGJTJY groups where the therapeutic effects were obvious in the high dose.

3.4. ZGJTJY Helps to Recover the Damages in Hippocampus Which Are Insulted by Diabetes-Related Depression. The alternations in hippocampus are present in Figure 4.

In control group, normal hippocampus cones were observed, while dark cell plasma and vacuolar degeneration occurred in vehicle. The recovery of hippocampus in DMGB/F and ZGJTJY groups was obvious. Compared with low level of ZGJTJY, the vacuolar degeneration and cell swelling were significantly decreased in the high level. Thus, there is positive relationship between the dosage of ZGJTJY and cytoprotection.

3.5. ZGJTJY Leads to a Decrease of CORT in Hippocampus. The content of CORT in hippocampus is presented in Figure 5.

The expression of CORT in vehicle (Figure 5) was obviously high when compared with the control. However, the expression was decreased significantly in DMGB/F and ZGJTJY/H groups, while the treatment effect in low level of ZGJTJY was slight. The result indicated that there is a positive correlated relationship between the decline of CORT and the dosage of ZGJTJY.

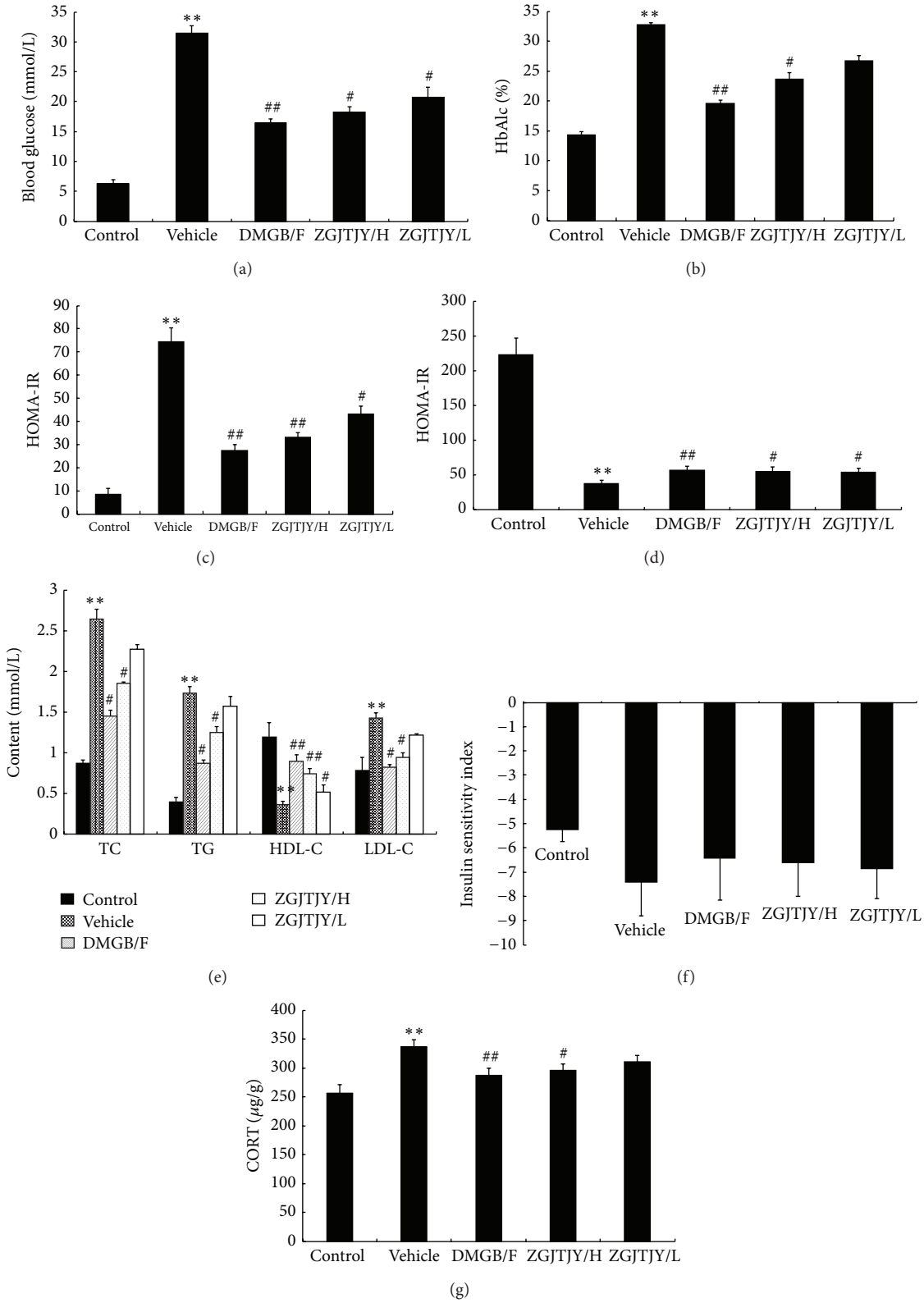

Figure 3: The disorder in blood glucose and the relative indexes in blood was relieved by DMGB/F and ZGJTJY and there was a positive relationship between the dosages of ZGJTJY. The levels of the relative indexes in blood were tested by specific kits, respectively, except the level of CORT which was measured by ELISA. $^{*}P < 0.05$ compared with control, $^{**}P < 0.01$ compared with control; $^{\#}P < 0.05$ compared with vehicle; $^{\#\#}P < 0.01$ compared with vehicle.

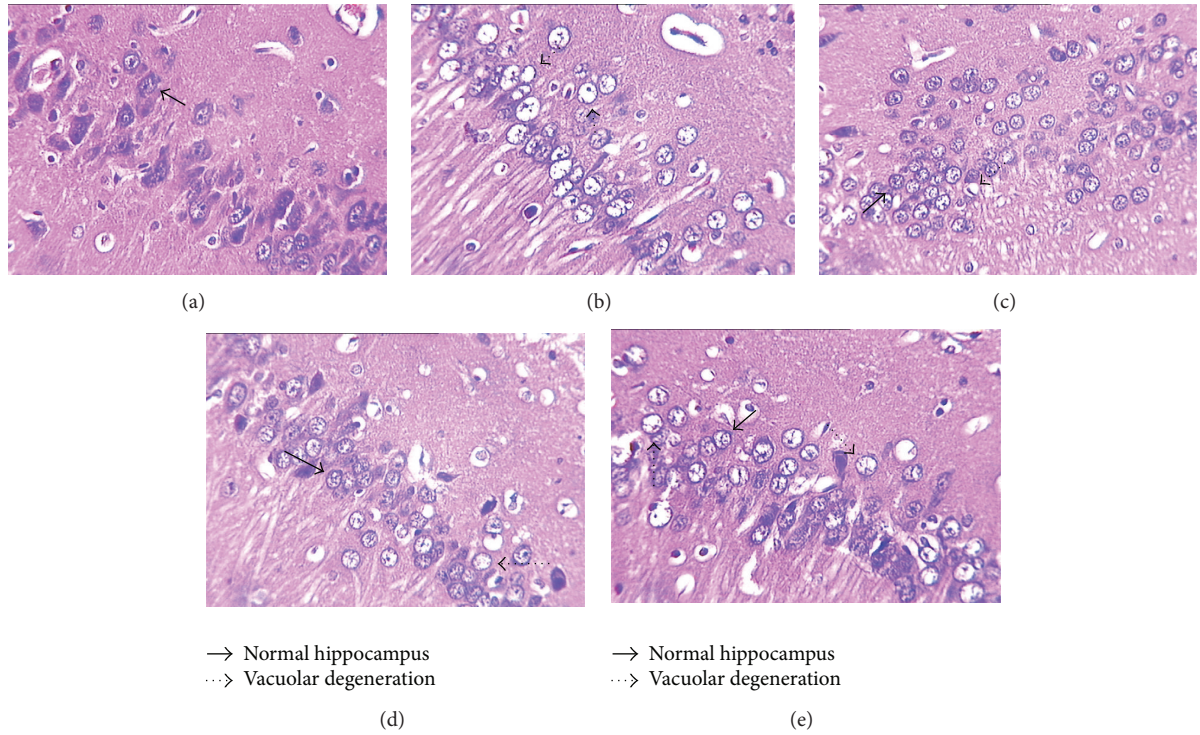

Figure 4: Cytoprotection was obvious in ZGJTJY group where the normal hippocampus appeared to increase. The morphology changes in hippocampus were observed by HE stain. (a) Control; (b) vehicle; (c) DMGB/F; (d) ZGJTJY/H; (e) ZGJTJY/L.

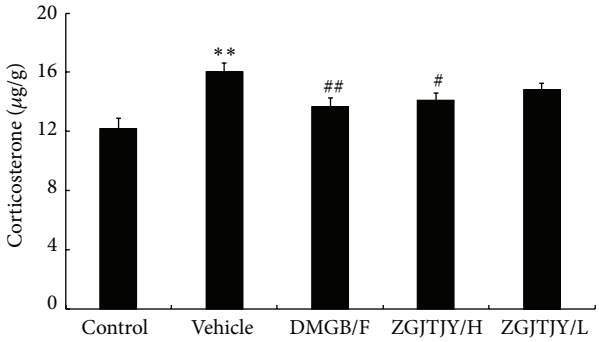

Figure 5: The expression of CORT was inhibited by treatment of ZGJTJY. The CORT expression in hippocampus was measured by ELISA kit following the manufacturer's protocol. $^{*}P < 0.05$ compared with control; $^{**}P < 0.01$ compared with control; $^{\#}P < 0.05$ compared with vehicle, $^{\#\#}P < 0.01$ compared with vehicle; $n = 8$, $\overline{x} \pm s$.

3.6. Downregulation of 11β-HSD1 Was Caused by ZGJTJY in Hippocampus. The protein level of 11β-HSD1 was measured by immunohistochemistry (Figures 6(a) and 6(b)) and western blotting (Figures 6(c) and 6(d)). The result (Figure 6(b)) shows that 11β-HSD1-like positive immunoreactivity neuron has become stronger in vehicle group when compared with control. Thus the luminous density of 11β-HSD1 positive cell was significantly higher in group vehicle (Figure 6(a)). However, there is an obvious decline of 11β-HSD1 in DMGB/F ($P < 0.05$, Figure 6(a)) and ZGJTJY groups. Furthermore, a positive correlation was found between the decrease of 11β-HSD1 and the dose of ZGJTJY where the high dose of ZGJTJY witnessed a dramatic decrease of 11β-HSD1 (Figure 6(a)). As shown in Figures 6(c) and 6(d), the western blotting test indicates that the changes between different groups nearly shared the same tendency with immunohistochemistry.

3.7. ZGJTJY Leads to an Increase of GR in Hippocampus. The protein level of GR in hippocampus was measured by immunohistochemistry and western blotting. The results indicate that the vehicle (Figure 7(b)) group witnessed a significant decrease in GR-like positive immunoreactivity neuron when compared with control group ($P < 0.05$) that means the expression of GR was restrained by diabetes-related depression. The content of GR was increased in DMGB/F and ZGJTJY groups. Noticeably, there is a positive correlation between the upregulation of GR and the dose of ZGJTJY. A remarkable increase was seen in the high dose of ZGJTJY (Figure 7(a)). When it comes to western blotting (Figures 7(c) and 7(d)), the trend of GR was almost the same as the result of immunohistochemistry where there is a positive relationship between the increase of GR and the dosage of ZGJTJY as well.

4. Discussion

In this study, we found that ZGJTJY can effectively lower blood glucose level in diabetes-related depression rats (Figure 3) and improve their depressive behavior (Figures 1 and 2). CORT can not only regulate blood glucose variation,

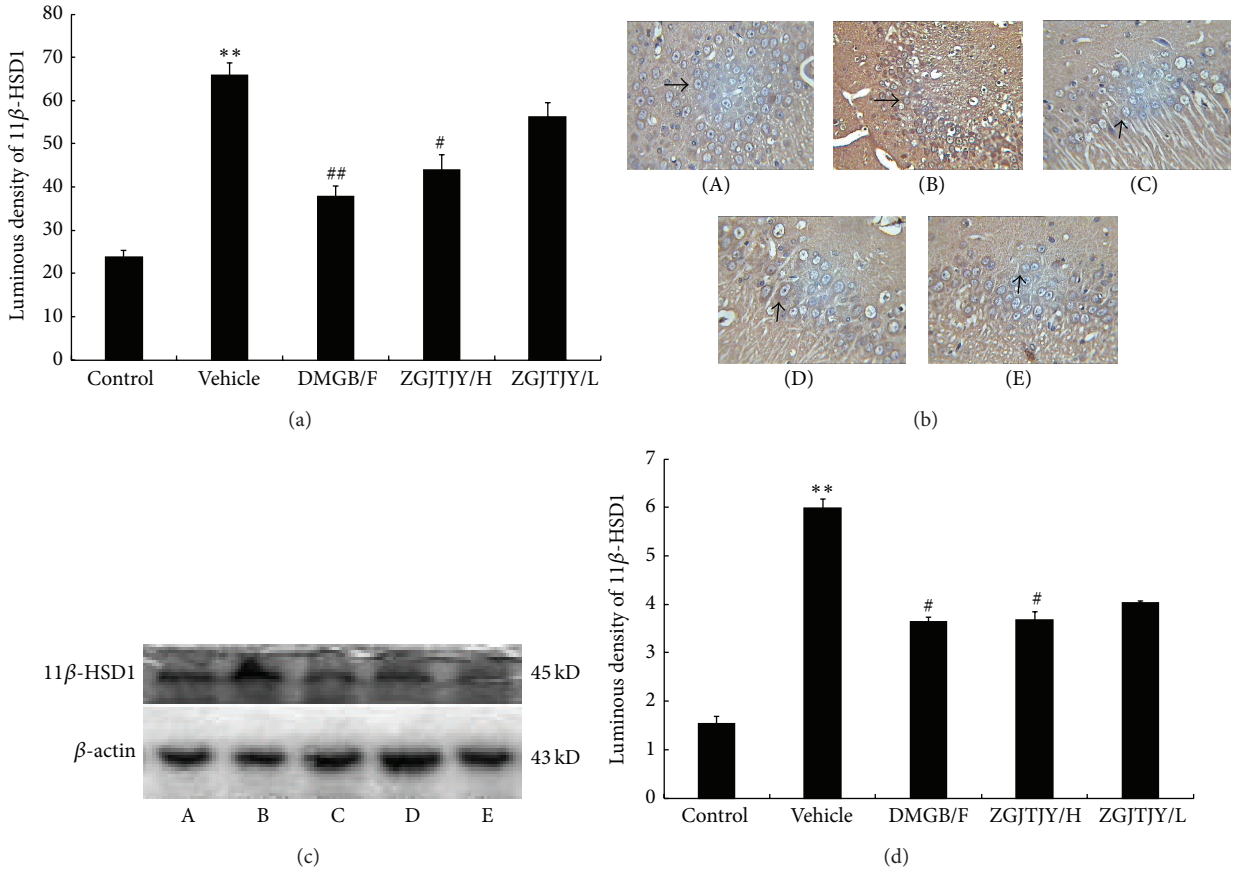

FIGURE 6: Inhibition of 11β-HSD1 was caused by ZGJTJY. The protein level was measured by immunohistochemistry (a, b) and western blotting (c, d). $^{*}P < 0.05$ compared with control, $^{**}P < 0.01$ compared with control; $^{\#}P < 0.05$ compared with vehicle; $^{\#\#}P < 0.01$ compared with vehicle; $n = 8$, $\overline{x} \pm s$. (A) Control group; (B) vehicle; (C) DMGB/F; (D) ZGJTJY/H; (E) ZGJTJY/L.

but also damage the hippocampus and lead to depressive behavior because of its high concentration. Our study found that the disordered blood glucose and behavior attributed to the abnormal increase of CORT in diabetes-related depression rats (Figure 3). Although a lot of studies have examined the relationship between CORT and blood glucose, few have observed the association between CORT and hippocampus. In this study, we speculated that the deregulated expression of 11β-HSD1 in hippocampus (Figure 6) can lead to increased CORT activity, while a decreased expression of glucocorticoid receptor (Figure 7) leads to a situation that CORT is unable to correct the HPA axis disorders through negative feedback and then causes CORT accumulation and damages the neurons. Those might be the important reasons to explain the hippocampal damage in diabetes-related depression. ZGJTJY could relieve hippocampal damage by improving CORT regulation through inhibiting the expression of 11β-HSD1 and increasing GR.

The methods of establishing the diabetes-related depression in the study consist of high fat diet, STZ injection, and 28 days of unpredictable chronic mild stress, which are reliable and stable. The chronic mild stress utilized in this research not only decreases the stimulus intensity, but better simulates the living pressure during the daily life as well. Consequently, physiological changes may occur in the rats after a series of stimulations; moreover, the randomly applied chronic mild stress made rats difficult to adopt, which is conducive to establishing the model. Although there are some other methods to establish a depression model, most of those approaches are inappropriate to build a diabetes-related depression. For instance, brain injury models including olfactory bulb resection model contribute to critical damages which are difficult for diabetes rats to bear. Force swim and tail suspension test with a short time model maintenance are instable in this study, which made the results not credible.

An increased HPA axis activity was found in diabetes, which then leads to secretion of GC in adrenal glands with an increase of CORT in blood circulation and local brain tissue. The elevated cortisol levels in the hippocampal neurons cause neurotoxicity and affect the cognitive function, which then results in depression. GC relied on the activation of 11β-HSD1 to pose effects on target tissues. 11β-HSD1, a NADP(H)-dependent with a low affinity dehydrogenation/oxidoreductase enzyme, was a stimulator that transforms the nonactive GC, namely, cortisone (human) and 11β-dehydrogenase corticosterone (rodents), into active cortisol (human) and corticosterone (rodents), respectively, and then it amplifies the local effect of GC [21, 22]. The

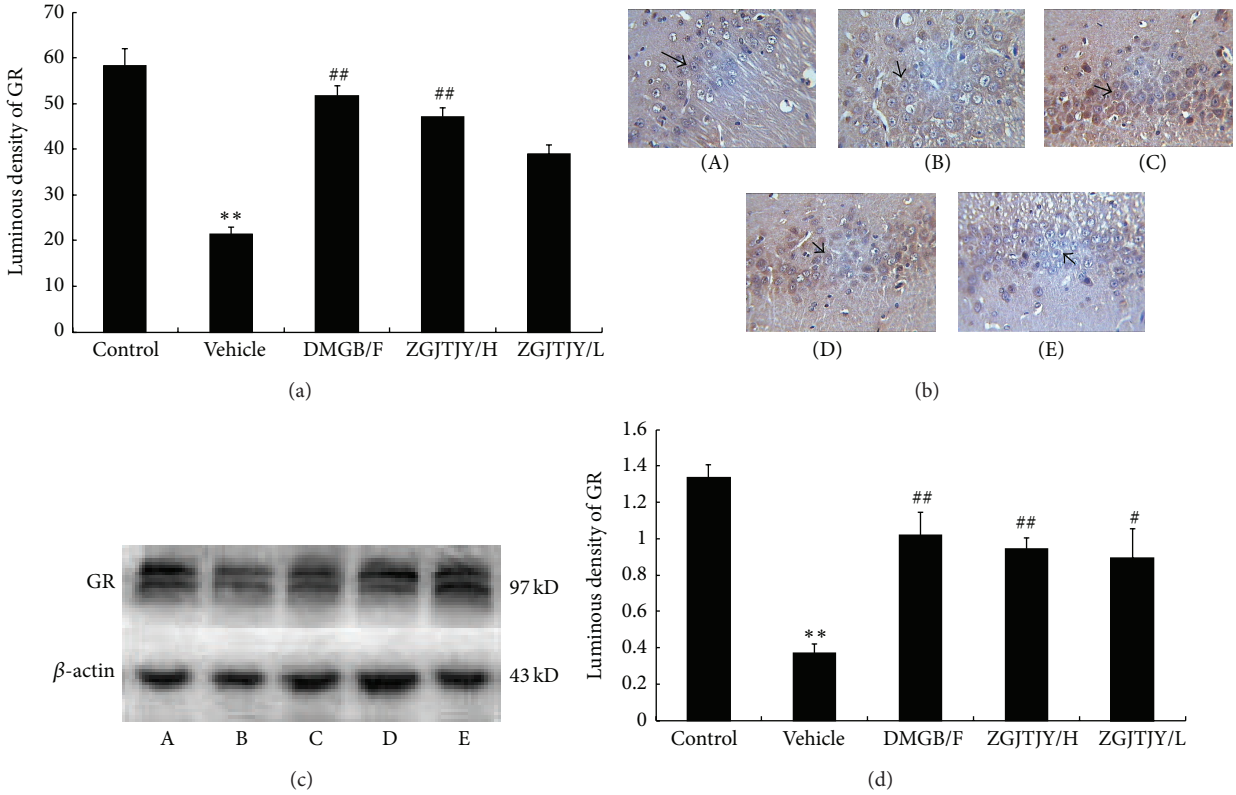

FIGURE 7: The expression of GR was restrained by ZGJTJY. The protein level of GR was measured by immunohistochemistry (a, b) and western blotting (c, d). $^{*}P < 0.05$ versus control, $^{**}P < 0.01$ versus control; $^{\#}P < 0.05$ versus vehicle, $^{\#\#}P < 0.01$ versus vehicle; $n = 8$, $\overline{x} \pm s$. (A) Control group; (B) vehicle; (C) DMGB/F; (D) ZGJTJY/H; (E) ZGJTJY/L.

enzyme is highly expressed in hippocampus which located in paraventricular nucleus of hypothalamus and cerebral cortex in the central nervous system. 11β-HSD1 expression was increased in diabetic rat [**?**]. Inactivated 11β-dehydrogenase corticosterone was circulated to hippocampus and stimulated by high expression of 11β-HSD1 into corticosterone, further elevating corticosterone levels in local brain [**? ?**], which then leads to the neuron damage and necrosis of hippocampus and reduces the number of neurons. Therefore spatial learning and memory declined. And eventually diabetes-related depression occurred. However, after being regulated by ZGJTJY, the expression of CORT was increased and 11β-HSD1 was inhibited in which the effects were related to the dosage of the prescription.

Hippocampus has a wealth of glucocorticoid receptor (GR) and mineralocorticoid receptor (MR). The affinity between GC and MR is almost saturated (>80%) which was ten times as much as it is between GC and GR; the affinity fluctuated from 10% to 90% randomly. Thus, the concentration of GC was the major element that affects the affinity with GR [18, 23]. Previous study found that the concentration of GC in diabetic rats was increased, but the expression of GR was reduced. And those may be due to the decreased number of neurons which are then attributed to the partially increased active glucocorticoids and hippocampal damage [24]. Elevated hippocampal GC combined with GR leads to negative feedback inhibition of the HPA axis under physiological condition [25, 26]. Reduced GR in the hippocampus decreases the inhibition of the HPA axis [27], which then stops the HPA axis circadian rhythm as a result, while stress responses continued, as well as increased secretion of GC level [28]. On one hand, increased GC circulated to the hippocampus, and then it was amplified by 11β-HSD1 to further increase the level of corticosterone, which eventually causes vicious cycle and aggravates hippocampal damage [29]. On the other hand, the upregulation of blood corticosterone contributes to a high level of blood glucose in that it was the counterregulatory factor of insulin to prevent insulin secretion. High level of blood glucose, followed by neuronal apoptosis, deteriorates hippocampal damage and leads to depressive disorder. In this study, the expression of GR was significantly reduced in diabetes mellitus with depression, while it was back to normal after treatment with ZGJTJY.

Currently, diabetes-related depression is still at clinical research stage, and there is no specific drug which is usually with negative side effects. However, traditional Chinese medicine is usually based on the overall aspect and it is extraordinarily efficient in complication therapy. ZGJTJY was based on the strength of Zuogui Wan from Jingyue Zhang, and it has shown better hypoglycemic and antidepressant effects. By this experiment studying, ZGJTJY can significantly improve blood glucose and depressive behavior in rats with diabetes-related depression, as well as reducing

corticosterone levels, and inhibit the expression of 11β-HSD1 in the hippocampus and increase the expression of GR. In order to have a further insight of ZGJTJY, our group intends to perform further study on the effect of ZGJTJY on cortisol regulation of diabetes-related depression rats in hippocampus.

Conflict of Interests

The authors declare that there is no conflict of interests regarding the publication of this paper.

Acknowledgments

The project was supported by the National Natural Science Fund Project (81373578, 81403379), the Natural Science Fund Project in Hunan Province (13JJ5030), and Innovation Platform Open-End Fund in Colleges and Universities of Hunan Province (13K074).

References

[1] International Diabetes Federation, (1950–2014), 2014, http://www.idf.org/about-diabetes.

[2] T. Wu, G. Xie, Y. Ni et al., "Serum metabolite signatures of type 2 diabetes mellitus complications," *Journal of Proteome Research*. In press.

[3] D. Selvarajah and S. Tesfaye, "Central nevous system involvement in diabetes mellitus," *Current Diabetes Reports*, vol. 6, no. 6, pp. 431–438, 2006.

[4] N. Sartorius and L. Cimino, "The co-occurrence of diabetes and depression: an example of the worldwide epidemic of comorbidity of mental and physical illness," *Annals of the Academy of Medicine Singapore*, vol. 41, no. 10, pp. 430–431, 2012.

[5] L. E. Egede and C. Ellis, "Diabetes and depression: global perspectives," *Diabetes Research and Clinical Practice*, vol. 87, no. 3, pp. 302–312, 2010.

[6] Y.-H. Wang, L.-T. Yin, H. Yang, X.-L. Li, and K.-G. Wu, "Hypoglycemic and anti-depressant effects of Zuogui Jiangtang Jieyu formulation in a model of unpredictable chronic mild stress in rats with diabetes mellitus," *Experimental and Therapeutic Medicine*, vol. 8, no. 1, pp. 281–285, 2014.

[7] S. M. Gold, I. Dziobek, V. Sweat et al., "Hippocampal damage and memory impairments as possible early brain complications of type 2 diabetes," *Diabetologia*, vol. 50, no. 4, pp. 711–719, 2007.

[8] Y. I. Sheline, "Depression and the hippocampus: cause or effect?," *Biological Psychiatry*, vol. 70, no. 4, pp. 308–309, 2011.

[9] K. Agyemang, L. Han, E. Liu, Y. Zhang, T. Wang, and X. Gao, "Recent advances in astragalus membranaceus anti-diabetic research: pharmacological effects of its phytochemical constituents," *Evidence-Based Complementary and Alternative Medicine*, vol. 2013, Article ID 654643, 9 pages, 2013.

[10] C. H. Park, J. S. Noh, T. Tanaka, S. S. Roh, J. C. Lee, and T. Yokozawa, "Polyphenol isolated from Corni Fructus, 7-*O*-galloyl-d-sedoheptulose, modulates advanced glycation endproduct-related pathway in type 2 diabetic *db*/*db* mice," *Archives of Pharmacal Research*, 2014.

[11] F. Z. Talukder, K. A. Khan, R. Uddin, N. Jahan, and M. A. Alam, "In vitro free radical scavenging and anti-hyperglycemic activities of *Achyranthes aspera* extract in alloxan-induced diabetic mice," *Drug Discoveries & Therapeutics*, vol. 6, no. 6, pp. 298–305, 2012.

[12] L. Zhang, J. Luo, M. Zhang, W. Yao, X. Ma, and S. Y. Yu, "Effects of curcumin on chronic, unpredictable, mild, stress-induced depressive-like behaviour and structural plasticity in the lateral amygdala of rats," *International Journal of Neuropsychopharmacology*, vol. 17, no. 5, pp. 793–806, 2014.

[13] J. Tian, F. Zhang, J. Cheng, S. Guo, P. Liu, and H. Wang, "Antidepressant-like activity of adhyperforin, a novel constituent of *Hypericum perforatum* L," *Scientific Report*, vol. 9, no. 4, article 5632, 2014.

[14] L. An, Y.-Z. Zhang, X.-M. Liu et al., "Total flavonoids extracted from xiaobuxin-tang on the hyperactivity of hypothalamic-pituitary-adrenal axis in chronically stressed rats," *Evidence-Based Complementary and Alternative Medicine*, vol. 2011, Article ID 367619, 7 pages, 2011.

[15] B. Budziszewska, "Effect of antidepressant drugs on the hypothalamic-pituitary-adrenal axis activity and glucocorticoid receptor function," *Polish Journal of Pharmacology*, vol. 54, no. 4, pp. 343–349, 2002.

[16] V. Butterweck, M. Hegger, and H. Winterhoff, "Flavonoids of St. John's Wort reduce HPA axis function in the rat," *Planta Medica*, vol. 70, no. 10, pp. 1008–1011, 2004.

[17] P. Willner, "Chronic Mild Stress (CMS) revisited: consistency and behavioural-neurobiological concordance in the effects of CMS," *Neuropsychobiology*, vol. 52, no. 2, pp. 90–110, 2005.

[18] R. Thieringer and A. Hermanowski-Vosatka, "Inhibition of 11β-HSD1 as a novel treatment for the metabolic syndrome: do glucocorticoids play a role?," *Expert Review of Cardiovascular Therapy*, vol. 3, no. 5, pp. 911–924, 2005.

[19] J. R. Seckl and B. R. Walker, "Minireview: 11β-hydroxysteroid dehydrogenase type 1—a tissue-specific amplifier of glucocorticoid action," *Endocrinology*, vol. 142, no. 4, pp. 1371–1376, 2001.

[20] Y. J. Liu, Y. Nakagawa, Y. Wang et al., "Increased glucocorticqid receptor and 11β-hydroxysteroid dehydrogenase type 1 expression in hepatocytes may contribute to the phenotype of type 2 diabetes in *db*/*db* mice," *Diabetes*, vol. 54, no. 1, pp. 32–40, 2005.

[21] N. Draper and P. M. Stewart, "11β-hydroxysteroid dehydrogenase and the pre-receptor regulation of corticosteroid hormone action," *Journal of Endocrinology*, vol. 186, no. 2, pp. 251–271, 2005.

[22] R. A. S. Schweizer, A. G. Atanasov, B. M. Frey, and A. Odermatt, "A rapid screening assay for inhibitors of 11β-hydroxysteroid dehydrogenases (11β-HSD): flavanone selectively inhibits 11β-HSD1 reductase activity," *Molecular and Cellular Endocrinology*, vol. 212, no. 1-2, pp. 41–49, 2003.

[23] J. L. W. Yau, T. Olsson, R. G. M. Morris, M. J. Meaney, and J. R. Seckl, "Glucocorticoids, hippocampal corticosteroid receptor gene expression and antidepressant treatment: relationship with spatial learning in young and aged rats," *Neuroscience*, vol. 66, no. 3, pp. 571–581, 1995.

[24] J. Beauquis, P. Roig, F. Homo-Delarche, A. de Nicola, and F. Saravia, "Reduced hippocampal neurogenesis and number of hilar neurones in streptozotocin-induced diabetic mice: reversion by antidepressant treatment," *European Journal of Neuroscience*, vol. 23, no. 6, pp. 1539–1546, 2006.

[25] W. Katon, J. Unützer, M.-Y. Fan et al., "Cost-effectiveness and net benefit of enhanced treatment of depression for older adults with diabetes and depression," *Diabetes Care*, vol. 29, no. 2, pp. 265–270, 2006.

[26] F. Thomson and M. Craighead, "Innovative approaches for the treatment of depression: targeting the HPA axis," *Neurochemical Research*, vol. 33, no. 4, pp. 691–707, 2008.

[27] L. An, Y.-Z. Zhang, X.-M. Liu et al., "Total flavonoids extracted from Xiaobuxin-Tang on the hyperactivity of hypothalamic-pituitary-adrenal axis in chronically stressed rats," *Evidence-Based Complementary and Alternative Medicine*, vol. 2011, Article ID 367619, 7 pages, 2011.

[28] P. J. Lustman and R. E. Clouse, "Treatment of depression in diabetes: impact on mood and medical outcome," *Journal of Psychosomatic Research*, vol. 53, no. 4, pp. 917–924, 2002.

[29] J. C. Fournier, R. J. DeRubeis, S. D. Hollon et al., "Antidepressant drug effects and depression severity: a patient-level meta-analysis," *The Journal of the American Medical Association*, vol. 303, no. 1, pp. 47–53, 2010.

Hindawi Publishing Corporation
Evidence-Based Complementary and Alternative Medicine
Volume 2015, Article ID 948376, 10 pages
http://dx.doi.org/10.1155/2015/948376

Research Article

Swertianlarin, an Herbal Agent Derived from *Swertia mussotii* Franch, Attenuates Liver Injury, Inflammation, and Cholestasis in Common Bile Duct-Ligated Rats

Liangjun Zhang,[1] Ying Cheng,[1] Xiaohuang Du,[2] Sheng Chen,[3] Xinchan Feng,[1] Yu Gao,[1] Shaoxue Li,[1] Li Liu,[1] Mei Yang,[1] Lei Chen,[1] Zhihong Peng,[1] Yong Yang,[4] Weizao Luo,[4] Rongquan Wang,[1] Wensheng Chen,[1] and Jin Chai[1]

[1]*Department of Gastroenterology, Southwest Hospital, Third Military Medical University, Chongqing 400038, China*
[2]*Department of Traditional Chinese Medicine, Southwest Hospital, Third Military Medical University, Chongqing 400038, China*
[3]*Department of Pediatrics, Southwest Hospital, Third Military Medical University, Chongqing 400038, China*
[4]*Chongqing Academy of Chinese Material Medicine, Chongqing 400065, China*

Correspondence should be addressed to Jin Chai; chaijinsw@yahoo.com

Received 29 September 2014; Revised 23 December 2014; Accepted 24 December 2014

Academic Editor: Sae Uchida

Swertianlarin is an herbal agent abundantly distributed in *Swertia mussotii* Franch, a Chinese traditional herb used for treatment of jaundice. To study the therapeutic effect of swertianlarin on cholestasis, liver injury, serum proinflammatory cytokines, and bile salt concentrations were measured by comparing rats treated with swertianlarin 100 mg/kg/d or saline for 3, 7, or 14 days after bile duct ligation (BDL). Serum alanine aminotransferase (ATL) and aspartate aminotransferase (AST) levels were significantly decreased in BDL rats treated with swertianlarin for 14 days ($P < 0.05$). The reduced liver injury in BDL rats by swertianlarin treatment for 14 days was further confirmed by liver histopathology. Levels of serum tumor necrosis factor alpha (TNFα) were decreased by swertianlarin in BDL rats for 3 and 7 days ($P < 0.05$). Moreover, reductions in serum interleukins IL-1β and IL-6 levels were also observed in BDL rats treated with swertianlarin ($P < 0.05$). In addition, most of serum toxic bile salt concentrations (e.g., chenodeoxycholic acid (CDCA) and deoxycholic acid (DCA)) in cholestatic rats were decreased by swertianlarin ($P < 0.05$). In conclusion, the data suggest that swertianlarin derived from *Swertia mussotii* Franch attenuates liver injury, inflammation, and cholestasis in bile duct-ligated rats.

1. Introduction

Accumulation of toxic bile acids in hepatocytes and the amplification of inflammation in cholestasis are the major factors resulting in liver injury and fibrosis [1–3]. Multiple pathologies, that is, gallstone obstruction of the bile duct, biliary atresia, pancreas tumors, and drug toxicity, can cause persisting cholestasis which can lead to liver failure, fibrosis, cirrhosis, and death [4–6]. Ursodeoxycholic acid (UDCA) and its analogs can inhibit inflammation and enhance elimination of toxic bile acids. It is the only approved drug that is widely clinically used to treat cholestatic patients such as primary biliary cirrhosis (PBC) [7, 8]. However, one-third to two-thirds of cholestatic patients with PBC do not completely respond to UDCA [9, 10]. INT747, an FXR agonist, is a Phase II studies drug that exerts anticholestatic effects by altering bile acids metabolism in experiment models [11–14]. Therefore, the search for potential drugs that target inflammation and bile acids pools for the treatment of cholestasis is important.

Swertianlarin is an iridoid compound that is present in *Swertia davidi* Franch and *Swertia mussotii* Franch [15–18]. These two types of Swertia Franch are the traditional herbs used for the treatment of jaundice caused by viral hepatitis. It has been used for many centuries in southwest China and is supposed to protect the liver from injury [15, 18],

have anti-inflammatory properties, and ameliorate cholestasis. Swertianlarin from *Enicostemma axillare* is known to have antioxidant and hepatoprotective effects against D-galactosamine-induced acute liver damage in rats [19]. Previous studies have also reported that swertianlarin inhibits inflammation in adjuvant-induced arthritis and in interleukin IL-1β-induced rat fibroblast-like synoviocytes [20–23]. However, the anti-inflammation effect of swertianlarin on cholestasis remains to be clarified. Furthermore, whether swertianlarin alters the bile acid pool and reduces liver injury on cholestasis is unclear.

To address whether swertianlarin derived from *Swertia mussotii* Franch attenuates inflammation and liver injury on cholestasis, we assessed the liver injury, serum proinflammatory cytokine levels, and the concentrations of serum bile acids in a bile duct-ligated rat model treated with swertianlarin.

2. Materials and Methods

2.1. Chemicals. Swertianlarin, isolated from *Swertia mussotii* Franch as reported previously [24], was kindly provided by Chongqing Academy of Chinese Material Medical with a purity of 98% as analyzed by HPLC. All other chemicals were of analytical grade and purchased from Sigma-Aldrich (Sigma-Aldrich Chemical Co., St. Louis, MO, USA).

2.2. Animals and Treatments. The male Sprague-Dawley (SD) rats were provided by the Center of Laboratory Animals of Third Military Medical University, Chongqing, China. All experimental protocols were approved by the Ethics Committee of Third Military Medical University. Efforts were made to reduce animal suffering and minimize animal number used. Animals were housed in plastic cages with free access to food and water under a 12 h light/dark cycle. The normal rats were given swertianlarin in 4 groups: 0, 10, 50, and 100 mg/(kg/d), dissolved in 1% Tween-20 saline, $n = 7$, by gavage for 14 days. All rats survived and the serum biochemistries alanine aminotransferase (ALT), aspartate aminotransferase (AST), alkaline phosphatase (ALP), total bile acids (TBA), total bilirubin (TBIL), and direct bilirubin (DBIL) were normal in the study (data not shown). In this study, rats were randomly divided into three groups ($n = 7$ per group): sham saline, BDL without swertianlarin, and BDL with swertianlarin with each containing from five to seven animals. In the BDL swertianlarin group, rats were pretreated with swertianlarin 100 mg/(kg/d) dissolved in 1% Tween-20 by gavage for 1 d and then underwent BDL followed by continued administration of swertianlarin for 3, 7, and 14 d. In the BDL saline groups, rats underwent BDL after pretreatment with only 1% Tween-20 saline by gavage for 1 d and then continued treatment with only 1% Tween-20 saline for 3, 7, and 14 d. In the sham saline control group, rats were pretreated with 1% Tween-20 saline by gavage for 1 d and underwent a sham-operation followed by only 1% Tween-20 saline for 3, 7, and 14 d. After 3, 7, and 14 d, animals were sacrificed randomly between 9:00 am and 11:00 am. Blood was placed on ice for 60 min and centrifuged (8000 g, 10 min) to prepare serum. The serum was immediately stored at −80°C until used. The liver samples were immediately cut into small pieces and frozen in liquid nitrogen until used. The collected serum and liver samples were used for biochemistry and histopathology studies as described previously [25].

2.3. Serum Biochemistry. The concentrations of alanine aminotransferase (ALT), aspartate aminotransferase (AST), alkaline phosphatase (ALP), total bile acids (TBA), total bilirubin (TBIL), and direct bilirubin (DBIL) in serum samples were analyzed by standard enzymatic assays using commercial kits.

2.4. Determination of Serum Proinflammatory Cytokines TNFα, Interleukin-1β, and Interleukin-6. Serum samples from sham operated rats and bile duct-ligated rats with and without swertianlarin were collected before sacrifice ($n = 7$ per each group) and stored at −80°C until analysis. Serum cytokines, tumor necrosis factor alpha (TNFα), interleukin-1 beta (IL-1β), and IL-6 levels were determined by ELISA Kits (BlueGene Biotechnology, Shanghai, China) according to the manufacturer's instructions [25, 26].

2.5. Serum Bile Salts and Lipids Determination. The concentrations of serum bile acids chenodeoxycholic acid (CDCA), taurochenodeoxycholic acid (TCDCA), cholic acid (CA), taurocholic acid (TCA), deoxycholic acid (DCA), taurodeoxycholic acid A (TDC), tauroursodeoxycholic acid (TUDCA), tauro-alpha/beta-muricholic acid (Tα/βMCA), alpha-muricholic acid (αMCA), and beta-muricholic acid (βMCA) levels, serum lipid triglyceride hydrolase (Tgh), triglyceride (TG), high-density lipoprotein cholesterol (HDL-C), and low-density lipoprotein cholesterol (LDL-C) were measured by standard enzymatic assays using commercial kits purchased from BlueGene Biotech (Shanghai, China), according to the manufacturer's protocol as described previously [27, 28].

2.6. Histopathology. Rat liver samples were fixed in 4% formalin and subjected to standard histological procedures and paraffin embedding. Liver sections (5 μm in thickness) were stained with hematoxylin and eosin and evaluated for histological lesions.

2.7. Statistical Analysis. All values were expressed as mean ± standard deviation (SD). One-way analysis of variance followed by Dunnett's multiple comparison post hoc test was used for statistical analysis of data using GraphPad Prism 6.01 (GraphPad Software Inc., San Diego, CA). A value of $P < 0.05$ was considered to be statistically significant.

3. Results

3.1. Swertianlarin Attenuates Liver Injury in Common Bile Duct-Ligated Rats. Figure 1(a) shows that serum ALT, AST, and ALP were significantly increased in both BDL rats treated with and those without swertianlarin for 3, 7, and 14 days, compared to sham group with saline ($P < 0.05$, Figure 1(a)).

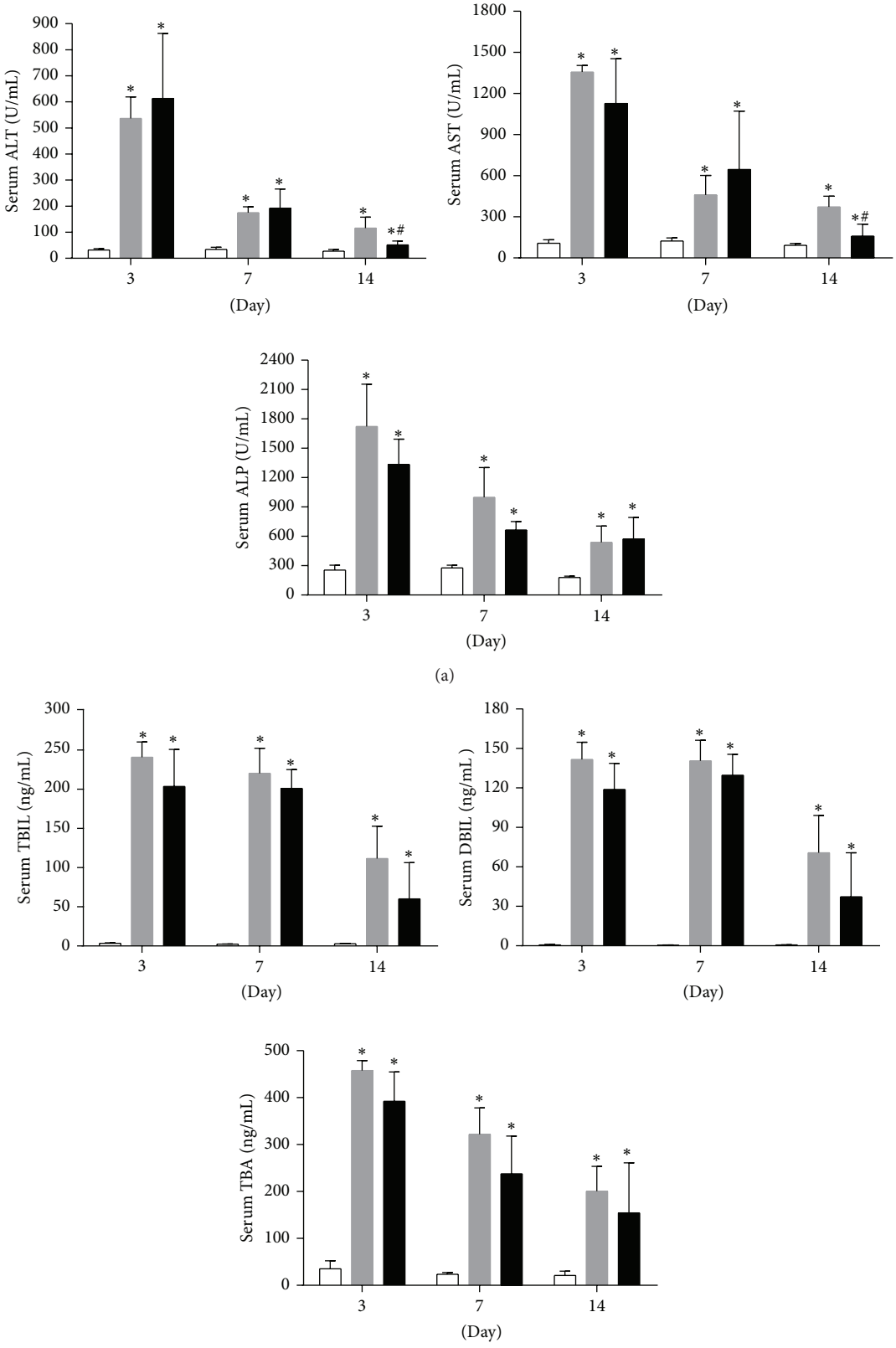

Figure 1: Continued.

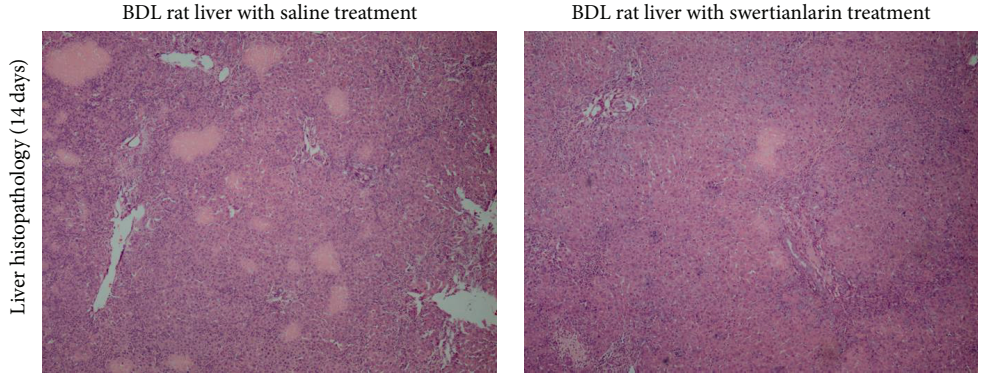

(c)

Figure 1: Changes of serum liver injury biomarkers and histopathology in swertianlarin-treated BDL rats. (a) Changes in ALT, AST, and ALP levels in sham rats with saline, BDL rats without swertianlarin, and BDL rats with swertianlarin for 3, 7, and 14 d. (b) Alterations of biomarkers TBIL, DBIL, and TBA levels in sham rats with saline, BDL rats without swertianlarin, and BDL rats with swertianlarin for 3, 7, and 14 d. (c) Liver histopathology (4X) in BDL rats with or without swertianlarin for 14 d. Data were analyzed using one-way analysis of variance followed by Dunnett's multiple comparison post hoc test. $^{*}P < 0.05$ versus sham group with saline; $^{\#}P < 0.05$, versus BDL group with saline. $n = 7$ per group. Saline, 1% Tween-20 saline; swertianlarin dissolved in 1% Tween-20 saline.

However, serum ALT and AST levels for 14 d were markedly decreased in the BDL rats with swertianlarin (54% and 52% of saline BDL group, resp.; $P < 0.05$). However, the levels of these two markers were not significantly different at the earlier time points of 3 and 7 d, compared to the BDL rats without swertianlarin (Figure 1(a)). Furthermore, the serum ALP levels for 3, 7, and 14 d were not significantly different in both BDL with and without swertianlarin groups at any time (Figure 1(a)). The reduced liver injury in BDL rats with swertianlarin for 14 d was further confirmed by liver histopathology (Figure 1(c)). Moreover, the serum TBIL, DBIL, and TBA levels were noticeably increased in all BDL groups. There were no significant differences in TBIL, DBIL, and TBA between BDL groups with or without swertianlarin (Figure 1(b)). Nevertheless, the serum levels of TBIL and DBIL tended to be lower in the BDL group with swertianlarin compared to the BDL group without swertianlarin for 14 d (Figure 1(b)). These results indicated that swertianlarin treatment decreased liver injury, whereas the serum TBIL and TBA levels in BDL rats remained unaltered for 14 d.

3.2. Swertianlarin Has Anti-Inflammatory Effect on BDL Rats. To investigate whether swertianlarin has anti-inflammatory effects, the concentration of serum proinflammatory cytokines TNFα, IL-1β, and IL-6 were measured by ELISA assay in the sham operated group and BDL groups with or without swertianlarin. The results showed that the serum TNFα levels for 3 and 7 d were dramatically increased while they were not significantly increased for 14 d in cholestatic rats without swertianlarin compared to sham operated rats (Figure 2(a)). However, the levels of serum TNFα in cholestatic rats with BDL for 3 and 7 d were significantly lower with swertianlarin treatment, 63% and 64% of saline BDL group, respectively ($P < 0.05$). However, they were not significantly different for 14 d, compared to the BDL group without swertianlarin (Figure 2(a)). Furthermore, serum IL-1β levels were significantly increased for 14 d while they were unchanged for 3 and 7 d in the BDL group with swertianlarin compared to those of the sham operated group (Figure 2(b)). However, the serum IL-1β levels for 3 and 14 d were noticeably lower in the swertianlarin BDL group (43% and 42% of BDL group without swertianlarin, resp.; $P < 0.05$). Moreover, the serum IL-1β levels were not altered by swertianlarin for 7 d (Figure 2(b)). Figure 2(c) shows that serum IL-6 levels were increased for 14 d but was decreased for 3 d ($P < 0.05$) and was not different for 7 d in BDL group without swertianlarin compared to the sham operated group (Figure 3(c)). Serum IL-6 in the swertianlarin BDL group for 14 d was 61% of saline BDL group ($P < 0.05$), whereas the serum IL-6 levels were not affected by swertianlarin for 3 and 7 d (Figure 3(c)). These results demonstrated that swertianlarin treatment reduced levels of serum proinflammatory cytokines TNFα, IL-1β, and IL-6 in this rat model.

3.3. Swertianlarin Alters the Concentration of Serum Bile Salts in Rats with Bile Duct Ligation. The accumulation of bile salts is the major factor resulting in the liver injury in cholestasis [1, 3, 21]. Because an apparent decrease in liver injury in cholestatic rats was associated with swertianlarin treatment, it was determined if swertianlarin alters the concentration of serum bile salts in cholestasis. The results showed that CDCA was lower in BDL rats without swertianlarin for 3, 7, and 14 days compared with sham operated rats ($P = 0.31$, $P < 0.05$, and $P < 0.05$, Figure 3(a)). In contrast, the TCDCA levels were increased in the BDL rats without swertianlarin for 7 d but were unaltered after 3 and 14 d (Figure 3(a)). The administration of swertianlarin decreased CDCA levels after 7 and 14 d and reduced TCDCA levels after 7 d in BDL rats ($P < 0.05$, Figure 3(a)). The concentration of serum CA was unchanged in BDL rats without swertianlarin, compared to the sham operated group. However, the serum CA levels were

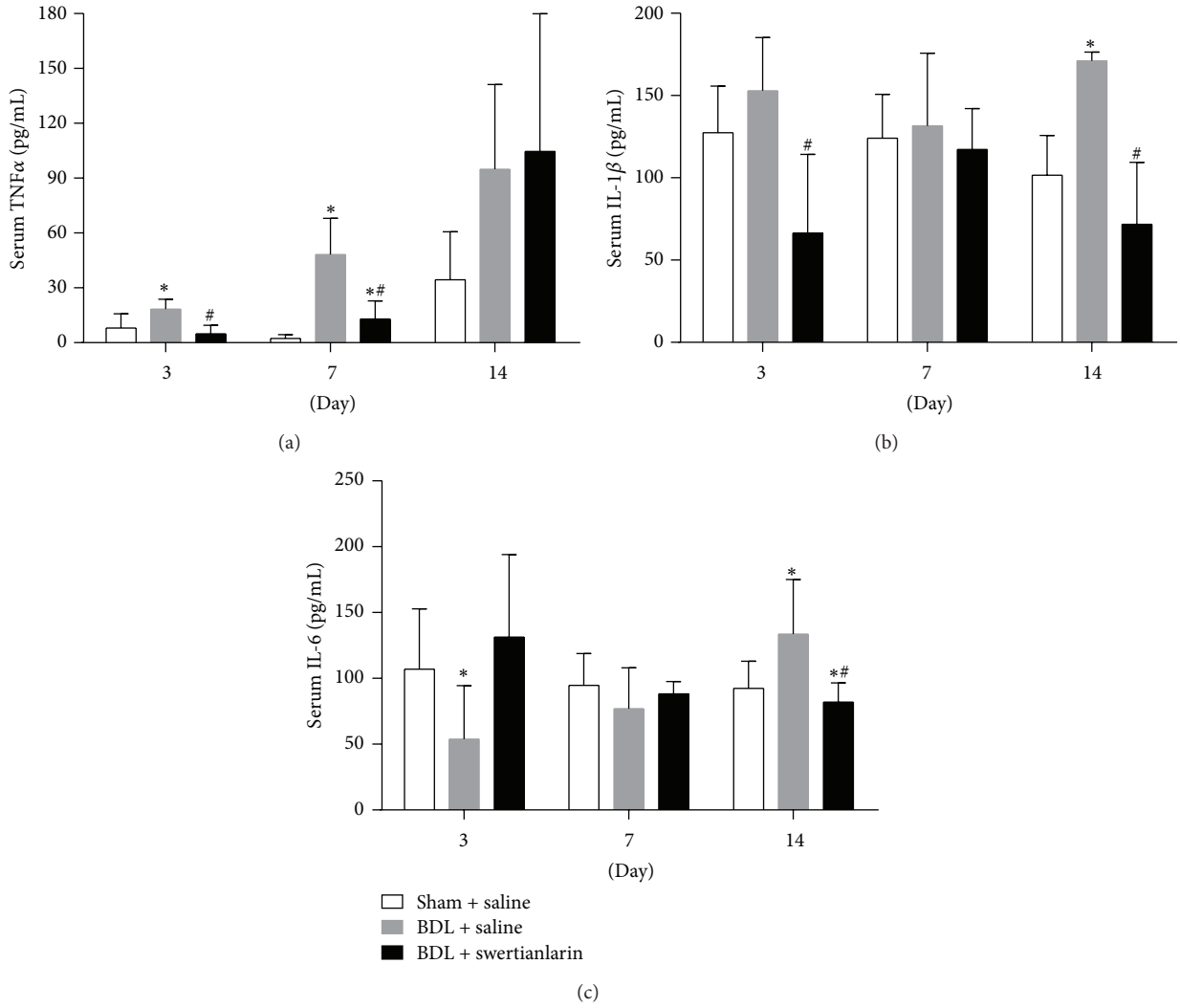

Figure 2: Alterations of serum proinflammatory cytokines TNFα, IL-1β, and IL-6 levels by swertianlarin in BDL rats. (a) The changes of serum TNFα in the sham operated, BDL with swertianlarin, and BDL without swertianlarin groups for 3, 7, and 14 d. (b) The alterations of serum IL-1β in sham operated, BDL with swertianlarin, and BDL without swertianlarin groups for 3, 7, and 14 d. (c) The determination of serum IL-6 in sham operated rats and BDL rats treated with or without swertianlarin after 3, 7, and 14 d. Data were analyzed as described in Materials and Methods. $^{*}P < 0.05$ versus sham group with saline; $^{\#}P < 0.05$, versus BDL group with saline. $n = 7$ per group. Saline, 1% Tween-20 saline; swertianlarin dissolved in 1% Tween-20 saline.

decreased in BDL rats with swertianlarin for 3 ($P < 0.05$), 7, and 14 d ($P < 0.05$, Figure 3(b)). Moreover, TCA levels were only decreased in BDL rats without swertianlarin after 3 and 7 d ($P < 0.05$, Figure 3(b)), but not significantly changed after 14 d. However, serum TCA was significantly lower in BDL rats with swertianlarin after 3 and 14 d ($P < 0.05$, Figure 3(b)), but not after 7 d, when compared to BDL rats without swertianlarin. Figure 3(c) (left) shows that serum DCA levels were similar in BDL rats without swertianlarin, compared with sham group. However, the serum DCA levels were decreased in BDL rats with swertianlarin for 3, 7, and 14 d ($P < 0.05$ for all, Figure 3(c) left). In contrast, serum TDCA levels were increased in BDL rats without swertianlarin for 14 d but were not elevated with swertianlarin treatment ($P < 0.05$, Figure 3(c) right). There were no difference in TDCA levels in BDL rats with or without swertianlarin after 3 d, whereas TDCA levels were lower in BDL rats with swertianlarin after 7 d, compared with BDL rats without swertianlarin ($P < 0.05$, Figure 3(c)). Figure 3(d) showed that TUDCA levels were lower in cholestatic rats without swertianlarin after 3 and 7 d ($P < 0.05$) but were not different after 14 days. Administration of swertianlarin decreased TUDCA levels in BDL rats after 14 d ($P < 0.05$, Figure 3(d)) compared to BDL rats without swertianlarin. Furthermore, serum Tα/βMCA levels were nonsignificantly different between the sham group and BDL groups without swertianlarin for 3, 7, and 14 d but were decreased in the BDL group with swertianlarin after 7 and 14 d, compared to the BDL group without swertianlarin ($P < 0.05$, Figure 3(e)). Figure 3(f) (left) shows that serum αMCA levels were similar in the BDL without swertianlarin

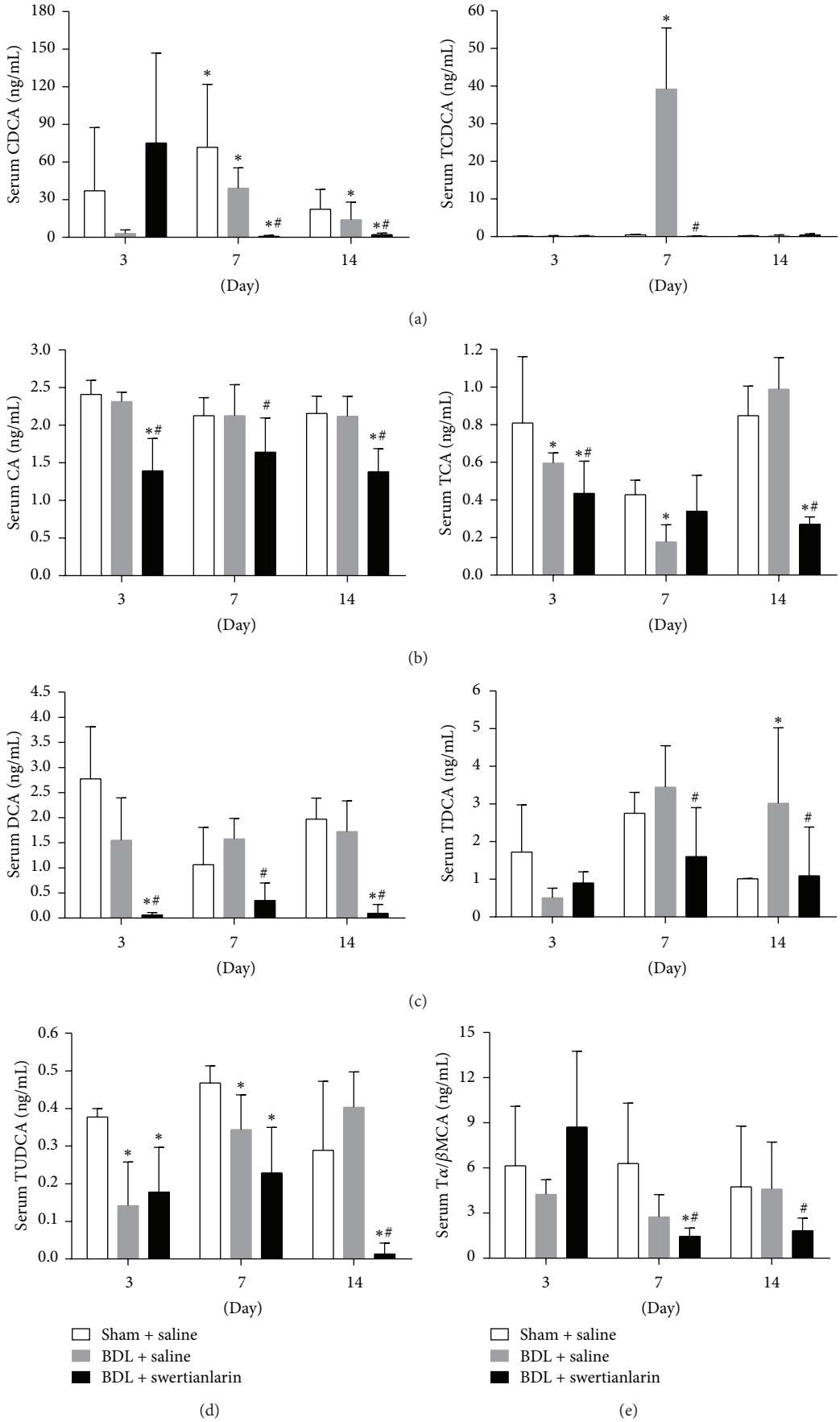

Figure 3: Continued.

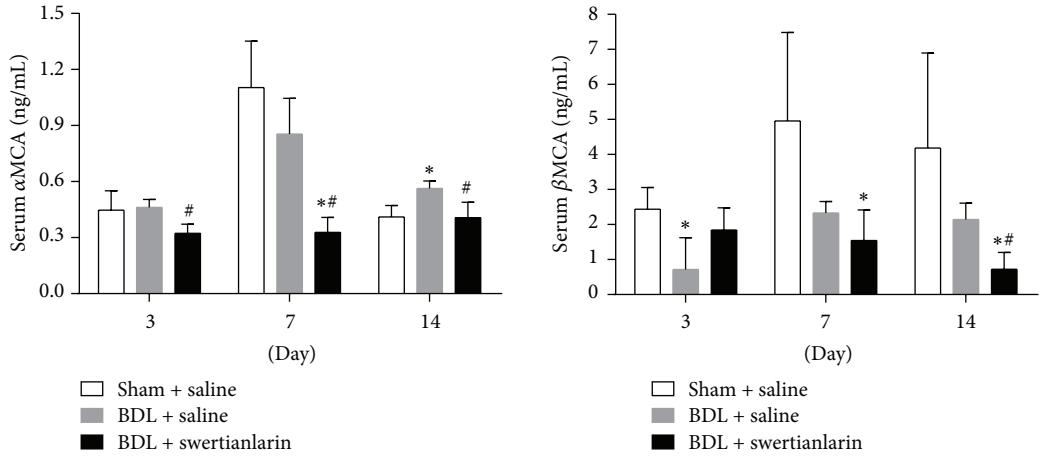

(f)

Figure 3: Alterations of serum bile salts by swertianlarin in BDL rats. (a) The concentrations of serum CDCA and TCDCA in sham operated rats and BDL rats with or without swertianlarin for 3, 7, and 14 d. (b) The changes in serum bile salts CA and TCA in sham operated, BDL with swertianlarin, and BDL without swertianlarin groups for 3, 7, and 14 d. (c) The determination of serum DCA and TDCA in sham operated rats and BDL rats treated with or without swertianlarin after 3, 7, and 14 d. (d) Serum TUDCA, (e) Tα/βMCA, and (f) αMCA and βMCA were measured in sham operated group, BDL with swertianlarin group, and BDL without swertianlarin group for 3, 7, and 14 d. Data were analyzed as described in Materials and Methods. $^{*}P < 0.05$ versus sham group with saline; $^{\#}P < 0.05$, versus BDL group with saline. $n = 7$ per group. Saline, 1% Tween-20 saline; swertianlarin dissolved in 1% Tween-20 saline.

group after 3 and 7 d but were higher in the BDL group without swertianlarin compared to the sham group for 14 d ($P < 0.05$). However, serum αMCA levels were decreased in the BDL group with swertianlarin for 3, 7, and 14 d ($P < 0.05$), compared with the BDL group without swertianlarin (Figure 3(f)). Serum βMCA levels were lower in the BDL group without swertianlarin for 3 d ($P < 0.05$) while they were not significantly changed for 7 d and 14 d, compared with the sham group. Administration of swertianlarin for 14 d significantly decreased serum βMCA levels in the BDL rats ($P < 0.05$, Figure 3(f), right). These results indicated that swertianlarin administration was associated with lower levels of conjugated and unconjugated bile salts in BDL rats.

3.4. Swertianlarin Does Not Affect Lipids Levels in BDL Rats. Serum Tgh, TG, and LDL-C levels for 3 and 7 d were higher, but unchanged for 14 d in BDL saline rats, compared with the sham group ($P < 0.01$, Figures 4(a), 4(b), and 4(d)). However, the HDL-C levels were increased for 3 d but decreased for 14 d in BDL rats (Figure 4(c)). Furthermore, there was no difference in serum HDL-C in BDL rats after 7 d (Figure 4(c)). The results showed that levels of Tgh, TG, HDL-C, and LDL-C were not significantly different in BDL rats with or without swertianlarin (Figure 4). These results suggest that lipid metabolism was not affected by swertianlarin in this model.

4. Discussion

Persisting cholestasis caused by bile duct obstruction (i.e., gallstones and pancreas tumors), hepatitis, and drugs can lead to liver failure, fibrosis, and cirrhosis [1–6]. The accumulation of bile acids in hepatocytes and hepatic chronic inflammation plays key roles in cholestatic liver injury [1–3]. The drugs that enhance elimination of toxic bile acids, such as UDCA and INT747 are beneficial for cholestatic patients [7–14]. In the present study, it was observed that swertianlarin attenuates liver injury and inflammation and is associated with lower concentrations of bile salts in BDL rats.

Models of cholestasis can be produced by administration of some drugs, for example, α-naphthylisothiocyanate (ANIT) (intrahepatic cholestasis), or by bile duct ligation (extrahepatic cholestasis) [27–29]. The presence of toxic bile acids is the major factor resulting in liver injury in cholestasis [1, 2]. The present study showed that certain conjugated and unconjugated bile acids in serum were reduced in BDL rats by swertianlarin treatment for 3, 7, and 14 d, implying that swertianlarin attenuates cholestasis. Serum bile acid levels were reduced in BDL rats treated with swertianlarin for 14 d. These data may explain why levels of serum markers of liver injury, ALT, and AST, as well as liver necrosis determined by histopathology, were significantly decreased in BDL rats treated with swertianlarin for 14 d. Many studies have demonstrated that inhibition of bile acid synthetic enzymes (e.g., Cyp7a1), upregulation of detoxification enzymes (e.g., Cyp3a11 and Ugt2b), and bile acids transporters (e.g., Mrp3 and Mrp4) contribute to the repression of bile acid synthesis, the reduction of bile salt toxicity. This may occur by increasing water solubility and elimination of bile acids, alleviating cholestasis and liver injury in cholestatic animal models and in human cholestatic patients using UDCA and INT747 [1, 2, 25]. The differences in timing of alterations of serum bile acids levels in BDL rats may be due to changes in hepatic bile acid transporters, synthetic and detoxification enzymes regulated by swertianlarin. However, this hypothesis

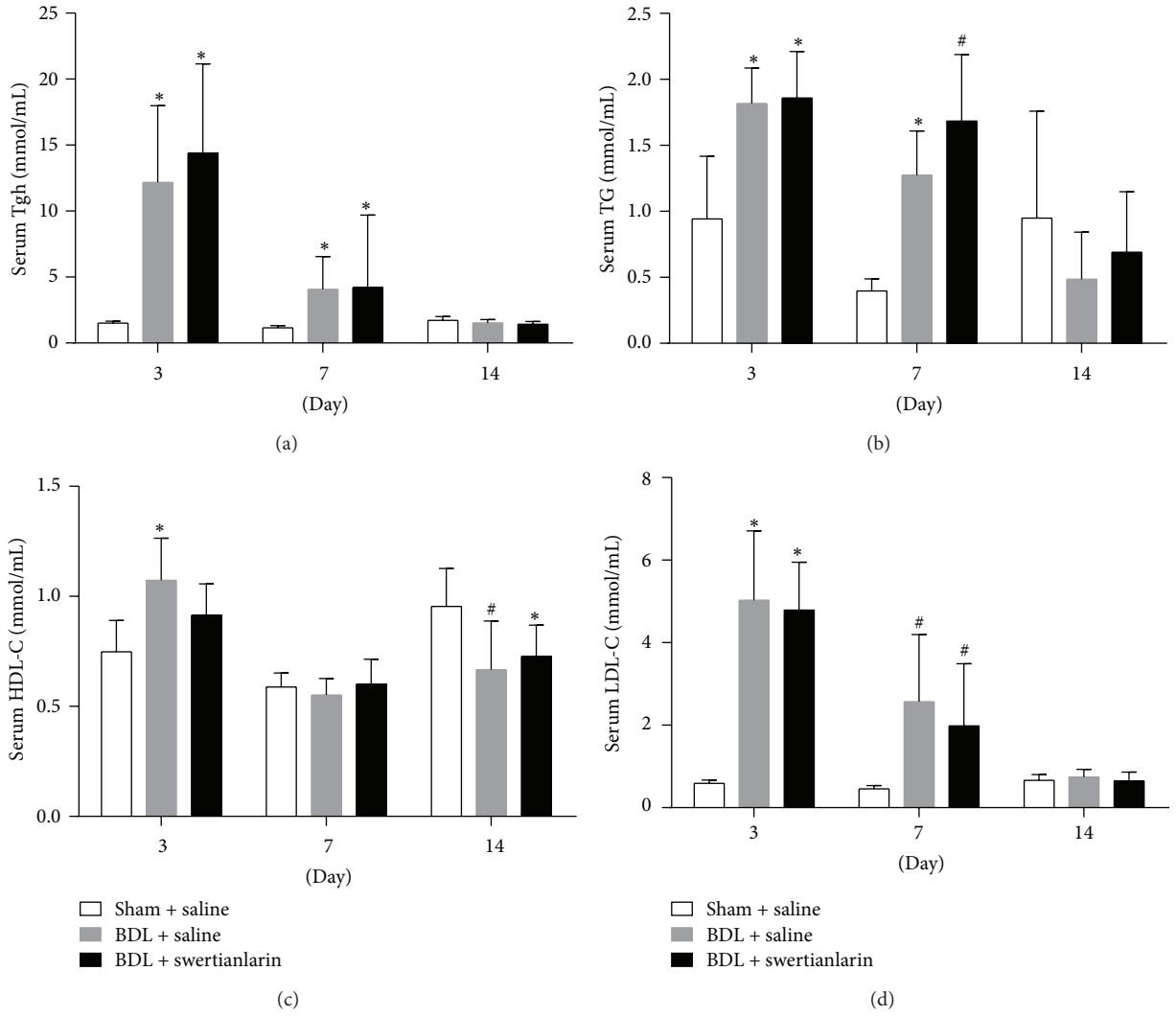

FIGURE 4: The lipids Tgh, TG, HDL-C, and LDL-C levels were unaffected by swertianlarin in bile duct-ligated rats. (a) Serum Tgh, (b) TG, (c) HDL-C, and (d) serum LDL-C levels were measured in sham operated rats, BDL rats without swertianlarin, and BDL rats with swertianlarin for 3, 7, and 14 d. Data were analyzed as described in Materials and Methods. $^{*}P < 0.01$; $^{\#}P < 0.05$, versus sham group with saline. $n = 7$ per group. Saline, 1% Tween-20 saline; swertianlarin dissolved in 1% Tween-20 saline.

needs to be tested by more in-depth studies in future. Moreover, it was found that the lipid levels Tgh, TG, HDL-C, and LDL-C were not different in swertianlarin-treated BDL rats compared to BDL rats without swertianlarin. However, serum lipid levels were severely disturbed in all of BDL rats. These results suggested that BDL not only affected bile acid homeostasis, but also interfered with lipid homeostasis. In addition, one recent study also reported that swertianlarin from *Enicostemma axillare* had antioxidant and hepatoprotective effects against D-galactosamine-induced acute liver damage in rats [19]. These support the protective role of swertianlarin on cholestasis.

We also demonstrated that elevated serum levels of proinflammatory cytokines TNFα for 3 and 7 d, IL-1β, and IL-6 for 14 d in BDL rats were significantly reduced by swertianlarin treatment, implying that swertianlarin has an anti-inflammatory effect on cholestatic process. These observations in BDL rats with swertianlarin treatment are similar to those previously described in adjuvant-induced arthritis and IL-1β-induced rat fibroblast-like synoviocyte models [20, 21]. A recent study reported that inflammation plays an important role in the progression of the pathology of cholestasis [3]. Knockout of TNFα in a cholestatic mouse model reduced liver injury and fibrosis [30]. Therefore, swertianlarin may also alter the progression of cholestasis by inhibiting inflammation. However, whether swertianlarin exerts an anti-inflammatory effect on cholestasis by the activation of NF-κB and JAK signaling, as reported previously [20], remains to be clarified.

Although the swertianlarin-treated BDL rats had less liver injury, inflammation, and cholestasis than those without swertianlarin, these results are from one cholestasis model. Whether swertianlarin also exerts the protective role in other cholestatic models (e.g., lipopolysaccharide-induced

cholestasis) or human cholestasis (e.g., primary biliary cirrhosis) needs further studies. Moreover, the molecular mechanism by which swertianlarin affects cholestasis remains to be determined.

5. Conclusions

The results demonstrated that swertianlarin from *Swertia mussotii* Franch attenuates liver injury, inflammation, and cholestasis in BDL rats. The findings of the present study contribute to understanding the protective role of swertianlarin in cholestasis and provide preliminary data for the development of potential drugs for the treatment of cholestasis.

Conflict of Interests

The authors declare that they have no conflict of interests regarding the publication of this paper.

Authors' Contribution

Liangjun Zhang and Ying Cheng equally contributed to this study.

Acknowledgments

This work was supported by National Natural Science Foundation of China (81070320, 81100280, and 81470880), Scholarship Foundation of China Scholarship Council (CSC no. 201307610015), and Scholarship Foundation of Third Military Medical University (2013).

References

[1] M. Trauner, P. J. Meier, and J. L. Boyer, "Mechanisms of disease: molecular pathogenesis of cholestasis," *The New England Journal of Medicine*, vol. 339, no. 17, pp. 1217–1227, 1998.

[2] M. Wagner, G. Zollner, and M. Trauner, "New molecular insights into the mechanisms of cholestasis," *Journal of Hepatology*, vol. 51, no. 3, pp. 565–580, 2009.

[3] B. L. Woolbright, D. J. Antoine, R. E. Jenkins, M. L. Bajt, B. K. Park, and H. Jaeschke, "Plasma biomarkers of liver injury and inflammation demonstrate a lack of apoptosis during obstructive cholestasis in mice," *Toxicology and Applied Pharmacology*, vol. 273, no. 3, pp. 524–531, 2013.

[4] W. R. Kim, J. Ludwig, and K. D. Lindor, "Variant forms of cholestatic diseases involving small bile ducts in adults," *The American Journal of Gastroenterology*, vol. 95, no. 5, pp. 1130–1138, 2000.

[5] R. Poupon, O. Chazouilleres, and R. E. Poupon, "Chronic cholestatic diseases," *Journal of Hepatology*, vol. 32, no. 1, supplement, pp. 129–140, 2000.

[6] H. Yang, D. J. Antoine, U. Andersson, and K. J. Tracey, "The many faces of HMGB1: molecular structure-functional activity in inflammation, apoptosis, and chemotaxis," *Journal of Leukocyte Biology*, vol. 93, no. 6, pp. 865–873, 2013.

[7] G. Paumgartner and T. Pusl, "Medical treatment of cholestatic liver disease," *Clinics in Liver Disease*, vol. 12, no. 1, pp. 53–80, 2008.

[8] P. Fickert, M. Wagner, H.-U. Marschall et al., "24-norUrsodeoxycholic acid is superior to ursodeoxycholic acid in the treatment of sclerosing cholangitis in Mdr2 (Abcb4) knockout mice," *Gastroenterology*, vol. 130, no. 2, pp. 465–481, 2006.

[9] A. Parés, L. Caballería, and J. Rodés, "Excellent long-term survival in patients with primary biliary cirrhosis and biochemical response to ursodeoxycholic acid," *Gastroenterology*, vol. 130, no. 3, pp. 715–720, 2006.

[10] C. Corpechot, L. Abenavoli, N. Rabahi et al., "Biochemical response to ursodeoxycholic acid and long-term prognosis in primary biliary cirrhosis," *Hepatology*, vol. 48, no. 3, pp. 871–877, 2008.

[11] Y. Liu, J. Binz, M. J. Numerick et al., "Hepatoprotection by the farnesoid X receptor agonist GW4064 in rat models of intra- and extrahepatic cholestasis," *The Journal of Clinical Investigation*, vol. 112, no. 11, pp. 1678–1687, 2003.

[12] M. Trauner, M. Wagner, P. Fickert, and G. Zollner, "Molecular regulation of hepatobiliary transport systems: clinical implications for understanding and treating cholestasis," *Journal of Clinical Gastroenterology*, vol. 39, no. 4, supplement 2, pp. S111–S124, 2005.

[13] L. Huang, A. Zhao, J. L. Lew et al., "Farnesoid X receptor activates transcription of the phospholipid pump MDR3," *The Journal of Biological Chemistry*, vol. 278, no. 51, pp. 51085–51090, 2003.

[14] A. Moschetta, A. L. Bookout, and D. J. Mangelsdorf, "Prevention of cholesterol gallstone disease by FXR agonists in a mouse model," *Nature Medicine*, vol. 10, no. 12, pp. 1352–1358, 2004.

[15] H. Yang, C. Ding, Y. Duan, and J. Liu, "Variation of active constituents of an important Tibet folk medicine *Swertia mussotii* Franch. (Gentianaceae) between artificially cultivated and naturally distributed," *Journal of Ethnopharmacology*, vol. 98, no. 1-2, pp. 31–35, 2005.

[16] C. Tian, T. Zhang, L. Wang, Q. Shan, and L. Jiang, "The hepatoprotective effect and chemical constituents of total iridoids and xanthones extracted from *Swertia mussotii* Franch," *Journal of Ethnopharmacology*, vol. 154, no. 1, pp. 259–266, 2014.

[17] R. L. Gao, L. Wang, Y. Yang et al., "Simultaneous determination of oleanolic acid, ursolic acid, quercetin and apigenin in *Swertia mussotii* Franch by capillary zone electrophoresis with running buffer modifier," *Biomedical Chromatography*, vol. 29, no. 3, pp. 402–409, 2015.

[18] G. Fan, W.-Z. Luo, S.-H. Luo et al., "Metabolic discrimination of *Swertia mussotii* and *Swertia chirayita* known as 'Zangyinchen' in traditional Tibetan medicine by ^{1}H NMR-based metabolomics," *Journal of Pharmaceutical and Biomedical Analysis*, vol. 98, pp. 364–370, 2014.

[19] V. Jaishree and S. Badami, "Antioxidant and hepatoprotective effect of swertiamarin from *Enicostemma axillare* against d-galactosamine induced acute liver damage in rats," *Journal of Ethnopharmacology*, vol. 130, no. 1, pp. 103–106, 2010.

[20] S. Saravanan, V. I. Hairul Islam, N. Prakash Babu et al., "Swertiamarin attenuates inflammation mediators via modulating kappaB /I kappaB and JAK2/STAT3 transcription factors in adjuvant induced arthritis," *European Journal of Pharmaceutical Sciences*, vol. 56, no. 1, pp. 70–86, 2014.

[21] S. Saravanan, V. I. H. Islam, K. Thirugnanasambantham et al., "Swertiamarin ameliorates inflammation and osteoclastogenesis intermediates in IL-1beta induced rat fibroblast-like synoviocytes," *Inflammation Research*, vol. 63, no. 6, pp. 451–462, 2014.

[22] K. S. Park, B. H. Kim, and I.-M. Chang, "Inhibitory potencies of several iridoids on cyclooxygenase-1, cyclooxygnase-2 enzymes activities, tumor necrosis factor-α and nitric oxide production in vitro," *Evidence-Based Complementary and Alternative Medicine*, vol. 7, no. 1, pp. 41–45, 2010.

[23] H. B. Vaidya, S. Giri, M. Jain, and R. K. Goyal, "Decrease in serum matrix metalloproteinase-9 and matrix metalloproteinase-3 levels in Zucker fa/fa obese rats after treatment with swertiamarin," *Experimental and Clinical Cardiology*, vol. 17, no. 1, pp. 12–16, 2012.

[24] J. Vaijanathappa and S. Badami, "Antiedematogenic and free radical scavenging activity of swertiamarin isolated from *Enicostemma axillare*," *Planta Medica*, vol. 75, no. 1, pp. 12–17, 2009.

[25] J. Chai, Y. He, S. Y. Cai et al., "Elevated hepatic multidrug resistance-associated protein 3/ATP-binding cassette subfamily C 3 expression in human obstructive cholestasis is mediated through tumor necrosis factor alpha and c-Jun NH2-terminal kinase/stress-activated protein kinase-signaling pathway," *Hepatology*, vol. 55, no. 5, pp. 1485–1494, 2012.

[26] H. He, A. Mennone, J. L. Boyer, and S.-Y. Cai, "Combination of retinoic acid and ursodeoxycholic acid attenuates liver injury in bile duct-ligated rats and human hepatic cells," *Hepatology*, vol. 53, no. 2, pp. 548–557, 2011.

[27] Y. Wang, L. Jing, X.-M. Zhao et al., "Protective effects of hydrogen-rich saline on monocrotaline-induced pulmonary hypertension in a rat model," *Respiratory Research*, vol. 12, no. 4, article 26, 2011.

[28] Y. Tanaka, L. M. Aleksunes, Y. J. Cui, and C. D. Klaassen, "ANIT-induced intrahepatic cholestasis alters hepatobiliary transporter expression via Nrf2-dependent and independent signaling," *Toxicological Sciences*, vol. 108, no. 2, pp. 247–257, 2009.

[29] B. L. Copple, H. Jaeschke, and C. D. Klaassen, "Oxidative stress and the pathogenesis of cholestasis," *Seminars in Liver Disease*, vol. 30, no. 2, pp. 195–204, 2010.

[30] A. Geier, C. G. Dietrich, M. Trauner, and C. Gartung, "Extrahepatic cholestasis downregulates Oatp1 by TNF-α signalling without affecting Oatp2 and Oatp4 expression and sodium-independent bile salt uptake in rat liver," *Liver International*, vol. 27, no. 8, pp. 1056–1065, 2007.

Hindawi Publishing Corporation
Evidence-Based Complementary and Alternative Medicine
Volume 2015, Article ID 973930, 12 pages
http://dx.doi.org/10.1155/2015/973930

Research Article

Serum Pharmacochemistry Analysis Using UPLC-Q-TOF/MS after Oral Administration to Rats of Shenfu Decoction

Jia-le He,[1,2] Jia-wei Zhao,[1,2] Zeng-chun Ma,[2] Yu-guang Wang,[2] Qian-de Liang,[2] Hong-ling Tan,[2] Cheng-rong Xiao,[2] Xiang-lin Tang,[2] and Yue Gao[2]

[1]*Graduate School, Anhui Medical University, Hefei, China*
[2]*Beijing Institute of Radiation Medicine, Tai-Ping Road 27, Beijing 100850, China*

Correspondence should be addressed to Zeng-chun Ma; mazchun@139.com and Yue Gao; gaoyue@bmi.ac.cn

Received 23 October 2014; Revised 27 May 2015; Accepted 28 May 2015

Academic Editor: Kazuo Toda

The purpose of this study was to study the serum pharmacochemistry of SFD as well as the material basis through analyzing the constituents absorbed in blood. The SFD was orally administrated to Wistar rats at 20 $g \cdot kg^{-1}$, and Ultra Performance Liquid Chromatography (UPLC) fingerprints of SFD were created. Serum samples were collected for analysis, and further data processing used MarkerLynx XS software. 19 ginsenosides and 16 alkaloids were detected in SFD. The absorption of alkaloids (mainly monoester diterpenoid alkaloids) increased when *Aconitum carmichaeli* Debx. was combined with *Panax ginseng*, while the ginsenosides remained stable. Diester diterpenoid alkaloids were not present in the serum samples. A suitable serum pharmacochemistry method was successfully established to study pharmacological effects and potential improvements in formulation. This may also be useful for toxicity reduction. We suspect that the increased absorption of the monoester diterpenoid alkaloids from the mixture of *Panax* and *Radix*, compared to the *Panax* only extract, may be the reason for the combination of the two herbs in popular medicine formulas in China.

1. Introduction

Shenfu Decoction (SFD) consisting of an equal ratio of ginseng root (radix ginseng, Renshen) and aconite root (*Radix Aconiti Lateralis Preparata*, Fuzi) is an example of a classic Chinese traditional herb-couple formulation, where two herbs are prescribed together to decrease toxicity and/or increase efficacy. For example, inclusion of *Glycyrrhiza uralensis* can prevent or destroy the toxicity of treated Fuzi [1]. The main components are ginsenosides and alkaloids. SFD was originally described in *Ji Sheng Xu Fang* (1253 in western calendar) written by Yonghe in the Song Dynasty. In many formulae of Traditional Chinese Medicine (TCM), Renshen is frequently prescribed in combination with other herbs to decrease toxicity and increase efficacy. Ginsenosides are the main bioactive constituents in the famous Chinese herb Renshen. They include protopanaxadiol, protopanaxatriol, octotillol, and oleanolic acid. Aconitines are the main constituents in *Aconitum carmichaelii* Debx. Aconitines include monoester diterpenoid alkaloids (MDAs) and diester diterpenoid alkaloids (DDAs) and have differences in esterification. Their chemical structures are shown in Figure 1. Due to the high toxicity of DDAs, *Fuzi* is combined with *Renshen* to decrease its toxicity.

SFD is used to treat cardiovascular diseases such as circulatory collapse, shock, thoracic obstruction, and acute thoracic pain. It has a therapeutic effect on heart failure and ischemia-reperfusion injury [2]. One study showed that blockage of the sodium channels in cardiac myocytes may be one of the important molecular mechanisms of its cardiac effect [3]. There are no detailed studies of its mechanism of action, and the bioactive compounds that account for its therapeutic effects remain unclear.

While they have the so-called active ingredients, there are no empirical data to prove its effectiveness. Oral administration is one of the primary modes for TCM. The bioactive compounds are absorbed in the blood and transferred to the

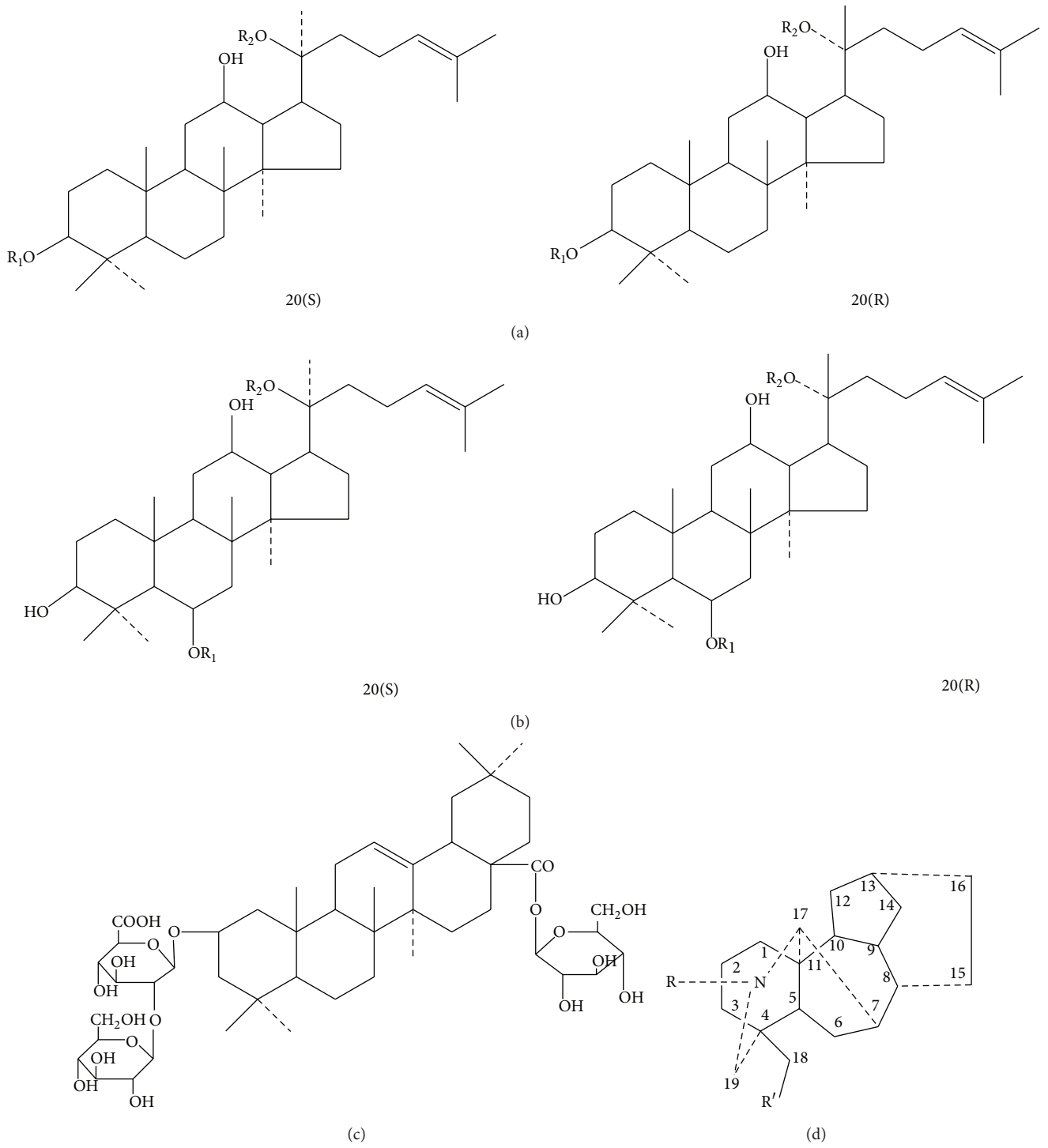

Figure 1: The chemical structure of 20(S)- and 20(R)-protopanaxadiol ginsenosides (a), 20(S)- and 20(R)-protopanaxatriol ginsenosides (b), oleanolic acid saponins type (c), and aconitines (d).

target. Thus, while there are multiple components in herbs, only those that are absorbed into circulation are effective [4].

Pharmacokinetics remains unresolved in the use of Chinese herbs. In our previous research, we focused on the influence of DDAs, drug metabolism enzymes, and transporters after the combination of *Renshen* and *Fuzi* [5–7]. Our previous study *in vitro* showed that there were significant differences between codecoction and mixed decoction of *Renshen* and *Fuzi* [5]. The content of toxic alkaloids was higher in mixed decoction than codecoction which was probably the attenuation basis. To confirm whether they behaved similarly *in vivo* is one of our goals. Here, we developed a rapid and sensitive Ultra Performance Liquid Chromatography/Quadrupole Time-of-Flight Mass Spectrometry

(UPLC/Q-TOF-MS) method to study the pharmacokinetics of SFD constituents.

2. Materials and Methods

2.1. Chemicals and Materials. HPLC-grade acetonitrile was purchased from Fisher Scientific (Waltham, MA, USA). Methanol was purchased from Sinopharm Chemical Reagent Co. (Shanghai, China). Formic acid was HPLC-grade (CNW Technologies GmbH, Dusseldorf, Germany). Renshen and Fuzi were purchased from Hebei Anguo Drug Market (Hebei, China) and authenticated by Professor Baipin Ma, Institute of Radiation Medicine Sciences of the Academy of Military Medical Sciences. The Renshen was at least 5-year growth white ginseng which was processed by the method of the *Chinese Pharmacopoeia* (2010) and the Fuzi was nonprocessed *Radix Aconiti Lateralis Preparata* (only for laboratory use). The vouched specimens were stored in storage room of the Department of Pharmacology and Toxicology of the Institute of Radiation Medicine Sciences of the Academy of Military Medical Sciences.

2.2. Preparation of Decoction and for LC-MS Analysis. Renshen (100 g) was soaked in 800 mL distilled water for 30 min and decocted for 1 h and then filtered. The residue was decocted in 500 mL distilled water for 1 h and filtered. The filtrate was then combined and labeled Renshen decoction. Fuzi (100 g) was decocted in 800 mL distilled water for 10 min and then filtered. The residue was decocted in 500 mL distilled water for 30 min and filtered and labeled Fuzi decoction. Then two different kinds of decoctions were prepared, namely, Renshen-Fuzi codecoction where the two herbs mixed together were extracted with water and Renshen-Fuzi mixed decoction where the individual herbs were extracted separately with water and the extracts then mixed together. The decoctions were evaporated to 1 g crude herb per mL. The decoctions were stored at 4°C, and the decoction samples were subjected to UPLC/Q-TOF-MS analysis, and the datasets were processed with MassLynx software.

2.3. Animals Handling and Serum Samples Preparation. Forty male Wistar rats (200 ± 20 g) were obtained from the Laboratory Animal Center of the Academy of Military Medical Sciences (Beijing, China, production certificate number SCXK-(M) 2007-004). All procedures were performed in accordance with the protocol outlined in the *Guide for the Care and Use of Laboratory Animals* published by the US National Institute of Health (NIH publication number 85-23, revised 1996) and approved by the Committee on the Ethics of Animal Experiments of the Academy of Military Medical Sciences. They were randomly divided into 5 groups: blank group (B-Group), *Renshen* decoction group (R-Group), *Fuzi* decoction group (F-Group), codecoction group (C-Group), and mixed decoction group (M-Group). There were 8 rats in each group. The rats were kept in an animal room with controlled environment (temperature: 22 ± 2°C, relative humidity: 55 ± 5%, and 12 h light-dark cycle) for 3 days before the experiment. All animals were free to access distilled water and standard food.

Every group except the blank group received an oral administration of 20 $g \cdot kg^{-1}$ decoction for 3 days. A distilled water vehicle control was given to the blank group. Blood samples (500 μL) were collected from the retroorbital sinus 1 h after oral administration on the 3rd day and centrifuged at 3000 rpm for 10 min. Then, 800 μL methanol was added to the 200 μL serum samples, vortexed, and then centrifuged at 13000 rpm for 10 min. The supernatant solution was transferred to another tube and dried with nitrogen gas. The residue was stored in 50% acetonitrile (200 μL) and frozen at −80°C until analysis.

2.4. Instrumentation and Chromatographic Conditions

2.4.1. Ultra Performance Liquid Chromatography. Chromatographic analysis was performed with an ACQUITY Ultra Performance Liquid Chromatography system (Waters, USA) controlled with MassLynx V4.1 software. Separation used an ACQUITY UPLC HSS T3 Column (2.1 × 100 mm, 1.8 μm, Waters). Water with 0.1% formic acid (v/v) and acetonitrile with 0.1% formic acid (v/v) were used as mobile phases A and B, respectively, at a flow rate of 0.45 $mL \cdot min^{-1}$. The gradient conditions of the mobile phase in positive mode were 0–2 min: 5% B; 2–6 min: 5–12% B; 6–8 min: 12–20% B; 8–16 min: 20–50% B; 16-17 min: 50–5% B; and 17-18 min: 5% B. The gradient conditions of the mobile phase in negative mode were 0-1 min: 25% B; 1–3 min: 25–30% B; 3–16 min: 30–35% B; 16-17 min: 35-25% B; and 17-18 min: 25% B.

2.4.2. Mass Spectrometry. A Waters Synapt High-Definition Time-of-Flight Mass Spectrometry (TOF-MS) system (Waters) equipped with an electrospray ionization (ESI) source operating in positive and negative mode was connected to the UPLC. A capillary voltage of 2.9 and 3.0 kV was used in positive and negative ionization mode, respectively. The desolvation temperature was 450°C, and the sampling cone voltage was 40 V. The extraction cone voltage was 4.0 V, source temperature was 100°C, and cone gas flow was 50 $L \cdot h^{-1}$. The desolvation gas flow rate was 900 $L \cdot h^{-1}$ in both positive and negative ionization modes. The mass was corrected during acquisition with leucine-enkephalin to generate a reference ion at m/z 556.2771 Da ($[M + H]^+$) in positive ion mode and m/z 554.2615 Da ($[M - H]^-$) in the negative ion mode. This ensured accurate mass measurements.

2.5. Data Analysis. All data were processed by MassLynx V4.1 software (Waters). The chromatographic peaks were integrated, aligned, and combined with accurate mass to charge ratios. A reference retention time was found for each expected compound. Using our previous work, the compounds in the decoction were identified [8–10]. The data were further processed by MarkerLynx XS software (Waters). The exported data list, partial least-squares-discriminant analysis (PLS-DA) as well as principal component analysis (PCA), was used to analyze the differences between the groups.

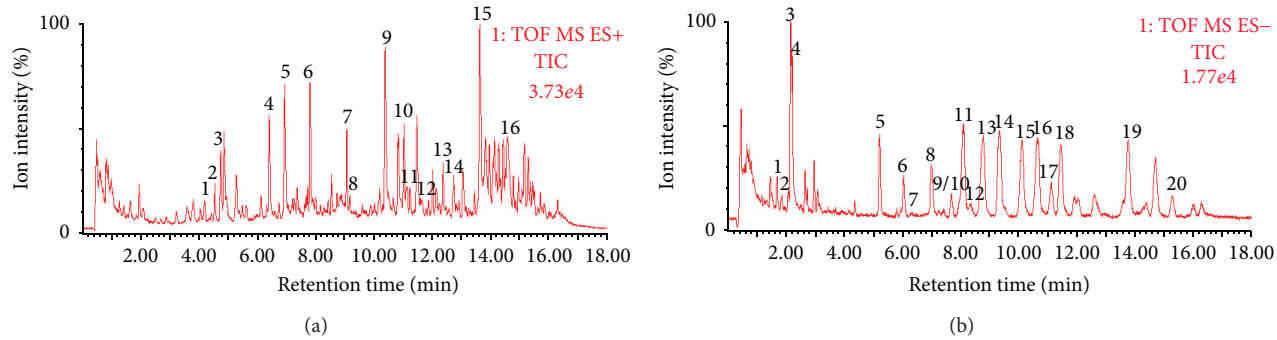

Figure 2: Total ion chromatogram of codecoction. (a) Positive ion mode detected alkaloids, (b) negative ion mode detected ginsenosides.

3. Results

3.1. Chemical Analysis of Codecoction. The ginsenosides and alkaloids in SFD were identified using UPLC combined with a TOF-MS detector. The total ion chromatogram of SFD in positive and negative ion modes is shown in Figure 2 and was processed with MassLynx V4.1 (Waters, USA). Comparing the retention time and mass data with reference compounds identified the target compounds. Both the MDAs and DDAs of alkaloids and 20(s)-protopanaxadiol type, 20(s)-protopanaxatriol type, and oleanolic acid saponin-type ginsenosides were detected in SFD. The chemical compositions are shown in Tables 1 and 2.

3.2. Alkaloids Difference in Serum Detected by Positive Mode

3.2.1. Differences in the Five Groups. All five groups were processed by PLS-DA and were used to highlight variation among the five groups (see Figure 3). Exported PCA plots and loading plots showed that the five groups formed five clusters. This indicated that the components in the serum were different.

3.2.2. Alkaloids Difference between B-Group, F-Group, M-Group, and C-Group. Comparing F-Group with B-Group, 14 kinds of alkaloids including DDAs, MDAs, and general alkaloids in aconitum plants were detected. Most of them were trace amount, which indicated the alkaloids poor absorption *in vivo*. The main reason was high efflux ratio reduced by P-glycoprotein [11–13]. These 14 kinds of alkaloids might be the chemical constituents involved in therapeutic efficacy of SFD. Some researchers thought that Fuzi's therapeutic activity (anti-inflammatory, analgesic, and cardiotonic activity) seems to have relevance to the presence of toxic alkaloids [14, 15] but the other researchers thought that Fuzi's toxicity compounds (mainly aconitine, mesaconitine, and hypaconitine) are not essential for its efficacy [16] (see Figure 4).

After detecting these 14 alkaloids, we further processed the data. Comparing C-Group with F-Group, the absorption of MDAs (benzoylaconine, mesaconine, 10-OH-benzoylmesaconine, and dehydrated benzoylmesaconine) decreased and the general alkaloids in aconitum plants (cammaconine, neoline, and talatizamine) increased. Most alkaloids (cammaconine, carmichaeline, talatizamine, acetyltalatizamine, and dehydrated benzoylhypaconine) absorption in M-Group was increased rather than F-Group. The increased or decreased absorption of alkaloids may contribute to the attenuation and synergistic effects. The decreased absorption of toxic alkaloids leads to attenuation and increased nontoxic alkaloids contribute to synergistic effects mainly because of compatibility of Renshen. The phenomenon was found in ancient year by the Chinese and we make it clear by analyzing the chemical compounds (see Figures 5 and 6).

The M-Group data showed that all alkaloids were absorbed more than the C-Group. The relative intensity of the ion indicated that the toxic chemicals (mesaconine, 10-OH-benzoylmesaconine, dehydrated benzoylmesaconine, and dehydrated benzoylhypaconine) were less absorbed than most general alkaloids in *Aconitum* plants (cammaconine, carmichaeline, fuziline, talatizamine, acetyltalatizamine, and neoline). The content of toxic alkaloids was higher in mixed decoction than codecoction which was probably the attenuation basis *in vitro*, and the results *in vivo* showed a similar consequence which indicated that the *Renshen* attenuated the toxicity of *Fuzi*. And ester exchange or degradation reactions occurring during the processing of codecoction with Renshen were considered to be the key factor of attenuation [5] (see Figure 7).

3.2.3. Ginsenosides Differences in the Serum in Negative Mode. The ginsenosides and alkaloids were detected in negative and positive mode, respectively. In our study, the codecoction and mixed decoction had small differences in the negative mode. This indicated that the ginsenosides behaved similarly, and the results presented the same tendency with an unpublished paper for the negative result *in vitro*. The same processing method used in positive mode was also applied to negative mode to analyze the ginsenoside differences. The PCA and PLS-DA/S-Plot showed no obvious distinction between the C-Group and the M-Group. However, 13 kinds of ginsenosides (GRg_1, GRe, GRd, GRo, GRc, GRb_2, GRb_3, GRb_1, GRa_2, GRa_1, MalonylGRc, $MalonylGRb_1$, and $MalonylGRb_2$) were detected in the serum of the *Panax ginseng* group. The extracted ion chromatogram and mass spectrogram of the ginsenosides are shown in Figures 8, 9, and 10.

Table 1: Alkaloids detected from codecoction.

Peak number	t_R (min)	Assigned identity	Molecular formula	$[M + H]^+/m/z$		
				Mean measured mass (Da)	Theoretical exact mass (Da)	Mass difference (ppm)
1	4.19	Mesaconine	$C_{24}H_{39}O_9N$	486.2725	486.2703	4.52
2	4.73	Carmichaeline	$C_{22}H_{35}O_4N$	378.2661	378.2644	4.49
3	4.86	Cammaconine	$C_{23}H_{37}O_5N$	408.2751	408.2750	0.24
4	6.39	Fuziline	$C_{24}H_{39}O_7N$	454.2806	454.2805	0.22
5	6.93	Neoline	$C_{24}H_{39}O_6N$	438.2863	438.2856	1.60
6	7.79	Talatizamine	$C_{24}H_{39}O_5N$	422.2898	422.2906	−1.89
7	9.05	Acetyltalatizamine	$C_{26}H_{41}O_6N$	464.3036	464.3012	5.17
8	9.16	10-OH-Benzoylmesaconine	$C_{31}H_{43}O_{11}N$	606.2959	606.2914	7.42
9	10.36	Benzoylmesaconine	$C_{31}H_{43}O_{10}N$	590.2980	590.2965	2.54
10	11.01	Benzoylaconine	$C_{32}H_{45}O_{10}N$	604.3125	604.3122	0.50
11	11.10	Dehydrated benzoylmesaconine	$C_{31}H_{41}O_9N$	572.2861	572.2860	0.17
12	11.86	10-OH-Mesaconitine	$C_{33}H_{45}O_{12}N$	648.3018	648.3020	−0.31
13	12.36	Dehydrated benzoylhypaconine	$C_{31}H_{41}O_8N$	556.2919	556.2910	1.62
14	12.70	Mesaconitine	$C_{33}H_{45}O_{11}N$	632.3054	632.3071	−2.69
15	13.61	Hypaconitine	$C_{33}H_{45}O_{10}N$	616.3087	616.3122	−5.68
16	14.58	Deoxyaconitine	$C_{34}H_{47}O_{10}N$	630.3254	630.3278	−3.81

Table 2: Ginsenoside identified from codecoction.

Peak number	t_R (min)	Assigned identity	Molecular formula	$[M-H]^-$ ($[M-H+HCOOH]^-$)/m/z		
				Mean measured mass (Da)	Theoretical exact mass (Da)	Mass difference (ppm)
1	1.72	Notoginsenoside R_1	$C_{47}H_{80}O_{18}$	977.5322	977.5321	0.10
2	1.76	20-Glucosylginsenoside Rf	$C_{48}H_{82}O_{19}$	961.5309	961.5372	−0.31
3	2.19	Ginsenoside Re	$C_{48}H_{82}O_{18}$	991.5481	991.5478	0.30
4	2.23	Ginsenoside Rg_1	$C_{42}H_{72}O_{14}$	845.4880	845.4899	−2.25
5	5.23	Ginsenoside Rf	$C_{42}H_{72}O_{14}$	799.4845	799.4844	0.13
6	6.06	Ginsenoside F_3	$C_{41}H_{70}O_{13}$	769.4738	769.4738	0.00
7	6.15	20(R)-Ginsenoside Rg_2	$C_{42}H_{72}O_{13}$	783.4873	783.4895	−2.81
8	7.01	Ginsenoside F_2	$C_{42}H_{72}O_{13}$	829.4943	829.4950	−0.84
9	7.69	Ginsenoside Ra_2	$C_{58}H_{98}O_{26}$	1209.5927	1209.5904	1.90
10	7.71	Ginsenoside Ra_1	$C_{58}H_{98}O_{26}$	1209.5928	1209.5904	1.98
11	8.11	Ginsenoside Rb_1	$C_{54}H_{92}O_{23}$	1107.5935	1107.5951	−1.44
12	8.70	Ginsenoside Ro	$C_{48}H_{76}O_{19}$	955.4913	955.4903	1.05
13	8.78	Malonylginsenoside Rb_1	$C_{57}H_{94}O_{26}$	1193.6003	1193.5955	4.02
14	9.33	Ginsenoside Rc	$C_{53}H_{90}O_{22}$	1077.5854	1077.5846	0.74
15	10.12	Malonylginsenoside Rc	$C_{56}H_{92}O_{25}$	1163.5876	1163.5850	2.23
16	10.64	Ginsenoside Rb_2	$C_{53}H_{90}O_{22}$	1077.5871	1077.5846	2.32
17	11.12	Ginsenoside Rb_3	$C_{53}H_{90}O_{22}$	1077.5871	1077.5846	−0.56
18	11.45	Malonylginsenoside Rb_2	$C_{56}H_{92}O_{25}$	1163.5879	1163.5850	2.49
19	13.76	Ginsenoside Rd	$C_{48}H_{82}O_{18}$	991.5476	991.5478	−0.20
20	15.25	Ginsenoside Ma-Rd	$C_{51}H_{84}O_{21}$	1031.5454	1031.5427	2.62

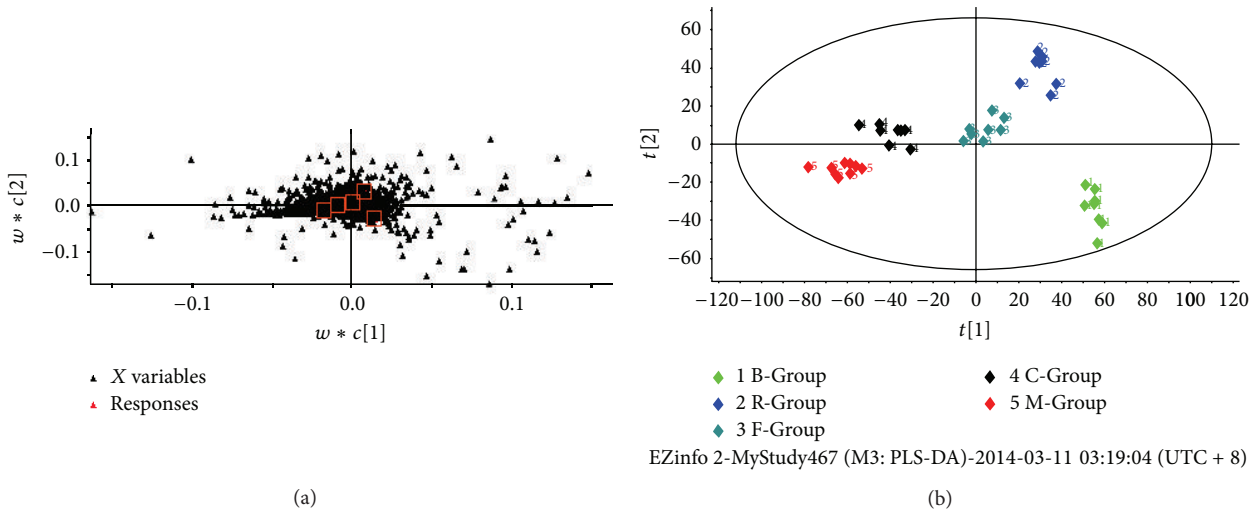

Figure 3: (a) PLS-DA loadings plot of five groups. (b) PCA score plot of the five groups. B-Group: blank group; R-Group: Renshen decoction group; F-Group: Fuzi decoction group; C-Group: codecoction group; M-Group: mixed decoction group. There were 8 rats in each group and each received an oral administration of 20 g·kg^{-1} decoction for 3 days. The blank group received an equivalent volume of distilled water.

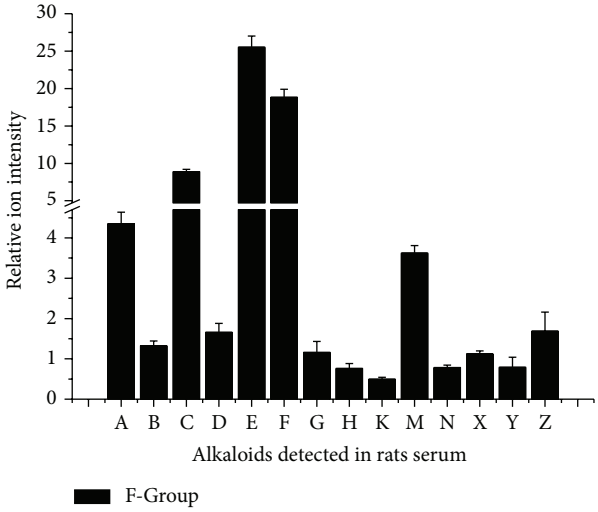

Figure 4: Relative content of alkaloids detected in F-Group serum. F-Group: Fuzi decoction group; A: cammaconine; B: carmichaeline; C: fuziline; D: neoline; E: talatizamine; F: acetyltalatizamine; G: mesaconine; H: 10-OH-benzoylmesaconine; K: benzoylaconine; M: benzoylmesaconine; N: dehydrated benzoylmesaconine; X: dehydrated benzoylhypaconine; Y: 10-OH-mesaconitine; Z: hypaconitine.

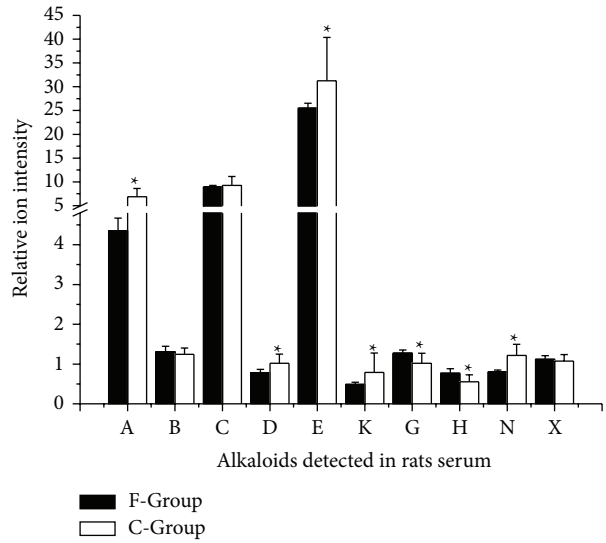

Figure 5: Relative content of alkaloids detected in rats serum of F-Group and C-Group. F-Group: Fuzi decoction group; C-Group: codecoction group. A: cammaconine; B: carmichaeline; C: fuziline; D: neoline; E: talatizamine; K: benzoylaconine; G: mesaconine; H: 10-OH-benzoylmesaconine; N: dehydrated benzoylmesaconine; X: dehydrated benzoylhypaconine.

4. Discussion

Researchers have reported quantitative analysis of aconitum alkaloids of SFD *in vitro* as well as the pharmacokinetic behavior of *Fuzi* and drug-drug interaction mechanisms in herb pair decoctions [17–19]. Relatively few studies have been conducted on the material basis of SFD *in vivo*, and most researchers focused on Shenfu injection which is a kind of processed Shenfu formulation [20, 21]. The material basis of toxicity reduction and pharmacological effect improvement *in vivo* remains unclear. In previous studies, the attenuation and synergistic effects of SFD including decoction time and herb ratio were studied *in vitro*. However, aconitum alkaloids serum levels were difficult to detect after oral administration, and only trace level was seen for its low bioavailability [18, 22]. Only Shenfu injected powder showed detectable alkaloids in serum [23]. Multicomponents and multitarget herbs resulted in complex systems with difficult detection. Recently, UPLC coupled with TOF-MS has become a vitally important tool in studying Chinese herbs. It is fast with good selectivity, high

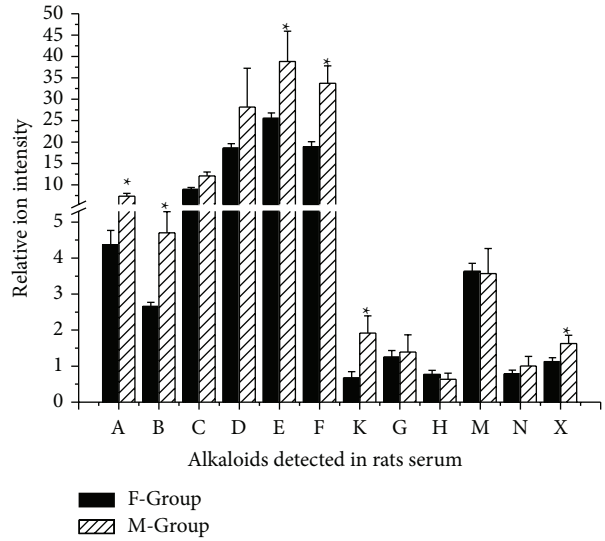

Figure 6: Relative content of alkaloids detected in rats serum of F-Group and M-Group. F-Group: Fuzi decoction group; M-Group: mixed decoction group. A: cammaconine; B: carmichaeline; C: fuziline; D: neoline; E: talatizamine; F: acetyltalatizamine; K: benzoylaconine; G: mesaconine; H: 10-OH-benzoylmesaconine; M: benzoylmesaconine; N: dehydrated benzoylmesaconine; X: dehydrated benzoylhypaconine.

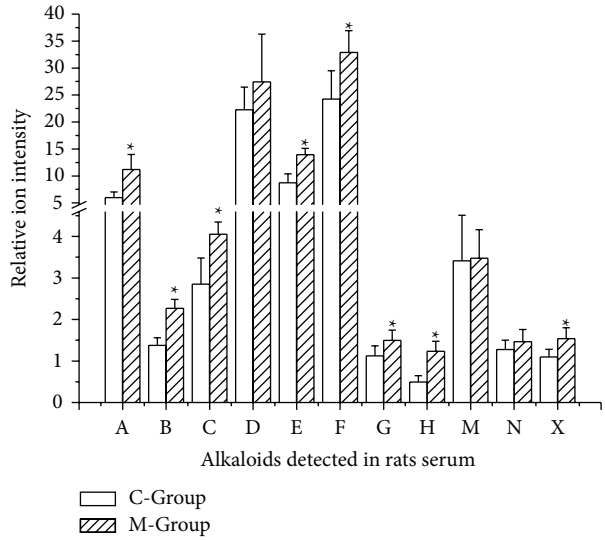

Figure 7: Relative content of alkaloids detected in rats serum of C-Group and M-Group. C-Group: codecoction group; M-Group: mixed decoction group. A: cammaconine; B: carmichaeline; C: fuziline; D: neoline; E: talatizamine; F: acetyltalatizamine; G: mesaconine; H: 10-OH-benzoylmesaconine; M: benzoylmesaconine; N: dehydrated benzoylmesaconine; X: dehydrated benzoylhypaconine.

resolution, and accurate mass measurements. This makes it attractive for the analysis of complex biological sample [24].

Shenfu formulation was a classical Chinese medicine for its obvious therapy efficiency on heart fail [25], but *Fuzi* in the formulation was a famous toxicity herb for its severe arrhythmia and neurological, cardiovascular, and gastrointestinal symptoms [26]. The herb pair was used for synergism and attenuation and the decoction method was thought to be the main reason for its chemical difference, but whether it behaves similarly *in vivo* was still a mystery, and here we approved an evidence to evaluate the Shenfu formulation *in vivo*. The concentration of hypaconitine and deoxyaconitine decreased, while benzoylmesaconine, benzoylhypaconine, and dehydrated benzoylmesaconine increased in the codecoction samples. The toxicity increased in single decocted or mixed decocted samples [5]. The codecoction inhibited toxic compounds, and the inhibited alkaloids dissolution resulted in a lower alkaloids content in the C-Group than the M-Group. They behaved similarly *in vivo* and *in vitro*. Here, *Renshen* showed evidence of increasing the absorption of alkaloids. These alkaloids were measured in a relative concentration range and found to be in accordance with the

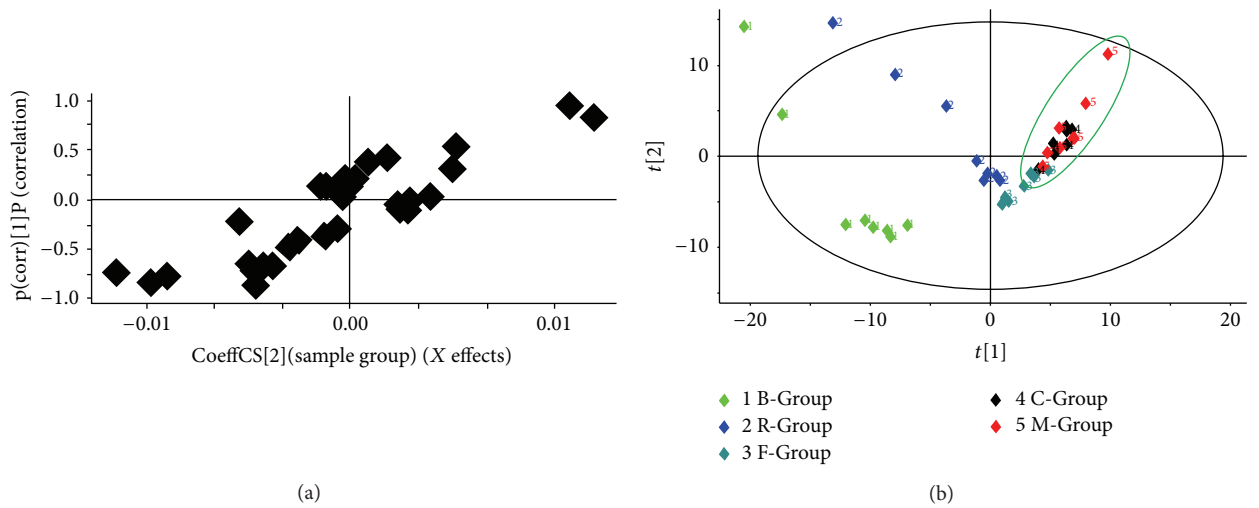

FIGURE 8: (a) PCA scores plot of C-Group and M-Group. (b) PLS-DA loadings plot of five groups. B-Group: blank group; R-Group: Renshen decoction group; F-Group: Fuzi decoction group; C-Group: codecoction group; M-Group: mixed decoction group. There were 8 rats in each group and each received an oral administration of 20 g·kg^{-1} decoction for 3 days. The blank group received an equivalent volume of distilled water.

tradition of TCM. We suspect that toxicity reduction is due to decoction *in vitro*; the pharmacological effect improvement is due to increased absorption and metabolism *in vivo*.

The pharmacological effect *in vivo* was affected by absorption and metabolism. In previous study, alkaloids were metabolized by Cytochrome P450 (CYP450) 3A [27]. A study on Shenfu injection indicated that it inhibited the enzyme activity of CYP3A at the mRNA level [6]. Mean Residence Time (MRT) increased when the enzyme activity was inhibited. Its absorption increase contributed to an increase in the Area under the Curve (AUC). The increased MRT and AUC indicated an increase in pharmacological effects.

Efflux transporters in the intestine play an important role in absorption. They also protect the body from toxin damage. The ATP-binding cassette transporters include P-glycoprotein (P-gp), multidrug resistance-associated protein isoform 2 (MRP2), and breast cancer resistance protein (BCRP). They modulate the absorption, distribution, metabolism, and excretion of medicine. These proteins are highly expressed in the apical membranes of intestinal epithelial, hepatic, and renal tubular cells. Transport studies show that the efflux ratios of aconitine, mesaconitine, and hypaconitine were significantly elevated due to P-gp and BCRP [11]. *Panax ginseng* and ginsenosides like ginsenoside Fl, ginsenoside Re, and ginsenoside Rb_2 induced the function of P-gp [28]. An important clue is seen in that Fuzi's toxicity compounds (aconitine, mesaconitine, and hypaconitine) are not essential for its efficacy [16]. While aconitine, mesaconitine, and hypaconitine were not detected in serum, it could be because they were below the detection limit.

The difference in molecular structure between DDAs and MDAs is an acetyl group. This caused the different efflux ratios. The lost acetyl group decreased the toxicity of the DDAs and the efflux ratio [29]. In another TCM herb pair *Fuzi-Ganjiang* formula, *Ganjiang* (*Rhizoma Zingiberis*, derived from the dry rhizome of *Zingiber officinale* Rosc.) was combined with *Fuzi* to decrease its toxicity and improve pharmacological effects. The authors showed that *Ganjiang* enhanced the absorption of MDAs and promoted the elimination of DDAs [30]. We could hypothesize that *Renshen* played the same role in these herb pairs. Our findings showed that nontoxic alkaloids in the M-Group and C-Group absorption increased more than F-Group. The absorption of alkaloids in mixtures or extractions was better than that of pure compounds seen in other experiments [12].

Like many other TCMs, SFD is always taken orally. Ginsenosides showed poor absorption and low bioavailability [31]. Major factors that limited the intestinal absorption of ginsenosides were poor membrane permeability and active biliary excretion. This limited systemic exposure to most ginsenosides and their deglycosylated metabolites [32]. The poor absorption and bioavailability of ginsenoside make them difficult to accurately measure in serum. Thus, we successfully developed a new method to measure ginsenoside previously. The different clearance rate of ginsenosides is considered to be the mechanism of Shenfu injection [10].

In the past decades, researchers have studied traditional Chinese formulas sufficiently, but the material basis and mechanism are still unclear with most data focusing on pharmacokinetics. Most studies are multicomponent herbs and with multiple targets *in vivo*. In addition to active compounds, there are also inactive and even toxic compounds in herbs. The material basis, pharmacology, component compatibility, and physiological disposition of TCM remain unclear. Understanding the attenuation and synergistic effects on absorption is an important goal of this study. Here, we studied the material basis of attenuation and synergistic effects by measuring the absorbed ingredients.

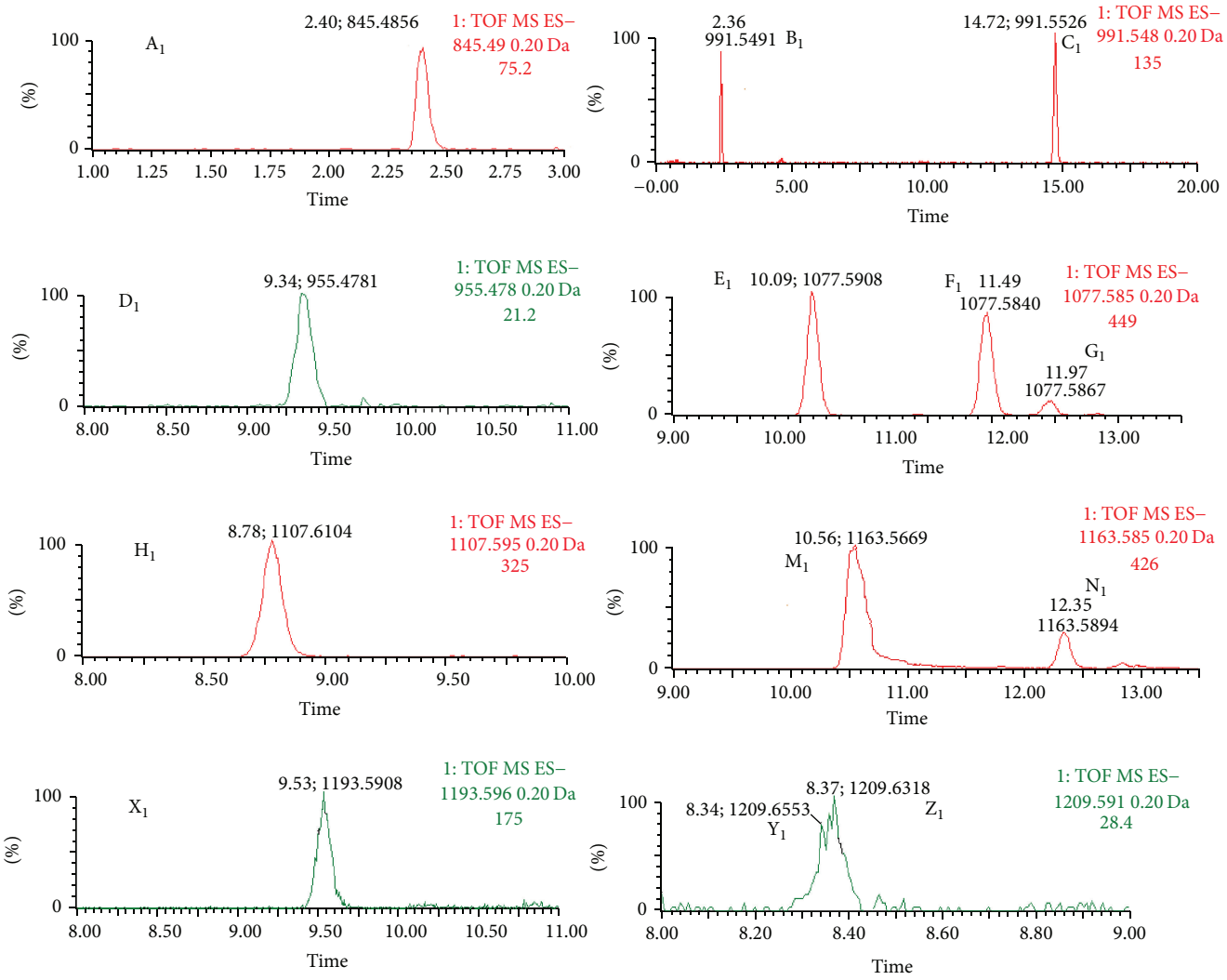

Figure 9: Extracted ion chromatogram of ginsenoside in negative ion mode. A_1: GRg_1 (Rt 2.40, *m/z* 845.4856), B_1: GRe (Rt 2.36, *m/z* 991.5491), C_1: GRd (Rt 14.72, *m/z* 991.5526), D_1: GRo (Rt 9.34, *m/z* 955.4781), E_1: GRc (Rt 10.09, *m/z* 1077.5908), F_1: GRb_2 (Rt 11.49, *m/z* 1077.5840), G_1: GRb_3 (Rt 11.97, *m/z* 1077.5867), H_1: GRb_1 (Rt 8.78, *m/z* 1107.6164), M_1: MalonylGRc (Rt 10.56, *m/z* 1163.5669), N_1: MalonylGRb$_1$ (Rt 12.35, *m/z* 1163.5894), X_1: MalonylGRb$_2$ (Rt 9.53, *m/z* 1193.5908), Y_1: GRa_2 (Rt 8.34, *m/z* 1209.6553), Z_1: GRa_1 (Rt 8.37, *m/z* 1209.6318).

Abbreviations

AUC:	Area under the Curve
B-Group:	Blank group
BCRP:	Breast cancer resistance protein
C-Group:	Codecoction group
CYP450:	Cytochrome P450
DDAs:	Diester diterpenoid alkaloids
F-Group:	Fuzi decoction group
MRT:	Mean Residence Time
MDAs:	Monoester diterpenoid alkaloids
M-Group:	Mixed decoction group
MRP2:	Multidrug resistance-associated protein isoform 2
P-gp:	P-glycoprotein
PLS-DA:	Partial least-squares-discriminant analysis
PCA:	Principal component analysis
R-Group:	Renshen decoction group
SFD:	Shenfu Decoction
TCM:	Traditional Chinese Medicine
UPLC/Q-TOF-MS:	Ultra Performance Liquid Chromatography/Quadrupole Time-of-Flight Mass Spectrometry.

Conflict of Interests

The authors declare no conflict of interests.

Authors' Contribution

Jia-le He and Jia-wei Zhao contributed equally to this work. Yu-guang Wang, Qian-de Liang, Hong-ling Tan, Cheng-rong Xiao, and Xiang-lin Tang carried out the animal surgery and

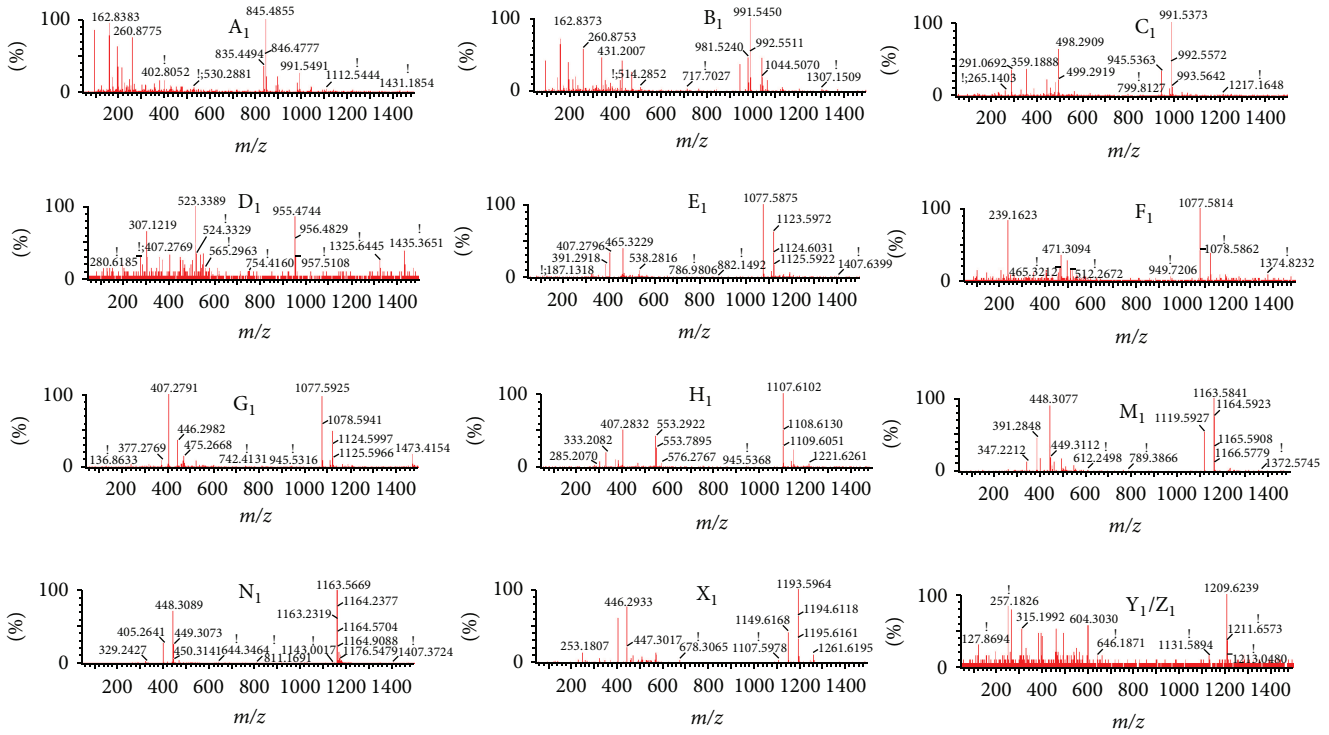

Figure 10: Mass spectrogram of ginsenoside in negative ion mode. A_1: GRg_1 (Rt 2.40, *m/z* 845.4856), B_1: GRe (Rt 2.36, *m/z* 991.5491), C_1: GRd (Rt 14.72, *m/z* 991.5526), D_1: GRo (Rt 9.34, *m/z* 955.4781), E_1: GRc (Rt 10.09, *m/z* 1077.5908), F_1: GRb_2 (Rt 11.49, *m/z* 1077.5840), G_1: GRb_3 (Rt 11.97, *m/z* 1077.5867), H_1: GRb_1 (Rt 8.78, *m/z* 1107.6164), M_1: MalonylGRc (Rt 10.56, *m/z* 1163.5669), N_1: $MalonylGRb_1$ (Rt 12.35, *m/z* 1163.5894), X_1: $MalonylGRb_2$ (Rt 9.53, *m/z* 1193.5908), Y_1: GRa_2 (Rt 8.34, *m/z* 1209.6553), Z_1: GRa_1 (Rt 8.37, *m/z* 1209.6318).

the blood collection. Zeng-chun Ma and Yue Gao contributed to critical review of the paper.

Acknowledgments

This work was supported by the National Natural Science Foundation of China (no. 81274127) and the National Basic Research Program of China ("973" Project nos. 2012CB518402 and 2011CB505304).

References

[1] J.-H. Chen, C.-Y. Lee, B.-C. Liau, M.-R. Lee, T.-T. Jong, and S.-T. Chiang, "Determination of aconitine-type alkaloids as markers in *fuzi* (*Aconitum carmichaeli*) by LC/(+)ESI/MS^3," *Journal of Pharmaceutical and Biomedical Analysis*, vol. 48, no. 4, pp. 1105–1111, 2008.

[2] Z.-J. Guo and C.-S. Li, "Therapeutic effects of shenfu injection on post-cardiac arrest syndrome," *Chinese Journal of Integrative Medicine*, vol. 19, no. 9, pp. 716–720, 2013.

[3] J. Luo, S. Min, K. Wei, and J. Cao, "Ion channel mechanism and ingredient bases of Shenfu Decoction's cardiac electrophysiological effects," *Journal of Ethnopharmacology*, vol. 117, no. 3, pp. 439–445, 2008.

[4] X. J. Wang, "Studies on serum pharmacochemistry of traditional Chinese medicine," *World Science and Technology*, vol. 4, no. 2, pp. 1–5, 2002.

[5] S.-S. Zhou, Z.-C. Ma, Y. Gao, and et al, "UPLC-TOF/MS based chemical profiling approach to evaluate toxicity-attenuated chemical composition in combination of ginseng and Radix Aconiti Praeparata," *Acta Pharmaceutica Sinica*, vol. 46, no. 12, pp. 1488–1492, 2011.

[6] H. Li, Y.-G. Wang, Z.-C. Ma et al., "Effect of Shenfu injection on CYP450s of rat liver," *Acta Pharmaceutica Sinica*, vol. 48, no. 5, pp. 728–733, 2013.

[7] Y.-G. Wang, H.-S. Liu, Y. Gao et al., "Screening of pregnane X receptor activation from ginsenosides," *Acta Pharmaceutica Sinica*, vol. 48, no. 1, pp. 144–148, 2013.

[8] S. S. Zhou, Z. C. Ma, Q. Liang et al., "UPLC/Q-TOF-MS based chemical profiling approach to evaluate chemical composition of augmentation toxicity in combination of radix aconiti and pinellia praeparata," *Acta Chimica Sinica*, vol. 70, no. 3, pp. 284–290, 2012.

[9] S. S. Zhou, Z. C. Ma, Y. Gao et al., "UPLC/Q-TOF-MS based chemical profiling approach to evaluate ginsenoside composition in combination of ginseng and radix ophiopogonis," *Journal of Chinese Mass Spectrometry Society*, vol. 34, no. 2, pp. 88–91, 2013.

[10] J.-L. He, S.-S. Zhou, Z.-C. Ma et al., "To evaluate the meterial basis of Shenfu injection based on UPLC-Q-TOF/MS," *Chinese Pharmacological Bulletin*, vol. 30, no. 3, pp. 429–433, 2014.

[11] L. Ye, X. S. Yang, Z. Q. Yang et al., "The role of efflux transporters on the transport of highly toxic aconitine, mesaconitine, hypaconitine, and their hydrolysates, as determined in cultured Caco-2 and transfected MDCKII cells," *Toxicology Letters*, vol. 216, no. 2-3, pp. 86–99, 2013.

[12] N. Li, R. Tsao, Z. G. Sui, J. Ma, Z. Lie, and Z. Lie, "Intestinal transport of pure diester-type alkaloids from an aconite extract across the Caco-2 cell monolayer model," *Planta Medica*, vol. 78, no. 7, pp. 692–697, 2012.

[13] C. Yang, Z. Li, T. Zhang, F. Liu, J. Ruan, and Z. Zhang, "Transcellular transport of aconitine across human intestinal Caco-2 cells," *Food and Chemical Toxicology*, vol. 57, pp. 195–200, 2013.

[14] A. Ameri, "The effects of *Aconitum* alkaloids on the central nervous system," *Progress in Neurobiology*, vol. 56, no. 2, pp. 211–235, 1998.

[15] A. M. Bello-Ramírez, J. Buendía-Orozco, and A. A. Nava-Ocampo, "A QSAR analysis to explain the analgesic properties of *Aconitum alkaloids*," *Fundamental and Clinical Pharmacology*, vol. 17, no. 5, pp. 575–580, 2003.

[16] P. J. Tong, C. L. Wu, X. F. Wang et al., "Development and assessment of a complete-detoxication strategy for Fuzi (lateral root of Aconitum carmichaeli) and its application in rheumatoid arthritis therapy," *Journal of Ethnopharmacology*, vol. 146, no. 2, pp. 562–571, 2013.

[17] N. Guo, M. T. Liu, D. W. Yang et al., "Quantitative LC-MS/MS analysis of seven ginsenosides and three *aconitum* alkaloids in Shen-Fu decoction," *Chemistry Central Journal*, vol. 7, no. 1, article 165, 7 pages, 2013.

[18] L. Tang, Y. Gong, C. Lv, L. Ye, L. Liu, and Z. Liu, "Pharmacokinetics of aconitine as the targeted marker of fuzi (*Aconitum carmichaeli*) following single and multiple oral administrations of fuzi extracts in rat by UPLC/MS/MS," *Journal of Ethnopharmacology*, vol. 141, no. 2, pp. 736–741, 2012.

[19] J.-M. Zhang, W. Liao, Y.-X. He, Y. He, D. Yan, and C.-M. Fu, "Study on intestinal absorption and pharmacokinetic characterization of diester diterpenoid alkaloids in precipitation derived from Fuzi-Gancao herb-pair decoction for its potential interaction mechanism investigation," *Journal of Ethnopharmacology*, vol. 147, no. 1, pp. 128–135, 2013.

[20] Z. Li, R. Zhang, X. Wang, X. Hu, Y. Chen, and Q. Liu, "Simultaneous determination of seven ginsenosides in rat plasma by high-performance liquid chromatography coupled to time-of-flight mass spectrometry: application to pharmacokinetics of Shenfu injection," *Biomedical Chromatography*, vol. 29, no. 2, pp. 167–175, 2015.

[21] H. Yang, L. Liu, W. Gao, K. Liu, L.-W. Qi, and P. Li, "Direct and comprehensive analysis of ginsenosides and diterpene alkaloids in Shenfu injection by combinatory liquid chromatography-mass spectrometric techniques," *Journal of Pharmaceutical and Biomedical Analysis*, vol. 92, pp. 13–21, 2014.

[22] T. Tazawa, H.-Q. Zhao, Y. Li et al., "A new enzyme immunoassay for aconitine and its application to quantitative determination of aconitine levels in plasma," *Biological and Pharmaceutical Bulletin*, vol. 26, no. 9, pp. 1289–1294, 2003.

[23] F. Zhang, M.-H. Tang, L.-J. Chen et al., "Simultaneous quantitation of aconitine, mesaconitine, hypaconitine, benzoylaconine, benzoylmesaconine and benzoylhypaconine in human plasma by liquid chromatography-tandem mass spectrometry and pharmacokinetics evaluation of 'SHEN-FU' injectable powder," *Journal of Chromatography B: Analytical Technologies in the Biomedical and Life Sciences*, vol. 873, no. 2, pp. 173–179, 2008.

[24] C.-Z. Wang, K. E. Kim, G.-J. Du et al., "Ultra-performance liquid chromatography and time-of-flight mass spectrometry analysis of ginsenoside metabolites in human plasma," *The American Journal of Chinese Medicine*, vol. 39, no. 6, pp. 1161–1171, 2011.

[25] C. X. Liu, Y. Z. Hou, X. L. Wang et al., "Clinical assessment of Shenfu injection loading in the treatment of patients with exacerbation of chronic heart failure due to coronary heart disease: study protocol for a randomized controlled trial," *Trials*, vol. 16, no. 1, article 222, 2015.

[26] Y. L. Zhao, J. B. Wang, X. J. Sun et al., "Microcalorimetry coupled with chemometric techniques for toxicity evaluation of *Radix Aconiti Lateralis Preparata (Fuzi)* and its processed products on *Escherichia coli*," *Applied Microbiology and Biotechnology*, vol. 98, no. 1, pp. 437–444, 2014.

[27] L. Ye, X.-S. Yang, L.-L. Lu et al., "Monoester-diterpene *aconitum* alkaloid metabolism in human liver microsomes: predominant role of CYP3A4 and CYP3A5," *Evidence-based Complementary and Alternative Medicine*, vol. 2013, Article ID 941093, 24 pages, 2013.

[28] Q. You, Z. C. Ma, Y. G. Wang et al., "Absorption characteristics of panax ginseng water extract in Caco-2 cell monolayer," *Chinese Pharmacology Bulletin*, vol. 29, no. 12, pp. 1711–1716, 2013.

[29] K. Wada, M. Nihira, H. Hayakawa, Y. Tomita, M. Hayashida, and Y. Ohno, "Effects of long-term administrations of aconitine on electrocardiogram and tissue concentrations of aconitine and its metabolites in mice," *Forensic Science International*, vol. 148, no. 1, pp. 21–29, 2005.

[30] W.-W. Peng, W. Li, J.-S. Li et al., "The effects of Rhizoma Zingiberis on pharmacokinetics of six *Aconitum alkaloids* in herb couple of Radix Aconiti Lateralis-Rhizoma Zingiberis," *Journal of Ethnopharmacology*, vol. 148, no. 2, pp. 579–586, 2013.

[31] J. Sun, W. Wu, Y. Y. Guo, Q. Qin, and S. Liu, "Pharmacokinetic study of ginsenoside Rc and simultaneous determination of its metabolites in rats using RRLC-Q-TOF-MS," *Journal of Pharmaceutical and Biomedical Analysis*, vol. 88, pp. 16–21, 2014.

[32] F. Zhao, L. Xu, and L. Xu, "Trains of thoughts and methods in studying substantial basis of effects of Chinese medicinal compounds," *Chinese Journal of Integrated Medicine*, vol. 27, no. 1, pp. 80–82, 2007.

Hindawi Publishing Corporation
Evidence-Based Complementary and Alternative Medicine
Volume 2015, Article ID 392405, 7 pages
http://dx.doi.org/10.1155/2015/392405

Research Article

Si Shen Wan Regulates Phospholipase Cγ-1 and PI3K/Akt Signal in Colonic Mucosa from Rats with Colitis

Duan-yong Liu,[1] Rong Xu,[2] Min-fang Huang,[2] Hong-yan Huang,[1] Xin Wang,[2] Yong Zou,[2] Hai-yang Yue,[2] and Hai-mei Zhao[3]

[1]*Science and Technology College, Jiangxi University of Traditional Chinese Medicine, Nanchang, Jiangxi 330025, China*
[2]*Department of Postgraduate, Jiangxi University of Traditional Chinese Medicine, Nanchang, Jiangxi 330004, China*
[3]*School of Basic Medical Sciences, Jiangxi University of Traditional Chinese Medicine, Nanchang, Jiangxi 330004, China*

Correspondence should be addressed to Duan-yong Liu; liuduanyong@163.com and Hai-mei Zhao; haimei79@163.com

Received 13 November 2014; Revised 29 January 2015; Accepted 2 February 2015

Academic Editor: Sae Uchida

The present study explored the feasible pathway of Si Shen Wan (SSW) in inhibiting apoptosis of intestinal epithelial cells (IECs) by observing activation of phospholipase Cγ-1 (PLC-γ1) and PI3K/Akt signal in colonic mucosa from rats with colitis. Experimental colitis was induced by 2,4,6-trinitrobenzene sulfonic acid (TNBS) in the Sprague-Dawley rats. After SSW was administrated for 7 days after TNBS infusion, western blot showed an increment in levels of PI3K, p-Akt, and IL-23 and a decrement in levels of PLC-γ1 and HSP70 in colonic mucosal injury induced by TNBS. Meanwhile, assessments by ELISA revealed an increment in concentrations of IL-2, IL-6, and IL-17 and a reduction in level of TGF-β after TNBS challenge. Impressively, treatment with SSW for 7 days significantly attenuated the expressions of PI3K and p-Akt and the secretion of IL-2, IL-6, IL-17, and IL-23 and promoted the activation of PLC-γ1, HSP70, and TGF-β. Our previous studies had demonstrated that SSW restored colonic mucosal ulcers by inhibiting apoptosis of IECs. The present study demonstrated that the effect of SSW on inhibiting apoptosis of IECs was realized probably by activation of PLC-γ1 and suppression of PI3K/Akt signal pathway.

1. Introduction

Inflammatory bowel disease (IBD) is an immunologically mediated chronic intestinal disorder, including ulcerative colitis and Crohn disease, which is characterized by bouts of severe intestinal inflammation and colonic mucosal ulcer [1, 2]. Although the exact etiology and pathogenesis of IBD still remains unclear, growing studies had indicated that intestinal epithelial cells (IECs) apoptosis played a significantly important role in the occur and procession of IBD [3, 4]. Excessive apoptosis with insufficient proliferation can disrupt intestinal mucosal integrity and barrier function and lead to injury of colonic mucous epithelium, ulcerative formation, and inflammatory cell infiltration and other changes associated with colitis [5, 6]. Therefore, inhibited excessive apoptosis of IECs is probably a necessary method to ameliorated colonic mucosal injury.

As a famous traditional Chinese herbal medicine formula, Si Shen Wan (SSW) is a classic prescription treated chronic colitis. In our previous studies, many evidences had proved that different dosages of SSW restored colonic mucosal ulcers induced by 2,4,6-trinitrobenzene sulfonic acid (TNBS) and dextran sulphate sodium salt (DSS); meanwhile, we found that SSW regulated colonic epithelial cell cycle and inhibited apoptosis of intestinal epithelial cells (IECs) from animals with colitis by intragastric administration. Furthermore, we observed that the antiapoptotic effect of SSW was probably realized by inhibiting mRNA expression of apoptosis-related molecules in p38 MAPK signal pathway. All results had demonstrated that SSW effectively treated colitis by inhibiting excessive apoptosis of IECs [7–9].

Although the molecular basis of IECs' apoptosis is unclear, it is known that cellular death of IECs is controlled by the intrinsic and extrinsic pathway. The extrinsic pathway activated by ligand-induced cell surface receptor (as tumor necrosis factor receptor 1 (TNFR1) and Fas) and the intrinsic mitochondrial apoptosis occurred by apoptotic-related proteins or signal pathway (as mitogen-activated

protein kinases (MAPKs), phospholipase C γ-1 (PLC-γ1) signal, phosphatidylinositol 3-kinase (PI3K)/Akt pathway, etc.) activation [5, 10].

PLC-γ, including two forms as PLC-γ1 and PLC-γ2, is a member of the family of phosphoinositide-specific PLCs (PI-PLC). PLC-γ1 is widely distributed in various kinds of tissues (e.g., colonic mucosa, intestine, lung, liver, etc.) [11]. PLC-γ1 plays an important protective role in cells apoptosis induced by H_2O_2 or ultraviolet C [12, 13]. Remarkably, elevated PLC-γ1 expression or activation of PLC-γ1 alone is sufficient to suppress cells apoptosis and involved their downstream targets (phosphatidylinositol 3-kinase (PI3K)/Akt signal proteins) of PLC-γ1 activation to mediate the protective effects [12, 13]. The present study sought to explore the molecular mechanism of SSW protecting apoptosis of IECs by observing activation of PLC-γ1 protein and their downstream signaling factors.

2. Materials and Methods

2.1. Animals. According to the Guidelines of Jiangxi University of Traditional Chinese Medicine (TCM), Animal Research Committee, forty Male Sprague-Dawley rats (weighing 200 to 220 g, certificate number: SCXK 2012-0001) were purchased from the Animal Center of Peking University Health Science Center. All rats were housed in a special room with a humidity of 50% ± 5% and lived in a 12 h light/dark cycle at 20 ± 2°C. Throughout the whole experiment, all animals were freely provided standard diet and water ad libitum. The rats were acclimatized for 3 days before experiments. The experimental protocols were supported by Jiangxi University of TCM Biomedical Ethics Committee, Experimental Animal Ethics Branch (JZ2014-79).

2.2. Drugs. Si Shen Wan (SSW) (batch number: 12080004) was purchased from Tongrentang (TRT) Pharma (Beijing, China). Mesalazine (batch number: 130407) was provided by Sunflower Pharma (Jiamusi, China). 2,4,6-Trinitrobenzene sulfonic acid (TNBS) (batch number: p2297) was gotten from Sigma (St. Louis, MO, USA).

2.3. Experimental Colitis Induced by TNBS. The animal model was induced according to the reported article with a little change [14, 15]. Briefly, the experimental colitis was induced by TNBS in rats. After 12 h of absolute diets, rat was lightly anesthetized with pentobarbital (60 mg/kg, i.p.) and received clyster with a dose of 100 mg/kg TNBS solution. The fresh solution was prepared in the light of the prescription (100 mg·kg^{-1} body TNBS was dissolved in 0.30 mL of 50% ethanol), and injected into the colon 8 cm proximal to the anus by a plastic hose tube whose diameter is 2 mm. And then, the rat was kept a head-down position for 15 min to full with the whole colon.

2.4. Experimental Protocol. According to calculating by body surface area between human and rat, we designed dosage of SSW and projected the experimental protocol on the basis of our previous studies [7–9]. Ten animals were in each group. The total 40 rats were randomly assigned into four groups: the Normal group (Normal; rats were induced and administrated by physiological saline), the TNBS 8d group (TNBS 8d; rats were induced by TNBS and 24 h thereafter physiological saline was administrated by gavage for 7 days), the TNBS 8d + SSW group (TNBS 8d + SSW; rats were induced by TNBS and 24 h thereafter SSW was administrated at 2.5 g/kg everyday by gavage for 7 days), and the TNBS 8d + Mesalazine group (TNBS 8d + Mesalazine; rats were induced by TNBS and 24 h thereafter Mesalazine was administrated at 300 mg/kg everyday by gavage for 7 days). At the end of treatment on day 9, all rats were fasted for 12 h and then sacrificed by cervical dislocation after anesthesia with intraperitoneally administrated urethane (2.0 g/kg). The whole colon was separated rapidly and opened longitudinally along colonic mesentery to clear its contents on an ice block. The colon was divided into two parts. One part was used to prepare colonic tissue homogenate, and the other was preserved in −80°C to Western blot analysis.

2.5. Enzyme-Linked Immunosorbent Assay. Colonic tissues were lysed in RIPA buffer (50 mM Tris-HCl at pH 7.4, 150 mM sodium chloride, 1% NP-40, 0.5% sodium deoxycholate, and 0.1% sodium dodecyl sulfate) with protease and phosphate inhibitor cocktail (Merk, Ashland, MA, USA) using a sonicator. Crude lysates were centrifuged at 19357 g for 20 min. The supernatant ($n = 10$) was used to measure the level of interleukin- (IL-) -2, IL-6, IL-17, and transforming growth factor- (TGF-) β1 by following the manufacturer instructions. Thecytokine ELISA kits (IL-2, IL-6, IL-17, and TGF-β1) were purchased from eBioscience (San Diego, CA).

2.6. Western Blot Analysis. Western blot analysis ($n = 6$ for each group) was performed as described previously [16]. Briefly, the protein concentration of the supernatants was measured by bicinchoninic acid (BCA) assay. The protein (10–30 μg) was separated by 9–12% sodium dodecyl sulphate-(SDS-) polyacrylamide gel electrophoresis for 1.5 h at 80 V and then blotted on polyvinylidene fluoride (PVDF) membranes (Amersham Pharmacia, Little Chalfont, UK). Membranes were treated with 5% nonfat dry milk in phosphate-buffered saline containing 0.01% Tween 20 (TBST) to block any nonspecific antibody binding sites and then probed overnight at 4°C with anti-PLC-γ1, phospho-PLC-γ1, -Akt, anti-phospho-Akt, PI3K, IL-23, HSP70, and GAPDH (Abcam, Cambridge, UK) monoclonal antibody at 1 : 1000–1 : 4,000 dilution with TBST containing 5% nonfat dry milk. After washing with TBST, the membranes were incubated for 1 h at room temperature with secondary HRP conjugated antibody (Dako, Glostrup, Denmark, 1 : 4,000) and visualized using ECL detection kit (Amersham Pharmacia, Uppsala, Sweden). Finally, bands were quantified using Image-Pro Plus 5.0 software (Media Cybernetic, Bethesda, MD, USA).

2.7. Statistical Analysis. All statistical analyses were performed with SPSS version 15.0 (SPSS Inc., Chicago, IL, USA) for Windows. Measurement data were expressed as

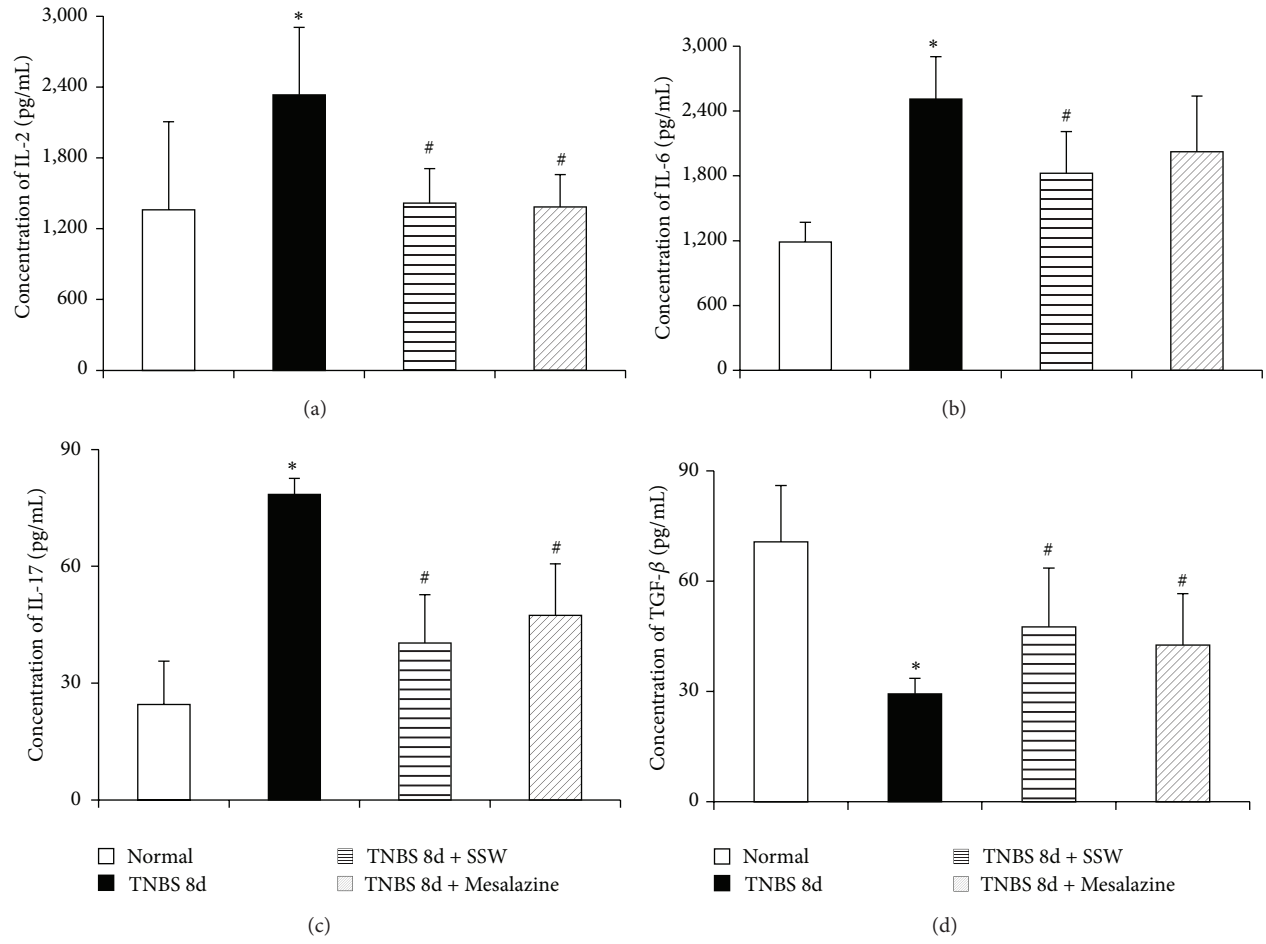

Figure 1: Concentration of IL-2, IL-6, IL-17, and TGF-β in colonic mucosa. (a) Concentration of IL-2 in colonic mucosa from different groups. (b) Concentration of IL-6 in colonic mucosa from different groups. (c) Concentration of IL-17 in colonic mucosa from different groups. (d) Concentration of TGF-β in colonic mucosa from different groups. Data were mean ± SD ($n = 10$). $^{*}P < 0.05$ versus Normal group; $^{\#}P < 0.05$ versus TNBS 8d group.

mean ± SD and analyzed using an analysis of variance (ANOVA) followed by the Tukey test for comparison of >2 condition. In this study, a difference was considered significant when $P < 0.05$.

3. Results

3.1. SSW Decreased the Levels of IL-2, IL-6, IL-17, and IL-23, and Increased the Level of TGF-β in Colonic Mucosa. After 7 days that experimental colitis was induced by TNBS and proinflammatory cytokines were released in inflammatory zone. In Figures 1(a), 1(b), 1(c), 3(a) and 3(b), the levels of IL-2, IL-6, IL-17, and IL-23 in colonic mucosa from colitis rats in the model group increased remarkably when they were compared with that in the Normal groups ($P < 0.05$). However, the expressions of the four cytokines decreased markedly in the TNBS 8d + SSW group ($P < 0.05$). While in Figure 1(d), compared with in the normal colonic mucosa, TGF-β was low expression in colonic mucosa from colitis rats in the model group ($P < 0.05$). But the level of TGF-β was higher in the TNBS 8d + SSW groups than that in the TNBS 8d group ($P < 0.05$). Except for IL-6, statistical results of the other three cytokines and TGF-β in the Mesalazine group were consistent with the TNBS 8d + SSW group. It is no statistical difference between the TNBS 8d + SSW group and the Mesalazine group.

3.2. SSW Elevated Expressions of PLC-γ1 and Hsp70 in Colonic Mucosa. The expressions of PLC-γ1 and Hsp70 were assessed by Western blot. In Figures 2(a), 2(b), 3(c), and 3(d), when they were compared with colitis rats without treatment, the expressions of PLC-γ1 and Hsp70 were elevated significantly after 7 days of treatment by SSW and Mesalazine or in the Normal group ($P < 0.05$).

3.3. SSW Inhibited Expression of PI3K, p-Akt in Colonic Mucosa, and Decreased the Ratio of p-Akt/Akt. The PI3K is one of downstream proteins of PLC-γ signal [17]. The expression of PI3K and the activation of phosphor-Akt (p-Akt) were analyzed by Western blot. As seen in Figures 2(a), 2(c) and 2(d), we found that the expressions of PI3K and

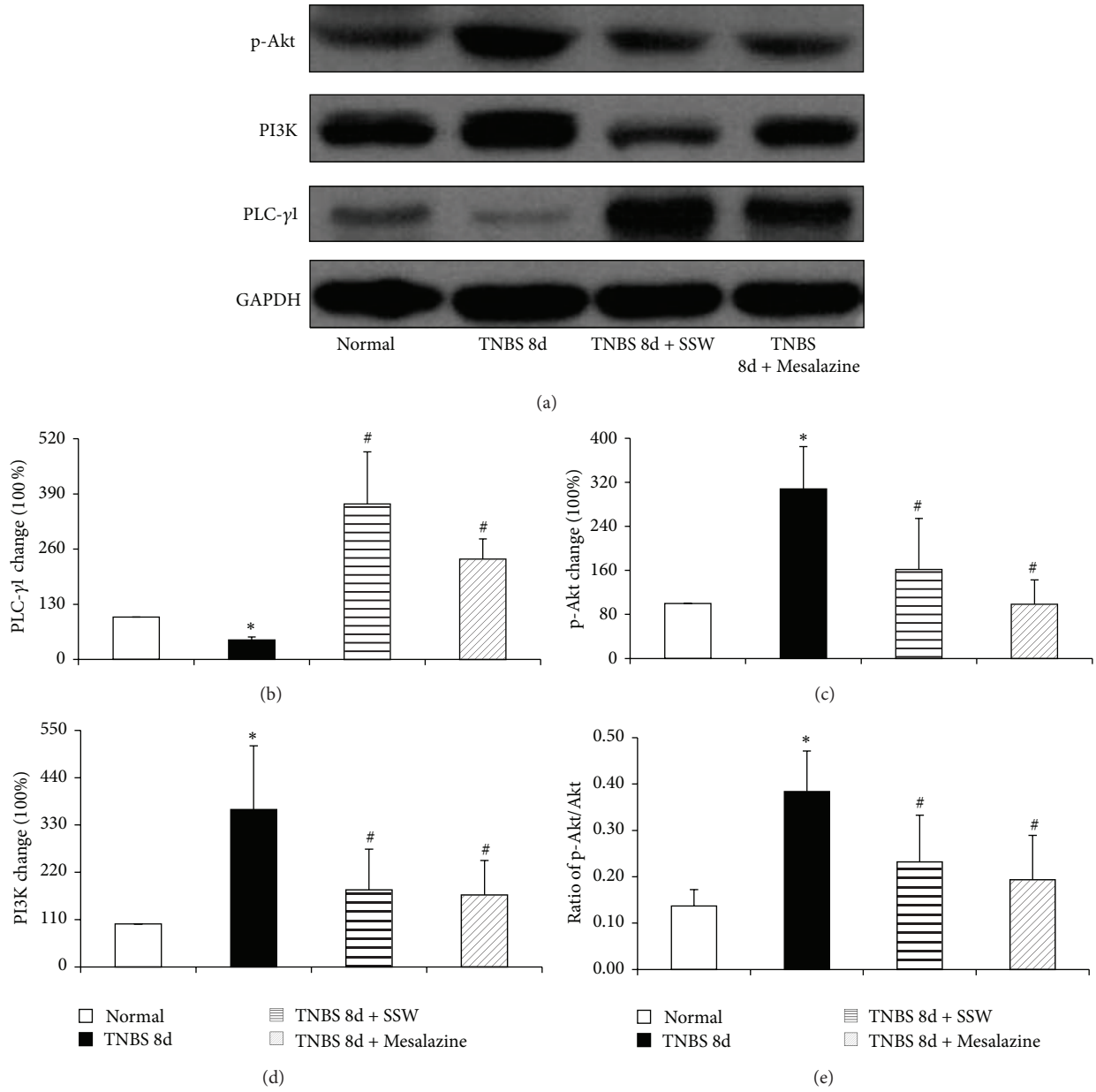

Figure 2: Western blot analysis of PLC-γ1, PI3K, and p-Akt. (a) Representative Western blot of PLC-γ1, PI3K, p-Akt, and GAPDH ($n = 6$). (b) Quantitative analysis of PLC-γ1 protein ($n = 6$). (c) Quantitative analysis of p-Akt protein ($n = 6$). (d) Quantitative analysis of PI3K protein ($n = 6$). (e) Ratio of p-Akt/Akt. Data were mean ± SEM ($n = 6$). $^{*}P < 0.05$ versus Normal group; $^{\#}P < 0.05$ versus TNBS 8d group.

p-Akt were distinctly heightened in the colonic mucosa from colitis rats without treatment when they compared with that in normal rats ($P < 0.05$). Nevertheless, it was very worthy that their expressions were reduced obviously in the colitis rats treated by 7 days of SSW and Mesalazine ($P < 0.05$). In the meantime, we computed the ratio of p-Akt/Akt to show the extent of phosphor-Akt in the present study ($P < 0.05$). The ratio was lower after 7 days of treatment with SSW and Mesalazine than in the TNBS 8d groups ($P < 0.05$) (Figure 2(e)). The results declared that the phosphorylation of Akt was inhibited after treatment by SSW.

4. Discussion

Increased apoptosis of colonic epithelial cells is an important character in the pathological change of IBD [3, 4]. In our previous studies, we had proved that SSW effectively treated TNBS- or DSS-induced experimental colitis by inhibiting IECs apoptosis [7–9]. In the present study, SSW significantly elevated expression of PLC-γ protein in the colonic mucosa from colitis rats and, meanwhile, inhibited activation of PI3K and p-Akt. Both of the two results hinted that the effect of SSW inhibiting IECs apoptosis was probably related to the activation of PLC-γ signal and PI3K/Akt pathway.

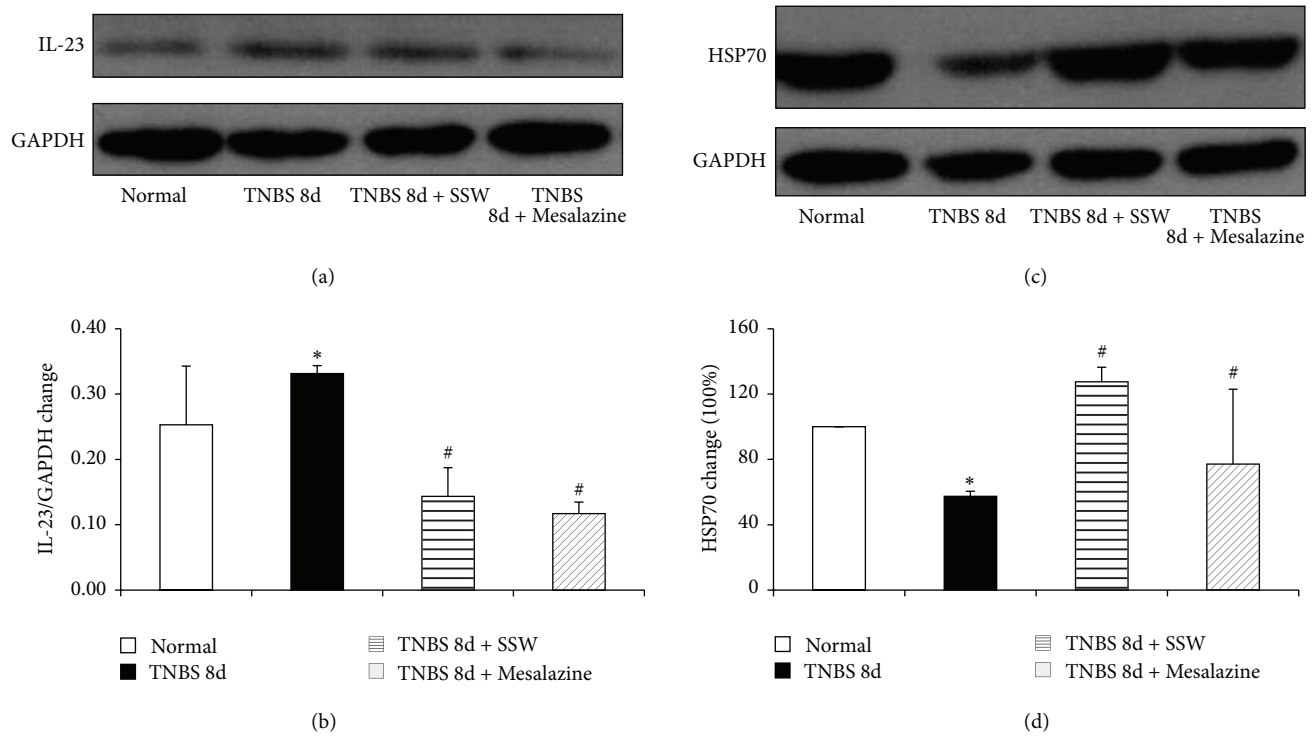

Figure 3: Western blot analysis of IL-23 and HSP70. (a) Representative Western blot of IL-23 and GAPDH ($n = 6$). (b) Quantitative analysis of IL-23 protein ($n = 6$). (c) Representative Western blot of HSP70 and GAPDH ($n = 6$). (d) Quantitative analysis of HSP70 protein ($n = 6$). Data were mean ± SEM ($n = 6$). $^{*}P < 0.05$ versus Normal group; $^{\#}P < 0.05$ versus TNBS 8d group.

As an important intermediary of growth factor signal pathway in the family of phosphoinositide-specific PLCs (PI-PLC), PLC-γ1 is double identity of important molecule in which PLC-γ1 can regulate and control cell proliferation and apoptosis [13, 18–20]. Growing evidences have demonstrated that PLC-γ1 plays a negative control role in the process of cell apoptosis. Some researchers had observed that obvious apoptotic morphology and the percentage of apoptotic cells were dramatically exhibited and rose when the PLC-γ1 signal pathway was inhibited by blocker [21]. In present and previous studies, we had found that low expression of PLC-γ1 and increased IECs apoptosis were simultaneously seen in the same animal model induced by TNBS, while SSW effectively decreased IECs apoptosis and improved expression of PLC-γ1 to alleviate colonic mucosal injury of rats with experimental colitis. The results had shown that the protective effect of SSW on damaged colonic mucosa was realized by promoting PLC-γ1 activation to inhibit IECs apoptosis [7–9]. The probable mechanism of PLC-γ1 signal is that proteolytic cleavage of PLC-γ1 is blocked by overexpression of Bcl-2, which can prevent apoptosis at a step during the activation of caspase family proteases such as caspase-9 and caspase-3 [22]. This point was in accord with our previous study showing that SSW heightened expression of Bcl-2 mRNA in colonic mucosa from rats with colitis [7].

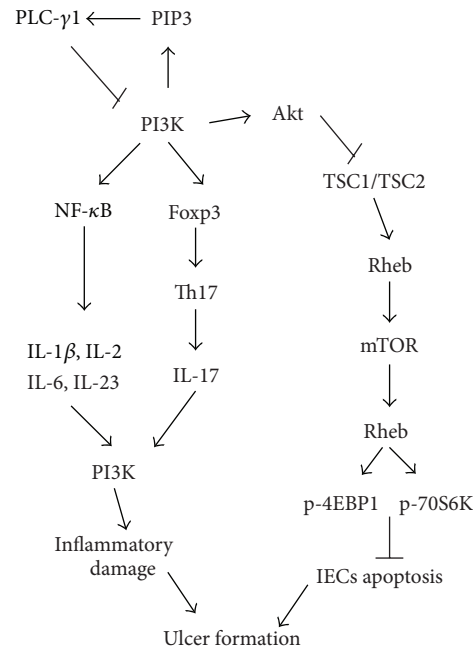

Figure 4: Schematic illustration of PLC-γ1 and PI3K/Akt signal.

As shown in Figure 4, many studies had indicated that PLC-γ1 pathway and PI3K-Akt pathway interacted with each other. However it is not known whether PLC-γ1 directly binds to Akt and well known that PI3K may affect the translocation of PLC-γ1 by generating PI3P [23] and that both PLC-γ1 and phosphatidylinositol 3-kinase (PI3K)/Akt signal are essential mediators of cellular processes such as growth, apoptosis, and cell proliferation [24, 25].

Recently, it is a hotspot that PI3K/Akt signal pathway, including PI3K, Akt, phosphatase, and tens in homolog on chromosome10 (PTEN), tuberous sclerosis complex 1/2 (TSC1/2) and target of rapamycin (mTOR), plays central roles in regulating cell growth and apoptosis. PIP3 is generated by activation of PI3K and can interact with PI3K to activate Akt by phosphorylation on Ser473 in a hydrophobic motif and Thr308 in the activation loop of the kinase domain. As a candidate, mTOR is activated by inhibiting TSC 1/2 or phosphorylated by phosphoinositide dependent protein kinase 1 (PDK1) [26, 27]. As a core controller of cyclin synthetic, activated mTOR may phosphorylate 4EBP1 and activate S6-kinase (p70S6 K) to enhance protein translation following Hsp70, Protor, and Deptor and finally inhibit cell apoptosis with independent of p53 [26, 28, 29]. Previous studies had shown that mesalazine effectively treated mice with Dss-induced colitis and affected the PI3K/Akt signal [30, 31].

Meanwhile, the primary function of PI3K-driven NF-κB activation is to promote expression and secretion of cytokines (IL-6, IL-23, IL-2, etc.) and chemokines [32]. Luyendyk and his colleagues had found that inhibition of PI3K/Akt pathway decreased transcriptional level of downstream cytokines (IL-6, IL-1β, and IL-2) to alleviate severity of inflammation [33]. And that PI3K signal can inhibit expression of Foxp3 and restrain activation of regulatory of T cell and activate Th17 cell. Activatory Th17 cells secreted abundant IL-17 and IL-23 contributed to the occurrence of several autoimmune diseases such as IBD and rheumatoid arthritis [34, 35].

In the present study, PI3K and p-Akt proteins were activated in the colonic mucosa from colitis rats without treatment; in the meantime, the levels of IL-2, IL-6, IL-17, and IL-23 were increased, and the expressions of HSP70 and TGF-β were decreased. This hinted that in the course of TNBS-induced colitis, activated PI3K/Akt signal pathway possibly heightened transcription of NF-κB, and then promoted to secrete proinflammatory cytokines (including IL-2, IL-6, IL-17, and IL-23), inhibited expressions of HSP70 and TGF-β, and finally led to inflammatory injury of colonic mucosa. Interestingly, PI3K signal was inactivated after treatment with SSW, the ratio of p-Akt/Akt was reduced, the secretions of those cytokines were downregulated, and the levels of HSP70 and TGF-β were elevated. These evidences indicated that SSW had inactivated PI3K/Akt signal pathway. Meanwhile, we found that there was no difference between SSW and Mesalazine to regulate expression of these cytokines and proteins. The results hinted that SSW had some extent similar to Mesalazine on curative effect and probable pharmacological mechanism. To sum up, SSW can restrain PI3K/Akt signal and activated PLC-γ1 protein in colonic mucosa from colitis rats. As a complex system, abundant active constituents of SSW and their pharmacological action are uncertain. However, several known constituents (including evodiamine and rutaecarpine) treated experimental colitis and controlled apoptosis by regulating PI3K/Akt signal (as evodiamine) [36, 37]. Nevertheless, a definite element of SSW to treat IBD by PLC-γ1 and PI3K/Akt signal has not been reported. Consequently, the next step would be very significant to seek out effective component of SSW.

5. Conclusions

According to our previous studies, in conclusion, effect of SSW on inhibiting IECs apoptosis is potentially related with activation of PLC-γ1 and retardant of PI3K/Akt signal pathway in the therapeutic process of IBD.

Conflict of Interests

All authors have declared that there is no conflict of interests.

Acknowledgments

This research is supported in part by the Project of National Natural Science Foundation of China (nos. 81460679 and 81260595) and funded by Chinese Scholarship Council and Jiangxi Province as visiting scholar (CSC: 201408360106, 201408360110), the Science and Technology Project of Education Department of Jiangxi Province (no. GJJ13611), and the Science and Technology Project of TCM from the Department of Health of Jiangxi Province (no. 2012A020).

References

[1] L. Eckmann, T. Nebelsiek, A. A. Fingerle et al., "Opposing functions of IKKβ during acute and chronic intestinal inflammation," *Proceedings of the National Academy of Sciences of the United States of America*, vol. 105, no. 39, pp. 15058–15063, 2008.

[2] X. Liu, J. M. Wang, and S. Bereswill, "Iridoid glycosides fraction of Folium syringae leaves modulates NF-κB signal pathway and intestinal epithelial cells apoptosis in experimental colitis," *PLoS ONE*, vol. 6, no. 9, Article ID e24740, 2011.

[3] J. B. Seidelin and O. H. Nielsen, "Attenuated apoptosis response to Fas-ligand in active ulcerative colitis," *Inflammatory Bowel Diseases*, vol. 14, no. 12, pp. 1623–1629, 2008.

[4] M. Strus, A. Janczyk, A. Gonet-Surowka et al., "Effect of hydrogen peroxide of bacterial origin on apoptosis and necrosis of gut mucosa epithelial cells as a possible pathomechanism of inflammatory bowel disease and cancer," *Journal of Physiology and Pharmacology*, vol. 60, no. 6, pp. 55–60, 2009.

[5] R. Dirisina, R. B. Katzman, T. Goretsky et al., "p53 and PUMA independently regulate apoptosis of intestinal epithelial cells in patients and mice with colitis," *Gastroenterology*, vol. 141, no. 3, pp. 1036–1045, 2011.

[6] G. S. Lichtenberger, R. A. Flavell, and L. Alexopoulou, "Innate immunity and apoptosis in IBD," *Inflammatory Bowel Diseases*, vol. 10, supplement 1, pp. S58–S62, 2004.

[7] H.-M. Zhao, X.-Y. Huang, F. Zhou et al., "Si Shen Wan inhibits mRNA expression of apoptosis-related molecules in p38 MAPK signal pathway in mice with colitis," *Evidence-based Complementary and Alternative Medicine*, vol. 2013, Article ID 432097, 8 pages, 2013.

[8] D.-Y. Liu, Y.-M. Guan, H.-M. Zhao et al., "The protective and healing effects of Si Shen Wan in trinitrobenzene sulphonic acid-induced colitis," *Journal of Ethnopharmacology*, vol. 143, no. 2, pp. 435–440, 2012.

[9] D. Liu, X. Huang, S. Cheng et al., "Regulation of Sishen Wan on Bax/Bcl-2 mRNA, Fas/FasL in colonic tissue from rats with colitis," *China Joural of Chinese Meteria Medica*, vol. 36, no. 24, pp. 3484–3488, 2011.

[10] D. Brenner and T. W. Mak, "Mitochondrial cell death effectors," *Current Opinion in Cell Biology*, vol. 21, no. 6, pp. 871–877, 2009.

[11] M. J. Smit, P. Verdijk, E. M. H. van der Raaij-Helmer et al., "CXCR3-mediated chemotaxis of human T cells is regulated by a G i-and phospholipase C-dependent pathway and not via activation of MEK/p44/p42 MAPK nor Akt/PI-3 kinase," *Blood*, vol. 102, no. 6, pp. 1959–1965, 2003.

[12] W. Yuan, J. Guo, X. Li et al., "Hydrogen peroxide induces the activation of the phospholipase C-γ1 survival pathway in PC12 cells: protective role in apoptosis," *Acta Biochimica et Biophysica Sinica*, vol. 41, no. 8, pp. 625–630, 2009.

[13] X.-C. Bai, D. Lu, J. Bai et al., "Oxidative stress inhibits osteoblastic differentiation of bone cells by ERK and NF-κB," *Biochemical and Biophysical Research Communications*, vol. 314, no. 1, pp. 197–207, 2004.

[14] J.-P. Segain, D. R. De la Blétière, V. Sauzeau et al., "Rho kinase blockade prevents inflammation via nuclear factor κB inhibition: evidence in Crohn's disease and experimental colitis," *Gastroenterology*, vol. 124, no. 5, pp. 1180–1187, 2003.

[15] D. Gao, A. H. Wagner, S. Fankhaenel et al., "CD40 antisense oligonucleotide inhibition of trinitrobenzene sulphonic acid induced rat colitis," *Gut*, vol. 54, no. 1, pp. 70–77, 2005.

[16] F. Huang, C.-Y. Kao, S. Wachi, P. Thai, J. Ryu, and R. Wu, "Requirement for both JAK-mediated PI3K signaling and ACT1/TRAF6/TAK1- dependent NF-κB activation by IL-17A in enhancing cytokine expression in human airway epithelial cells," *Journal of Immunology*, vol. 179, no. 10, pp. 6504–6513, 2007.

[17] S. K. Sukumaran, G. McNamara, and N. V. Prasadarao, "*Escherichia coli* K-1 interaction with human brain microvascular endothelial cells triggers phospholipase C-γ1 activaiotn downstream of phosphatidylinositol 3-kinase," *The Journal of Biological Chemistry*, vol. 278, no. 46, pp. 45753–45762, 2003.

[18] A. Wells and J. R. Grandis, "Phospholipase C-γ1 in tumor progression," *Clinical and Experimental Metastasis*, vol. 20, no. 4, pp. 285–290, 2003.

[19] S. Khoshyomn, P. L. Penar, J. Rosso, A. Wells, D. L. Abramson, and A. Bhushan, "Inhibition of phospholipase C-γ1 activation blocks glioma cell motility and invasion of fetal rat brain aggregates," *Neurosurgery*, vol. 44, no. 3, pp. 568–577, 1999.

[20] D. Hanahan and R. A. Weinberg, "The hallmarks of cancer," *Cell*, vol. 100, no. 1, pp. 57–70, 2000.

[21] J. Liu, M. Li, W. S. Zeng, X. C. Bai, and S. Q. Luo, "Inhibition of phospholipase C γ1 signaling pathway promotes apoptosis of human colorectal carcinoma cells," *Di Yi Jun Yi Da Xue Xue Bao*, vol. 25, no. 2, pp. 177–180, 2005.

[22] J. Yang, X. Liu, K. Bhalla et al., "Prevention of apoptosis by Bcl-2: Release of cytochrome c from mitochondria blocked," *Science*, vol. 275, no. 5303, pp. 1129–1132, 1997.

[23] Y. Wang and Z. Wang, "Regulation of EGF-induced phospholipase C-gamma1 translocation and activation by its SH2 and PH domains," *Traffic*, vol. 4, no. 9, pp. 618–630, 2003.

[24] L. C. Cantley, "The phosphoinositide 3-kinase pathway," *Science*, vol. 296, no. 5573, pp. 1655–1657, 2002.

[25] J. Luo, B. D. Manning, and L. C. Cantley, "Targeting the PI3K-Akt pathway in human cancer: rationale and promise," *Cancer Cell*, vol. 4, no. 4, pp. 257–262, 2003.

[26] M. Razmara, C.-H. Heldin, and J. Lennartsson, "Platelet-derived growth factor-induced Akt phosphorylation requires mTOR/Rictor and phospholipase C-γ1, whereas S6 phosphorylation depends on mTOR/Raptor and phospholipase D," *Cell Communication and Signaling*, vol. 11, article 3, pp. 1–12, 2013.

[27] D. D. Sarbassov, D. A. Guertin, S. M. Ali, and D. M. Sabatini, "Phosphorylation and regulation of Akt/PKB by the rictor-mTOR complex," *Science*, vol. 307, no. 5712, pp. 1098–1101, 2005.

[28] N. Hay and N. Sonenberg, "Upstream and downstream of mTOR," *Genes and Development*, vol. 18, no. 16, pp. 1926–1945, 2004.

[29] B. A. Jacobson, A. De, M. G. Kratzke et al., "Activated 4E-BP1 represses tumourigenesis and IGF-I-mediated activation of the eIF4F complex in mesothelioma," *British Journal of Cancer*, vol. 101, no. 3, pp. 424–431, 2009.

[30] J. E. Hutti, A. D. Pfefferle, S. C. Russell, M. Sircar, C. M. Perou, and A. S. Baldwin, "Oncogenic PI3K mutations lead to NF-κB-dependent cytokine expression following growth factor deprivation," *Cancer Research*, vol. 72, no. 13, pp. 3260–3269, 2012.

[31] Y. Hirotani, K. Mikajiri, K. Ikeda, M. Myotoku, and N. Kurokawa, "Changes of the peptide YY levels in the intestinal tissue of rats with experimental colitis following oral administration of mesalazine and prednisolone," *Yakugaku Zasshi*, vol. 128, no. 9, pp. 1347–1353, 2008.

[32] A. Reinacher-Schick, A. Schoeneck, U. Graeven, I. Schwarte-Waldhoff, and W. Schmiegel, "Mesalazine causes a mitotic arrest and induces caspase-dependent apoptosis in colon carcinoma cells," *Carcinogenesis*, vol. 24, no. 3, pp. 443–451, 2003.

[33] J. P. Luyendyk, G. A. Schabbauer, M. Tencati, T. Holscher, R. Pawlinski, and N. Mackman, "Genetic analysis of the role of the PI3K-Akt pathway in lipopolysaccharide-induced cytokine and tissue factor gene expression in monocytes/macrophages," *Journal of Immunology*, vol. 180, no. 6, pp. 4218–4226, 2008.

[34] Z. Zhang, M. Zheng, J. Bindas, P. Schwarzenberger, and J. K. Kolls, "Critical role of IL-17 receptor signaling in acute TNBS-induced colitis," *Inflammatory Bowel Diseases*, vol. 12, no. 5, pp. 382–388, 2006.

[35] S. Sauer, L. Bruno, A. Hertweck et al., "T cell receptor signaling controls Foxp3 expression via PI3K, Akt, and mTOR," *Proceedings of the National Academy of Sciences of the United States of America*, vol. 105, no. 22, pp. 7797–7802, 2008.

[36] T. Zhang, S. Qu, Q. Shi, D. He, and X. Jin, "Evodiamine induces apoptosis and enhances TRAIL-induced apoptosis in human bladder cancer cells through mTOR/S6K1-mediated downregulation of Mcl-1," *International Journal of Molecular Sciences*, vol. 15, no. 2, pp. 3154–3171, 2014.

[37] B. L. Liu, W. W. Wu, C. F. Jin et al., "Effects of rutaecarpine on ulcerative colitis in mice," *Chinese Journal of Clinical Pharmacology and Therapeutics*, vol. 9, no. 11, pp. 1273–1277, 2004.